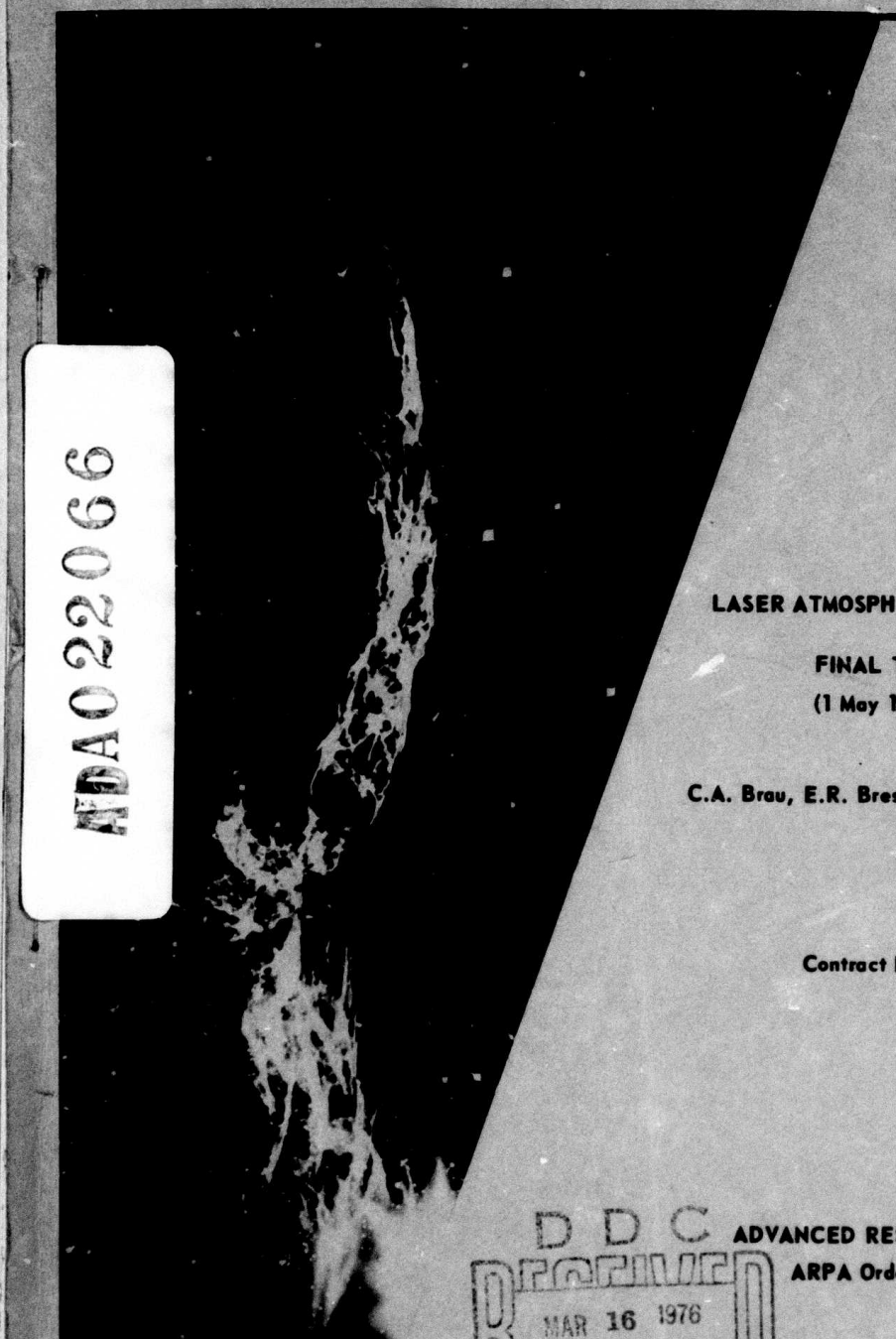

LASER ATMOSPHERIC PROPAGATION KINETICS

FINAL TECHNICAL REPORT

(1 May 1973 – 15 August 1974)

C.A. Brau, E.R. Bressel, S.L. Glickler and R.T.V. Kung

Contract No. N00014-73-C-0311

July 1975

sponsored by

ADVANCED RESEARCH PROJECTS AGENCY

ARPA Order No. 1806 Amendment 9

AVCO EVERETT RESEARCH LABORATORY, INC.

A SUBSIDIARY OF AVCO CORPORATION

LASER ATMOSPHERIC PROPAGATION KINETICS

FINAL TECHNICAL REPORT
(1 May 1973 - 15 August 1974)

by

C. A. Brau, E. R. Bressel, S. L. Glickler and R. T. V. Kung

AVCO EVERETT RESEARCH LABORATORY, INC.
a Subsidiary of Avco Corporation
Everett, Massachusetts

Contract No. N00014-73-C-0311

July 1975

sponsored by

ADVANCED RESEARCH PROJECTS AGENCY
ARPA Order No. 1806 Amendment 9

and

monitored by

OFFICE OF NAVAL RESEARCH
DEPARTMENT OF THE NAVY
Arlington, Virginia 22217

UNCLASSIFIED

SECURITY CLASSIFICATION OF THIS PAGE (When Data Entered)

REPORT DOCUMENTATION PAGE

READ INSTRUCTIONS BEFORE COMPLETING FORM

1. REPORT NUMBER

2. GOVT ACCESSION NO.

3. RECIPIENT'S CATALOG NUMBER

4. TITLE (and Subtitle)

LASER ATMOSPHERIC PROPAGATION KINETICS.

5. TYPE OF REPORT & PERIOD COVERED

Final Technical Report.
1 May 73 — 15 August 74

6. PERFORMING ORG. REPORT NUMBER

7. AUTHOR(s)

C. A. Brau, R. R. Bressel, A. L. Glickler and R. T. V. Kung

8. CONTRACT OR GRANT NUMBER(s)

N00014-73-C-0311
ARPA Order-1806

9. PERFORMING ORGANIZATION NAME AND ADDRESS

Avco Everett Research Laboratory, Inc.
2385 Revere Beach Parkway
Everett, Massachusetts 02149

10. PROGRAM ELEMENT, PROJECT, TASK AREA & WORK UNIT NUMBERS

11. CONTROLLING OFFICE NAME AND ADDRESS

Advanced Research Projects Agency
ARPA Order No. 1806, Amendment 9

12. REPORT DATE

July 1975

13. NUMBER OF PAGES

96

14. MONITORING AGENCY NAME & ADDRESS (if different from Controlling Office)

Office of Naval Research
Department of the Navy
Arlington, Virginia 22217

15. SECURITY CLASS. (of this report)

Unclassified

15a. DECLASSIFICATION/DOWNGRADING SCHEDULE

16. DISTRIBUTION STATEMENT (of this Report)

17. DISTRIBUTION STATEMENT (of the abstract entered in Block 20, if different from Report)

18. SUPPLEMENTARY NOTES

19. KEY WORDS (Continue on reverse side if necessary and identify by block number)

Infrared Lasers
Atmospheric Absorption
Vibrational Kinetics

20. ABSTRACT (Continue on reverse side if necessary and identify by block number)

The absorption of high power laser radiation by the atmosphere is important because the resultant heating of the air causes "thermal lensing" and nonlinear distortion of the beam. The effects of kinetics manifest themselves in the form of transient, unsteady heating at the beginning of the laser pulse, and bleaching at high intensities. The vibrational and rotational kinetics of the absorption of DF and CO laser radiation have been studied and are described.

DD FORM 1473 JAN 73 EDITION OF 1 NOV 65 IS OBSOLETE

UNCLASSIFIED

SECURITY CLASSIFICATION OF THIS PAGE (When Data Entered)

048450

20. (Continued)

CO laser radiation is absorbed principally by H_2O vapor in the wings of 6.3 μm band. DF laser radiation is absorbed by several species, including N_2 (collision induced fundamental band), N_2O (ν_1 overtone and ν_2 bands), CO_2 (ν_3 band), CH_4 (ν_4 overtone and $\nu_2 + \nu_4$ combination bands), H_2O and HDO. The degree of absorption by the latter two species and the precise assignments of the transitions are subject to some disagreement in the literature, and probably introduce the greatest uncertainty in the results.

Rotational relaxation is found to be fast, and bleaching is predicted only at intensities of the order of 10^3 MW/cm^2 and above. The vibrational kinetics have been studied by means of a detailed numerical model for a variety of atmospheric conditions at sea level. The rate of relaxation of N_2O by H_2O (a major uncertainty at the beginning of the program) has been measured by a laser fluorescence technique. The results for CO show that although thermal lensing is important for laser pulse energies above about 1 J/cm^2, transient effects are generally limited to a few microseconds or less, and bleaching is not important at intensities below 10^3 MW/cm^2. Likewise, thermal lensing becomes important for DF at laser pulse energies above a few joules per square centimeter. However, bleaching may become important for some lines at intensities as low as 4 MW/cm^2, and for some other lines transient effects may last for times of the order of a millisecond.

FOREWORD

ARPA Order No. 1806

Program Code No. 3E90

Name of Contractor: Avco Everett Research Laboratory, Inc.

Effective Date of Contract: 1 May 1973

Contract Expiration Date: 15 August 1974

Amount of Contract: $136,582

Contract No. N00014-73-C-0311

Principal Investigator and Phone No: C. A. Brau - (617)389-3000, Ext. 532

Scientific Officer: Director, Physics Program, Physical Sciences Division
Office of Naval Research Department of the Navy,
Arlington, Virginia 22217

Short Title of Work: Propagation Kinetics

The AERL personnel who authored this report are Drs. Charles A. Brau, R. T. V. Kung, Ellen R. Bressel, and Mr. Sheldon L. Glickler.

The authors gratefully acknowledge the contributions of Drs. Lee A. Young, H. A. Hyman, Bennet Kivel and C. Bradley Moore to this program.

ABSTRACT

The absorption of high power laser radiation by the atmosphere is important because the resultant heating of the air causes "thermal lensing" and nonlinear distortion of the beam. The effects of kinetics manifest themselves in the form of transient, unsteady heating at the beginning of the laser pulse, and bleaching at high intensities. The vibrational and rotational kinetics of the absorption of DF and CO laser radiation have been studied and are described.

CO laser radiation is absorbed principally by H_2O vapor in the wings of 6.3 μm band. DF laser radiation is absorbed by several species, including N_2 (collision induced fundamental band), N_2O (ν_1 overtone and ν_2 bands), CO_2 (ν_3 band), CH_4 (ν_4 overtone and $\nu_2 + \nu_4$ combination bands), H_2O and HDO. The degree of absorption by the latter two species and the precise assignments of the transitions are subject to some disagreement in the literature, and probably introduce the greatest uncertainty in the results.

Rotational relaxation is found to be fast, and bleaching is predicted only at intensities of the order of 10^3 MW/cm^2 and above. The vibrational kinetics have been studied by means of a detailed numerical model for a variety of atmospheric conditions at sea level. The rate of relaxation of N_2O by H_2O (a major uncertainty at the beginning of the program) has been measured by a laser fluorescence technique. The results for CO show that although thermal lensing is important for laser pulse energies above about 1 J/cm^2, transient effects are generally limited to a few microseconds or less, and bleaching is not important at intensities below 10^3 MW/cm^2. Likewise, thermal lensing becomes important for DF at laser pulse energies above a few joules per square centimeter. However, bleaching may become important for some lines at intensities as low as 4 MW/cm^2, and for some other lines transient effects may last for times of the order of a millisecond.

TABLE OF CONTENTS

LIST OF ILLUSTRATIONS

LIST OF TABLES

I. INTRODUCTION

As a laser beam propagates through the atmosphere, a portion of the energy of the beam is absorbed by the molecules in its path. For laser wavelengths in transparent regions of the atmosphere the total energy absorbed is only a small fraction of the initial beam energy. Nevertheless, the effect of absorption on beam propagation may be serious due to "thermal lensing" effects. That is, the small amount of absorbed energy ultimately appears in the form of thermal energy, and the corresponding temperature rise causes the gas to expand, reducing its index of refraction. The index of refraction gradients thus induced in the gas by the laser beam tend to distort and defocus the beam in a nonlinear fashion, which may be extremely serious at high power levels.

The description of thermal lensing and the resulting effect on propagation is an extremely complex problem involving vibrational (and possibly rotational) kinetics, aerodynamics and optics. The propagation of CO_2 (10.6 μm) laser radiation, including all the above effects, has been studied theoretically by Wood, Camac, Gerry[1] and Wallace at AERL and by other workers at Lincoln Laboratories, Air Force Weapons Laboratory and Naval Research Laboratory.[2] Experimental results obtained by Gebhardt and Smith[3] are generally in agreement with the theoretical predictions. The results of these studies have demonstrated the important role played by vibrational kinetics, particularly with regard to absorption by CO_2 on the inverse laser transition

$$CO_2(100) + h\nu \rightarrow CO_2(001). \qquad (1)$$

In this transition the asymmetric stretch level (001) is heated by the laser radiation. This energy is then rapidly transferred to N_2 (v=1) where it is "stored" for a relatively long time, due to the slow relaxation of N_2. At the same time, the symmetric stretch made is cooled by the transition. Since this mode relaxes very rapidly via the bending modes, the initial result is to cool the gas, with heating taking place only on the much longer time scale corresponding to N_2 vibrational relaxation. Thus, the vibrational kinetics play a dramatic role, reversing the sign of the thermal lensing.

The objective of the present program has been to examine the effects of vibrational and rotational relaxation on the absorption of DF (3.5 μ) and CO (5 μ) radiation by the atmosphere. At the beginning of the program, much was already known about the absorption of CO radiation by H_2O (the major atmospheric absorber), and the vibrational kinetics of H_2O in N_2/O_2 (air) were fairly well understood. Thus, it has been sufficient just to make a critical evaluation of the available data and to apply this knowledge to the atmospheric absorption problem. Similarly, much was known about the absorption of DF radiation by the atmosphere, enough to establish that the

most important absorbers are N_2 (pressure induced vibrational band), CO_2 (ν_3), H_2O (ν_2), N_2O (ν_1 and ν_2), CH_4 (ν_2 and ν_4) and HDO (ν_1). However, some important gaps were found in the available data regarding the vibrational relaxation of this complex system. In particular, the relaxation of N_2O (ν_2) by H_2O was expected to be fast because of the similarity of N_2O to CO_2, making this a very important process. Since no data were available, an experiment was undertaken to measure the rate of this process, as described below, and the results confirmed the expectation.

The remaining sections describe the results obtained under the program. Section II summarizes the atmospheric absorption coefficients used in this work. These are based on a critical evaluation of the available data regarding atmospheric constituents, molecular absorption cross sections, line shapes and laser wavelengths. Section III presents a discussion of the important rotational and vibrational relaxation processes and a critical evaluation of the available data. Section III also describes the mathematical model used to calculate the relaxation of the vibrational degrees of freedom in response to a laser pulse of arbitrary wavelength distribution, intensity and duration. Section IV describes the experiment which was carried out to measure the rate of relaxation of N_2O by atmospheric species. Section V describes the calculations which were carried out, using the vibrational relaxation model, to investigate the thermal response of the atmosphere to high intensity laser pulses. Due to the large number of absorbing species and the complicated mechanisms by which they relax, the calculations are rather complex. Thus, it has been found useful to summarize the results in terms of global parameters, such as the bleaching flux and relaxation time, which may be used to characterize the thermal response of the atmosphere under various conditions. Finally, in Section VI, the results are summarized and their implications for laser propagation are discussed.

II. SPECTROSCOPY

A. SELECTION OF DF LASER TRANSITIONS

In a DF chemical laser the DF molecules are formed by chemical reaction in high vibrational and rotational states. As they lase and relax by collisional processes they cascade down to lower, thermally populated levels. Thus, in pulsed DF lasers the various transitions do not all lase simultaneously. Rather, the higher vibrational levels tend to lase first with lower levels appearing later in the pulse. Even in continuous wave (CW) lasers the relative strength of the various lines is a complex function of the chemical and relaxation processes occurring in the laser. The various DF lines are absorbed by different species with widely varying absorption cross sections. Therefore, it may be found desirable to suppress certain transitions, even though they may be strong laser lines, if they are strongly absorbed and adversely affect the propagation of other lines. However, this may be difficult to accomplish in DF lasers due to their intrinsic high gain and the complex nature of the processes controlling the relative strength of the various lines.

The eight DF laser transitions shown in Table I were chosen from the experimental work on pulsed DF lasers of Deutsch[4] and Basov, et al.[5] Reference 4, which contains the most accurate experimental measurements of line position ($\pm$ 0.08 cm^{-1}), was used to determine the transition frequency, and the relative energy data of Ref. 5 were used to select lines of strong output in pulsed lasers. Care was employed to ensure that all known atmospheric absorbers were included for these lines.

TABLE I

PULSED DF LASER TRANSITIONS

Laser Line Identification	Laser Frequency (cm^{-1})	Relative Energy*
2P (8)	2631.09	2.37
2P (9)	2605.87	2.68
2P (10)	2580.16	4.24
2P (11)	2553.97	3.46
3P (8)	2546.37	2.74
3P (9)	2521.81	5.38
3P (10)	2496.61	3.35
3P (11)	2471.34	2.26

*Energy of 1P (10) transition is taken as 1.

B. SELECTION OF ATMOSPHERIC ABSORBERS AND ABSORPTION COEFFICIENTS FOR DF LASER LINES

The atmospheric absorbers of importance at DF laser wavelengths are N_2, N_2O, CH_4, H_2O, HDO and CO_2. This is confirmed by both absorption cell experiments[6] and theoretical calculations based on experimental data.[7] McClatchey, et al.,[8] at Air Force Cambridge Research Laboratory (AFCRF) have compiled the molecular spectroscopic parameters for a number of infrared-active molecules (including those listed above) which occur naturally in the terrestrial atmosphere. Parameters included in the compilation for each absorption line are: frequency, intensity, half-width, energy of the lower state of the transition, vibrational and rotational identifications of the upper and lower energy states, an isotopic identification, and a molecule identification. We have written a code which sorts the AFCRL data according to absorbing molecules and vibrational transition over a given frequency interval and calculates the absorption cross section for the absorbing molecule at the laser frequency of interest.

The absorption cross sections are calculated from the integrated absorption coefficient assuming a Lorentz line shape using the relation:

$$\sigma = \frac{S}{\pi} \frac{\Delta\nu}{(\nu - \nu_o)^2 + \Delta\nu^2}, \tag{2}$$

where σ is the cross section in cm^2/particle, S (the integrated absorption cross section cm^{-1}/particle-cm^{-2}) = $\int \sigma(\nu)\, d\nu$, $\Delta\nu$ is the half-width in cm^{-1} and $(\nu - \nu_o)$ is the difference in wave number between the laser line frequency and the center of the absorbing line. The computed N_2O cross sections are in excellent agreement with the absorption cell measurements in Ref. 6 for all the laser transitions considered. For CH_4 the agreement between these cross sections and the absorption cell measurements of Ref. 6 are not as good. For the calculations discussed in Section V, we have used the cross sections computed from the AFCRL data, which average about a factor of 3 to 4 lower than the absorption cell measurements. The effects of any errors thus introduced on the calculated atmospheric temperature rise are small, because in no case is CH_4 the major absorber. This procedure gives too high a value for CO_2, since CO_2 is known to be sub-Lorentzian far from line center. Reference 9 reports measurements of CO_2 absorption both in pure CO_2 and in mixtures of CO_2 with N_2 and O_2. The absorption due to the wings of the strong lines in the $\nu 3$ band centered at 2349 cm^{-1} is much less than that calculated with the Lorentz shape. The data in N_2 and O_2 have been[9] fit with the following equation, which retains the Lorentz pressure dependence but requires a nearly exponential modification of the frequency dependence:

$$\sigma = \frac{S}{\pi} \frac{\Delta\nu}{(\nu - \nu_o)^2 + \Delta\nu^2} e^{-0.46\,(|\nu - \nu_o| - 5)^{0.46}}. \tag{3}$$

Use of this relation gives values for CO_2 absorption cross sections at the DF laser frequencies of interest, which are lower than those of Ref. 6. Therefore, for CO_2, where the absorption is due to lines of the 4.3 μm band (hundreds of wave numbers removed from the laser frequency) we have used the experimental results of Ref. 6. These fall between the values calculated from the AFCRL data using a Lorentz line shape and the experimental line shape fit to CO_2 absorption data.

The absorption due to water vapor is sometimes arbitrarily divided into the contribution due to lines whose centers lie near the wavelength of interest (within a few cm^{-1}) and that due to the far wings of distant lines. The latter contribution varies slowly with wavelength, and is referred to as the water vapor continuum. Measurements of this "continuum" absorption, which may be induced by self-collisions as well as by collisions with N_2 and other gases, are difficult, and the data are not complete.[10] However, the "continuum" absorption calculated using the Lorentz line shape, Eq. (2), is in fair agreement with the observed value at 2400 cm^{-1} at the experimental temperature of 65°C.[10] In fact, the calculated value is about a factor of two larger than the observed value, so that it is not necessary to account for any further contribution to the "continuum" absorption. Due to the lack of experimental measurements for conditions appropriate to this report, the calculations described in Section V use the theoretical value for the total absorption by water vapor due to both nearby and distant lines, based on Eq. (2) and the data compiled by McClatchey, et al.[8] For water vapor the situation is further complicated by the fact that both H_2O and HDO are absorbers, with HDO such a strong absorber that it is significant even in its natural isotopic abundance of 300 ppm of H_2O. The calculated cross sections for H_2O and HDO obtained from the AFCRL data and the experimental results of Ref. 6 are in sharp disagreement for individual laser lines. Because the experimental absorption cross sections were obtained by subtracting the very large absorption due to D_2O from the measured absorption, we have rather arbitrarily assumed the error to be in the experiment and have chosen to use the values calculated from the AFCRL data which for H_2O are in agreement with data of Bates.[11] It turns out that when the laser power is evenly distributed over all the laser lines with equal powers, either set of cross-section values gives about the same temperature rise. This is because the sum over all lines of the absorption cross sections for HDO + H_2O happens to be about the same for both the AFCRL and Ref. 6 cases. It should be noted, however, that for individual laser lines the values are very different and that any calculations of the temperature rise due to H_2O + HDO which use less than all of the eight laser lines of Table I or employ different power levels on the lines may be sensitive to which set of cross-section values is chosen.

The final contribution to atmospheric absorption of DF laser radiation comes from the collision-induced vibrational band of N_2. Since it is centered around the N_2 fundamental frequency at 2331 cm^{-1}, this band is important only for the longest wavelength DF lines. The effective absorption cross section for this band in pure N_2 scales with the density.[10, 12] The temperature dependence has not been accurately determined beyond

about 3.9 μm, but apparently is small.[10] Because of the similar behavior of N_2 and O_2 on the collision-induced vibrational band of O_2,[12] the effect of O_2 on the collision-induced band of N_2 is assumed to be the same as that of N_2 itself. Thus, the effective cross section is given by the expression

$$\sigma = \rho_{tot}\, \tilde{\sigma}(\lambda), \tag{4}$$

where ρ_{tot} is the total (essentially $N_2 + O_2$) density and $\tilde{\sigma}$ is a function only of the wavelength λ.

The absorption cross sections of the various absorbers are summarized in Table II for a total pressure of one atmosphere and a temperature of 300°K.

C. SELECTION OF CO LASER LINES

In contrast to DF chemical lasers, the CO molecules in electric CO lasers are first excited to relatively low vibrational levels by the discharge. They are then pumped to rather high vibrational levels by intermolecular V-V transfer processes. Due to anharmonic effects the vibrational distribution function is generally strongly distorted from a Boltzmann distribution in a manner which favors the higher vibrational levels. As a result, the highest gain is usually observed in relatively high levels (typically $7 < \nu < 15$). Recently, lasing has been observed on the lower levels (down to the $1\tilde{-}0$ transition) in high gain - low loss systems.

As we shall see, the higher vibrational levels, which emit at longer wavelengths, are more strongly absorbed by the H_2O (ν_2) 6.3-μm band. In addition, the kinetics of the lower levels take place more rapidly, offering the possibility of greater specific power. For these reasons it may be desirable to suppress lasing on the high vibrational levels (with a grating or passive H_2O absorber, for example) and force lasing on the low vibrational levels.

To assess the relative advantages of low and high vibrational levels it is necessary to consider a wide range of transitions. The positions of the CO laser lines used in calculating the results presented here are given in Table III. The wavenumber positions for CO, listed in this table, were calculated from spectroscopic constants given by Mantz.[13,14] These should be good to $\pm$ 0.01 cm^{-1}. The wavenumbers agree well with those used by Long[15] and McClatchey.[16]

D. SELECTION OF CO ATMOSPHERIC ABSORBERS AND ABSORPTION COEFFICIENTS

Survey calculations have been made of absorption of CO laser lines by H_2O, CO_2, O_3, N_2O and CH_4. Compared with H_2O, the absorption by O_3 N_2O and CH_4 is negligible. The absorption of the 6P(9) CO line at 1977.28 cm^{-1} by CO_2 is also negligible. For the 2P(9) CO line at

TABLE II

ABSORPTION CROSS SECTIONS OF DF LASER RADIATION
BY ATMOSPHERIC CONSTITUENTS

(Pressure = 1 atm; Temperature = 300°K)

Laser Transition	$\sigma(N_2)$ (cm^2)	$\sigma(N_2O)$ (cm^2)		$\sigma(CH_4)$ (cm^2)		$\sigma(H_2O)$ (cm^2)	σ(HDO) (cm^2)		$\sigma(CO_2)$ (cm^2)	
	Present	Present	Ref. 6	Present	Ref. 6	Present	Present	Ref. 6	Present	Ref. 6
2P(8)	7×10^{-28}	---	---	2.0×10^{-22}	2.2×10^{-22}	6.8×10^{-26}	5.0×10^{-22}	3.3×10^{-22}	---	---
2P(9)	1.0×10^{-27}	3.6×10^{-22}	8.5×10^{-22}	1.5×10^{-23}	2.4×10^{-22}	1.0×10^{-27}	1.5×10^{-21}	4.5×10^{-22}	---	---
2P(10)	1.6×10^{-27}	2.9×10^{-20}	6.6×10^{-20}	---	5.6×10^{-23}	1.4×10^{-28}	1.8×10^{-22}	1.4×10^{-22}	---	---
2P(11)	2.9×10^{-27}	1.0×10^{-20}	1.8×10^{-20}	---	5.3×10^{-23}	8.0×10^{-29}	3.7×10^{-23}	6.1×10^{-22}	---	---
3P(8)	3.4×10^{-27}	2.9×10^{-20}	3.3×10^{-20}	2.5×10^{-22}	9.4×10^{-22}	7.4×10^{-28}	5.7×10^{-23}	1.7×10^{-21}	---	---
3P(9)	5.9×10^{-27}	4.7×10^{-22}	9.4×10^{-22}	---	1.7×10^{-23}	8.0×10^{-28}	1.2×10^{-23}	8.3×10^{-22}	3.2×10^{-22}	3.2×10^{-24}
3P(10)	1.1×10^{-26}	2.4×10^{-22}	6.3×10^{-22}	---	2.4×10^{-23}	9.3×10^{-26}	3.0×10^{-24}	4.6×10^{-22}	6.5×10^{-24}	8.4×10^{-24}
3P(11)	1.7×10^{-26}	4.2×10^{-21}	3.7×10^{-21}	---	1.3×10^{-22}	1.3×10^{-22}	1.1×10^{-25}	6.7×10^{-23}	1.4×10^{-23}	1.3×10^{-23}

TABLE III

POSITIONS OF CO LASER LINES

Laser Line	ν (cm-1)
2P(8)	2085.343
2P(9)	2081.285
2P(15)	2056.047
3P(10)	2051.075
3P(15)	2030.158
3P(16)	2025.875
4P(8)	2033.143
4P(9)	2029.128
4P(15)	2004.337
5P(9)	2003.167
6P(9)	1977.277
6P(10)	1973.299

2081.26 cm^{-1}, the CO_2 absorption is down from that due to H_2O by a factor of 6. The sub-Lorentz CO_2 line contour of Winters, et al.,[9] was used. In the remainder of this work we concern outselves only with absorption by H_2O.

Extensive calculations of absorption of CO laser radiation by atmospheric H_2O have been made by McClatchey.[16,17] However, this work has two limitations. First, the Lorentz contour, Eq. (2) was used for the H_2O spectral absorption coefficient. The experiments of Long, et al.,[15] show that the absorption of CO laser lines in the wings of H_2O lines is typically 40-percent greater than given by Eq. (2). To fit their data they assume that the absorption coefficient follows the lorentz contour for $|\nu - \nu_o| \leq \nu_m$, but that outside this range it is given by

$$\sigma(\nu) = \frac{S}{\pi} \frac{(\nu_m)^2 \Delta\nu}{\left[(\nu_m)^2 + \Delta\nu^2\right] |\nu - \nu_o|^m} \quad |\nu - \nu_o| \geq \nu_m . \tag{5}$$

Equations (2) and (4) agree at $|\nu - \nu_o| = \nu_m$. The best fit was obtained using $\nu_m = 3\,\Delta\nu$ and $m = 1.77$.

McClatchey[17] and Long[15] consider absorption by H_2O lines whose centers lie within 20 or 25 cm^{-1}, respectively, of the CO laser line. This amounts to a cutoff; $\sigma(\nu) = 0$, $\nu > \nu_{max}$ or $\nu < \nu_{min}$. However, we find by allowing $\nu_{min} = \nu_o - 350\ cm^{-1}$, that in some cases half the absorption is due to lines 150 cm^{-1} distant. The true contour in the far wings of H_2O lines cannot be determined from the available data. Unfortunately, H_2O does not form sharp band heads as does CO_2, whose far wing line profile may be determined more reliably. We consider the extrapolation of Eq. (5) to be less arbitrary than cutting it off. Using the extended line profile we find that Long's data may be fitted using $\nu_m = 3\,\Delta\nu$ and $m \sim 1.88$. Values of m for various individual lines ranged from 1.85 to 1.91.

In mixtures of water vapor and air, the H_2O half-width is given by

$$\Delta\nu = a_o p_t [1 + (B-1)\,\chi], \tag{6}$$

where a_o is the half-width per atmosphere of air, p_t is the total pressure in atmospheres, χ is the mole fraction of H_2O in the mixture and B is the self-broadening coefficient. Long, et al.,[15] find B = 8 to 27. We use the value B = 5 from Ref. 18. The difference is insignificant because $\chi < 0.01$ in cases of interest.

Our results are presented in Table IV. Equation (4) was used with $\nu_m = 3\,\Delta\nu$ and $m = 1.88$. The cutoffs were $\nu_{min} = \nu_o - 350\ cm^{-1}$ and $\nu_{max} = \nu_o + 50\ cm^{-1}$. Absorption at larger wavenumbers, farther away from the center of the 6.3-μm H_2O band is negligible. The absorption coefficients are larger than those scaled from McClatchey's calculations[16] for $p_{H_2O} = 3.3$ Torr (mid-latitude winter case), due to the use of the

TABLE IV

ABSORPTION CROSS SECTIONS FOR
CO LASER RADIATION BY H_2O IN AIR

(Pressure = 1 atm; Temperature = 300°K)

Laser Transition	σ (cm^2) Present	σ (cm^2) Ref. 19	σ (cm^2) Ref. 17
2P(8)	4.7×10^{-24}	6.5×10^{-24}	---
2P(9)	4.2×10^{-24}	6.2×10^{-24}	---
2P(15)	5.1×10^{-24}	---	---
3P(10)	9.0×10^{-24}	1.1×10^{-23}	---
3P(15)	7.0×10^{-24}	---	---
3P(16)	2.4×10^{-23}	---	---
4P(8)	7.0×10^{-24}	8.7×10^{-24}	---
4P(9)	7.2×10^{-24}	9.3×10^{-24}	---
4P(15)	1.1×10^{-23}	---	2.5×10^{-24}
5P(9)	1.3×10^{-23}	1.5×10^{-23}	3.8×10^{-24}
6P(9)	1.5×10^{-23}	2.0×10^{-23}	---
6P(10)	1.7×10^{-23}	2.1×10^{-23}	4.0×10^{-24}

"super-Lorentz" profile and its extension farther into the wings of the H_2O lines. There are no Ohio State[15] experimental or theoretical results for many of these lines. Their work has generally been on lines at smaller wavenumbers (higher CO vibrational levels) located nearer the center of the 6.3-μm band of H_2O, for which the attenuation coefficients are typically larger.

Table IV shows the cross sections we have used for water vapor based on the above discussion. They are in good agreement with the results of Harris and Glowacki.[19]

III. KINETICS OF ABSORPTION OF DF AND CO LASER RADIATION

The absorption of DF laser radiation is complicated by the number of atmospheric species which absorb this radiation and by the fact that the upper level of the absorbing transition is frequently a high-lying vibrational level, as in N_2O and CH_4. Thus, to describe the absorption kinetics it is necessary to include a large number of levels. A complete diagram of all the important vibrational levels of the atmospheric species important for DF and CO absorption kinetics is shown in Fig. 1. It is important to keep in mind that each vibrational level shown actually consists of a manifold of vibration-rotation states.

A. ROTATIONAL RELAXATION

Because of the large number of levels, it is necessary to make approximations in which groups of levels are lumped together and treated as a single level. To begin with, it will be assumed that all the rotational levels belonging to a given vibrational level remain in equilibrium with one another at the translational temperature T. This assumption will be valid if the rotational relaxation time τ_R is short compared with the time for a radiatively induced transition, that is, if

$$\Phi_\nu \sigma_\nu \tau_R \ll 1, \tag{7}$$

where Φ_ν is the flux of laser photons, and σ_ν is the absorption cross section. Both the rotational relaxation time and the absorption cross section depend upon the pressure through the molecular collision frequency ν_c. Thus, the adequacy of assumption (7) will depend on the pressure. For a purely Lorentz broadened line, the cross section at the frequency ν is given by Eq. (2). The line half-width $\Delta\nu$ is proportional to the pressure and may be represented by the relation

$$\Delta\nu = ap,$$

where p is the pressure.

The rotational relaxation time is more difficult to quantify precisely. Since rotational relaxation involves a great many levels, it is inevitably a complex process. For example, an extremely short laser pulse (shorter than the time between molecular collisions) will affect only molecules in specific quantum states. The population of the perturbed states will then relax by reorientation of the remaining molecules having the same total angular momentum and by transitions from nearby rotational energy levels. The appropriate relaxation time for this case corresponds to the gain relaxation time measured following a Q-switched laser pulse.[20] Longer laser pulses will perturb the populations of all the rotational levels around the

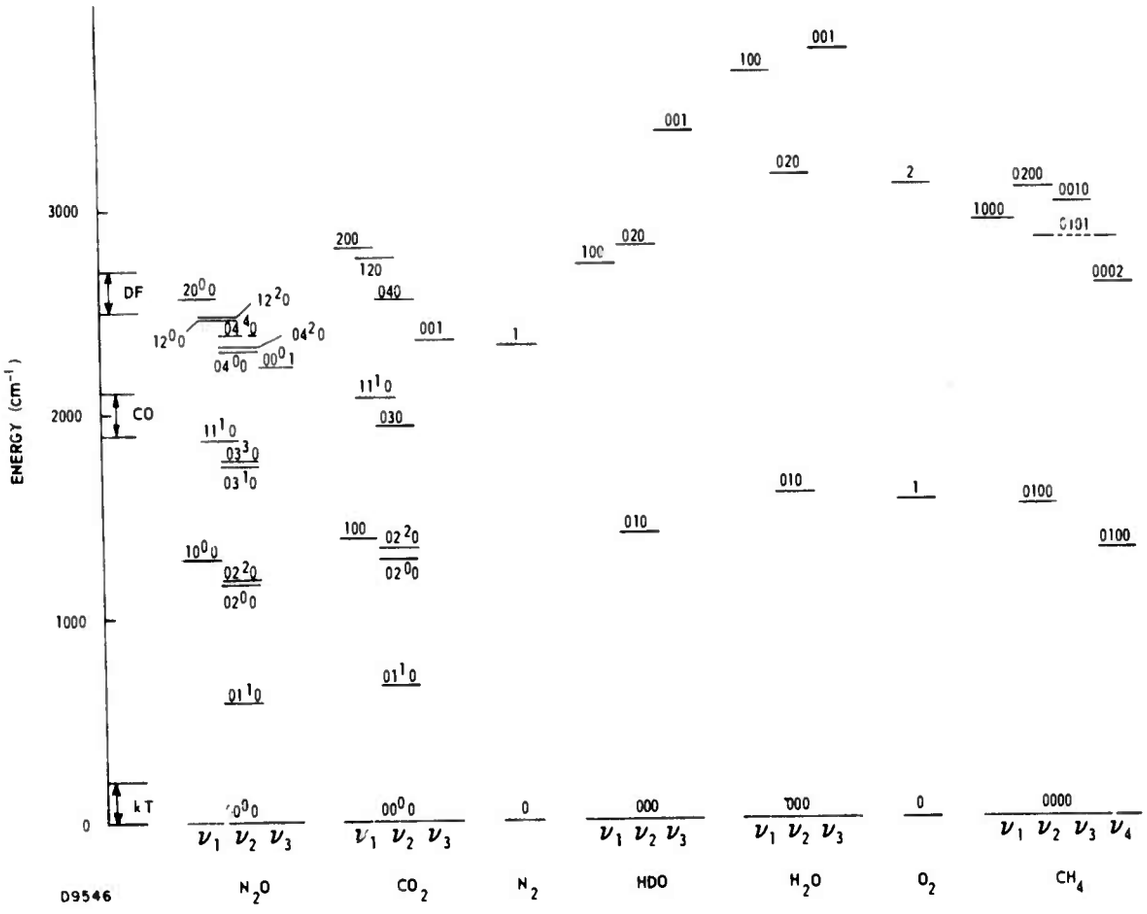

Fig. 1 Vibrational Energy Level Diagram for DF and CO Laser Atmospheric Absorption Kinetics

level from which the transition originates; in this case the time for the system to relax to equilibrium will be considerably longer. Moreover, experimental evidence indicates that the thermally averaged relaxation time (measured acoustically) may correspond to as small as a few collisions or as large as 30 collisions or more (for rotationally light molecules, such as HCl, at elevated temperatures).[21] Moreover, it has been found both theoretically and experimentally that for molecules in high rotational levels the rotational relaxation time increases exponentially with rotational energy.[22]

To examine the importance of rotational relaxation it is convenient to express the relaxation time in the form

$$p\tau_R = \beta, \tag{8}$$

where β is independent of pressure. Equation (7) may then be expressed

$$\Phi_\nu \, \nu \tau_R = \Phi_\nu \frac{\alpha\beta}{\pi} \frac{S}{(\nu - \nu_o)^2 + (\alpha p)^2} \ll 1. \tag{9}$$

When the laser lies in the wing of the absorber ($|\nu - \nu_o| / \alpha p \gg 1$) we obtain the inequality

$$\Phi_\nu \ll \frac{\pi(\nu - \nu_o)^2}{\alpha\beta S} \tag{10}$$

The right-hand side is a function only of the laser frequency and the absorbing level and is independent of the pressure. The limiting fluxes for the most important DF laser lines, calculated using this expression, are summarized in Table V. At sufficiently high pressures ($\alpha p / |\nu - \nu_o| \gg 1$) the laser line will lie within the Lorentz width of the absorber. The limiting flux Φ_ν will then increase as p^2. At sufficiently low pressures, of course, the line will become Doppler broadened and the cross section σ_ν will be independent of pressure. The limiting flux Φ_ν at which rotational relaxation becomes important will then be proportional to the pressure; at a sufficiently low pressure rotational relaxation will always become important. However, as shown in Table V, this occurs only at very low pressures ($\lesssim$ 0.01 atm).

When rotational relaxation becomes important the atmosphere will begin to "bleach", that is, molecules will be removed from the absorbing level and deposited in the upper level faster than they can be relaxed by collisions and the atmosphere will become transparent. Thus, by ignoring rotational relaxation we place an upper bound on the extent of absorption. The results shown in Table V indicate that rotational bleaching should not be important for DF laser intensity levels below 10^{10} W/cm^2. Although a few isolated lines may be bleached at this power level, their contribution to the total absorption on the vibrational bands to which they belong will not be significant. Because of the high rotational bleaching fluxes calculated for DF absorption and limitations of time, similar calculations were not

TABLE V

DF LASER INTENSITY AT WHICH ROTATIONAL RELAXATION BECOMES IMPORTANT

DF Laser Transition	Absorbing Species	Relaxation Time (collisions)	Laser Intensity (W/cm^2)	Pressure Range (atm)
2P(8)	CH_4	10	8×10^9	$0.01 < p < 0.2$
2P(10)	N_2O	2	4×10^9	$0 < p < 1$
2P(11)	N_2O	2	1×10^{10}	$0 < p < 3$
3P(8)	N_2O	2	1×10^9	$0.02 < p < 0.04$

NOTES:

At lower pressures the absorbing lines become Doppler broadened, and the intensity at which rotational relaxation becomes important decreases linearly with the pressure. At higher pressures the laser line falls within the Lorentz width of the absorbing line and the intensity at which rotational relaxation becomes important increases as the square of the pressure.

Laser transitions and absorbing species not indicated in the above table show no rotational relaxation effects at laser intensities below 10^{10} W/cm^2.

performed for CO absorption. It should be emphasized, however, that the DF results cannot be simply extrapolated to all IR lasers. All the important absorbers for DF radiation have rather small absorption cross sections because either the absorbing bands correspond to vibrational overtones (as in the case of N_2O and CH_4), or the laser line lies in the far wings of the absorbing line (as in CO_2), or the rotational structure of the band reduces the contribution of individual lines (as in HDO and H_2O). For laser lines overlapped by strong absorbing lines, rotational relaxation may become important.

B. VIBRATIONAL RELAXATION

Even if rotational equilibrium is assumed, there remain a great many vibrational levels of importance for the absorption kinetics, as indicated in Fig. 1. Although it is not difficult to handle this number of levels on the computer, it is appropriate to make some further simplifications since there do not exist enough kinetic rate data to enable one to describe the system in complete detail. The kinetics of the important atmospheric absorbers are discussed in the following sections.

1. Kinetics of Absorption of DF Laser Radiation by N_2

DF laser radiation is absorbed by N_2 on the collision-induced vibrational continuum band centered around 4.3 μm:

$$N_2(v = 0) + h\nu + M \rightarrow N_2(v = 1) + M + \Delta E. \qquad (11)$$

The excess energy $\Delta E = h\nu - E_{vib} \sim 250\ cm^{-1}$ appears immediately as translational and rotational heating of the N_2 and M molecules.

The relaxation of $N_2(v = 1)$ by the dominant atmospheric species (N_2, O_2, H_2O) has been extensively studied as a result of interest in the CO_2 - N_2 laser.[23] T-V deactivation of $N_2(v = 1)$ by N_2 and O_2 and V-V transfer to O_2 are extremely slow. The most important relaxation path is provided by H_2O. It has not been established directly whether the quenching of N_2 by H_2O proceeds by a T-V (or vibration-to-rotation) process, or by V-V transfer to the $\nu 2$ mode of H_2O,

$$N_2(v = 1) + H_2O(000) \rightarrow N_2(v = 0) + H_2O(010) + 735\ cm^{-1}. \qquad (12)$$

However, the subsequent relaxation of $H_2O(010)$ is so fast that for practical purposes it does not matter.

These processes are summarized in Fig. 2. The time scales for the various processes in this and the following sections are based on an atmosphere composed of

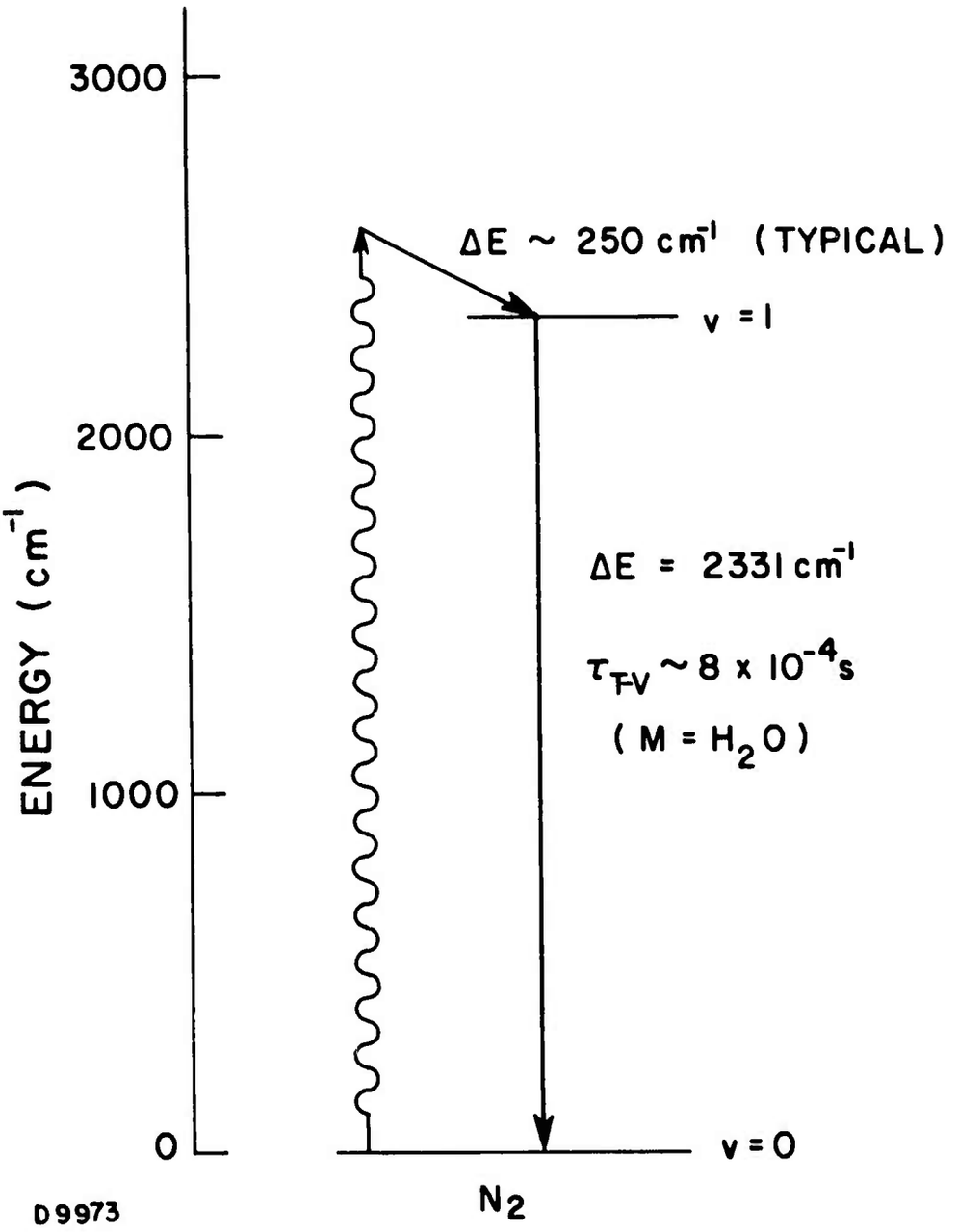

Fig. 2 Kinetics of Absorption of DF Laser Radiation by N_2

N_2 (2×10^{19} molecules/cm^3),

O_2 (5×10^{18} molecules/cm^3),

H_2O (3×10^{17} molecules/cm^3),

at a temperature of 300°K. The amount of energy which appears as thermal (translational + rotational) energy at each step is also indicated. We see that under the above conditions, absorption on the N_2 continuum band results in a small amount of essentially instantaneous heating followed by slow heating on the N_2 relaxation time scale, which is on the order of 8×10^{-4} s.

2. Kinetics of Absorption of DF Laser Radiation by CO_2

DF laser radiation is absorbed by CO_2 on the ν_3 fundamental band centered at 4.3 μm:

$$CO_2(000) + h\nu \rightarrow CO_2(001) + \Delta E. \qquad (13)$$

The absorption takes place principally in the far wings of the lines corresponding to low, thermally populated, rotational levels. Thus most of the excess energy ΔE (~250 cm^{-1}) appears instantaneously as translational energy of the CO_2 and collisional broadening molecules.

The relaxation of $CO_2(001)$ by the dominant atmospheric species (N_2, O_2, H_2O) has been extensively studied as a result of interest in the CO_2 - N_2 laser.[23] Relaxation takes place principally via intermolecular V-V transfer to N_2.

$$CO_2(001) + N_2(v = 0) \rightarrow CO_2(000) + N_2(v = 1) - 18 \text{ cm}^{-1}. \qquad (14)$$

The subsequent relaxation of $N_2(v = 1)$ is described above.

These processes are summarized in Fig. 3, where the relaxation times correspond to the same atmospheric conditions as in Fig. 2. Aside from the small amount of heat released by the absorption process, the overwhelming effect of absorption by CO_2 is to heat the gas on a slow time scale (~10^{-3} s) corresponding to the relaxation of the $N_2(v = 1)$ level.

3. Kinetics of Absorption of CO and DF Laser Radiation by H_2O

CO laser radiation is absorbed by H_2O on the ν_2 fundamental transition,

$$H_2O(000) + h\nu \rightarrow H_2O(010) + \Delta E. \qquad (15)$$

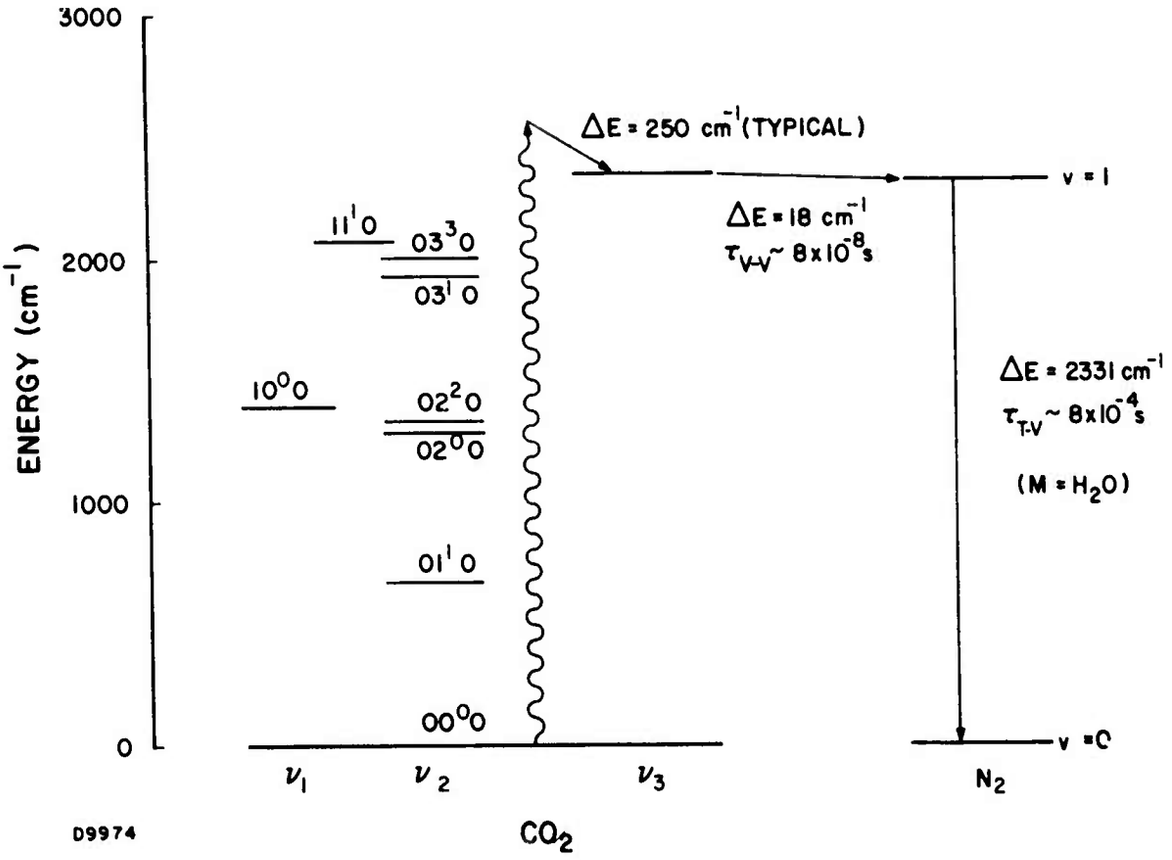

Fig. 3 Kinetics of Absorption of DF Laser Radiation by CO_2

The excess energy ($\Delta E \sim 400\ cm^{-1}$) appears as translational and rotational energy of the H_2O molecule, and is assumed to be thermalized instantly.

The absorption of DF radiation by H_2O, while somewhat controversial, as mentioned above, is alleged to occur on the same vibrational transition. The relatively large excess energy ($\Delta E \sim 900\ cm^{-1}$ for DF lasers) appears as translational and rotational energy of the H_2O molecule, and is presumed to be thermalized instantaneously.

The relaxation of the H_2O (ν_2) mode has been studied experimentally for a long time, and while considerable uncertainty remains for some of the important rates, a broad understanding is possible.[23] The most important processes for the relaxation of H_2O (ν_2) are near resonant V-V transfer to O_2,

$$H_2O(010) + O_2(v = 0) \rightarrow H_2O(000) + O_2(v = 1) + 38\ cm^{-1}, \qquad (16)$$

and T-V quenching,

$$H_2O(010) + M \rightarrow H_2O(000) + M + 1595\ cm^{-1}, \qquad (17)$$

where M = N_2, O_2 and (most importantly) H_2O itself. There is considerable scatter in the data on the T-V quenching of H_2O (ν_2) by H_2O, but the rate is apparently quite fast, on the order of $(2 \times 10^{-12}) - (5 \times 10^{-11})\ cm^3/s$ (about 10 to 100 collisions). The most recent data favor the fastest rate. The data on V-V transfer to O_2 (reaction (16)) are somewhat confused due to apparent errors in most of the papers. The correct rate seems to be about $1.5 \times 10^{-12}\ cm^3/s$. The energy which is transferred to O_2 relaxes relatively slowly by T-V quenching of O_2 by H_2O,

$$O_2(v = 1) + H_2O(000) \rightarrow O_2(v = 0) + H_2O(000) + 1556\ cm^{-1}, \qquad (18)$$

and by transfer back to H_2O followed by quenching of the H_2O.

These processes are summarized in Fig. 4, where the times indicated correspond to the atmospheric conditions of Figs. 2 and 3. The absorption of a laser photon leads to some immediate heating (for a time on the order of the rotational relaxation time) as indicated. T-V quenching of the H_2O leads to further very rapid heating (with a time scale on the order of 10^{-7} to 10^{-6} s. The energy that is transferred to O_2 produces heating on a somewhat larger time scale, on the order of 10^{-5} s. The extent of heating occurring on the fast and slow time scales depends on the relative rates of T-V quenching and V-V transfer to O_2. If the faster H_2O/O_2 V-V transfer rate and/or slower H_2O/H_2O T-V quenching rate is correct, or if the humidity is low (as it will surely be at higher altitudes) then the bulk of the H_2O vibrational energy will be transferred to O_2. This will shift the heating to significantly longer times. These uncertainties become even more important for the absorption of CO laser radiation, since $H_2O(\nu_2)$ is the dominant absorber.

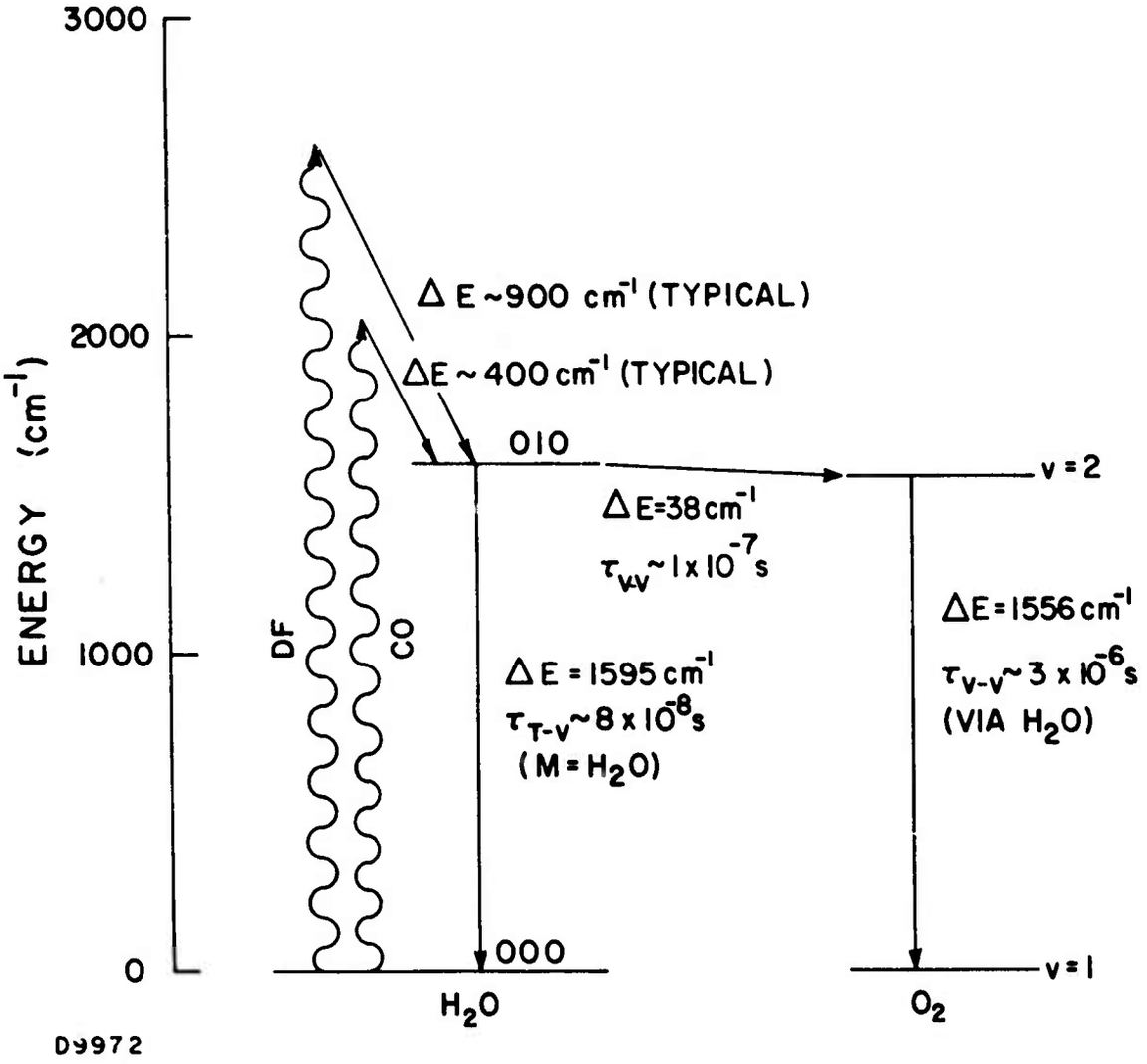

Fig. 4 Kinetics of Absorption of CO and DF Laser Radiation by H_2O

4. Kinetics of Absorption of DF Laser Radiation by N_2O

DF laser radiation is absorbed by N_2O principally on the ν_1 overtone transition,

$$N_2O(00^00) + h\nu \rightarrow N_2O(20^00) + \Delta E, \tag{19}$$

and the combination band transition

$$N_2O(00^00) + h\nu \rightarrow N_2O(12^{\ell}0) + \Delta E. \tag{20}$$

A small amount of absorption takes place on the corresponding transitions from the $N_2O(01^10)$ level, but this may be ignored.

Most of the available data on N_2O vibrational relaxation[24-27] were obtained in pure N_2O and N_2O/N_2 mixtures, and do not shed much light on the most important processes in the atmosphere. However, under the present program the relaxation of modes ν_1 and ν_2 has been studied experimentally. The results are described in detail in Section IV. They show that modes ν_1 and ν_2 are rapidly coupled by collisions with N_2 and H_2O. On the other hand, Yardley[27] finds that mode ν_3 is only weakly coupled to modes ν_1 and ν_2. He observes that N_2O mode ν_3 rapidly couples to N_2 by V-V transfer in about 1100 collisions. However, at the end of this (short) time the extent of residual excitation in mode ν_3 indicates that modes ν_1 and ν_2 have not been excited by either direct intramolecular V-V processes or intermolecular V-V transfer back from N_2.[28]

We are therefore led to neglect the coupling of modes ν_1 and ν_2 to mode ν_3 and to assume that modes ν_1 and ν_2 are rapidly coupled. This leads to the model shown in Fig. 5. According to this model, modes ν_1 and ν_2 are reduced to four lumped levels, each consisting of several near-resonant levels as indicated by the dotted lines.

The relaxation of the N_2O (ν_2) mode by N_2 has been determined by acoustical and spectrophonic techniques[24] and, under the present program, by laser fluorescence techniques, and found to be 2.0×10^{-14} cm^3/s. This is approximately a factor of five faster than the corresponding relaxation rate for CO_2 as might be expected from the slightly lower vibrational frequency of N_2O (ν_2). Using the laser fluorescence technique, the rate of quenching of N_2O (ν_2) by H_2O has been found to be 4.3×10^{-12} cm^3/s. This is about a factor of four slower than the corresponding rate for CO_2. To scale the rates to different temperatures we assume that the temperature dependence for N_2O (ν_2) is the same as that for CO_2 (ν_2). To scale the rate to higher levels we assume the harmonic oscillator rule, which says that for level ($0\,m^{\ell}\,0$) the quenching rate is proportional to m.

These processes are summarized in Fig. 5 where the times indicated correspond to the atmospheric conditions of Figs. 2 through 4. Only a small amount of heating accompanies the absorption of a laser photon. The bulk of the heating occurs on a time scale of the order of 2×10^{-7} s, corresponding to the quenching of N_2O (ν_2) by H_2O.

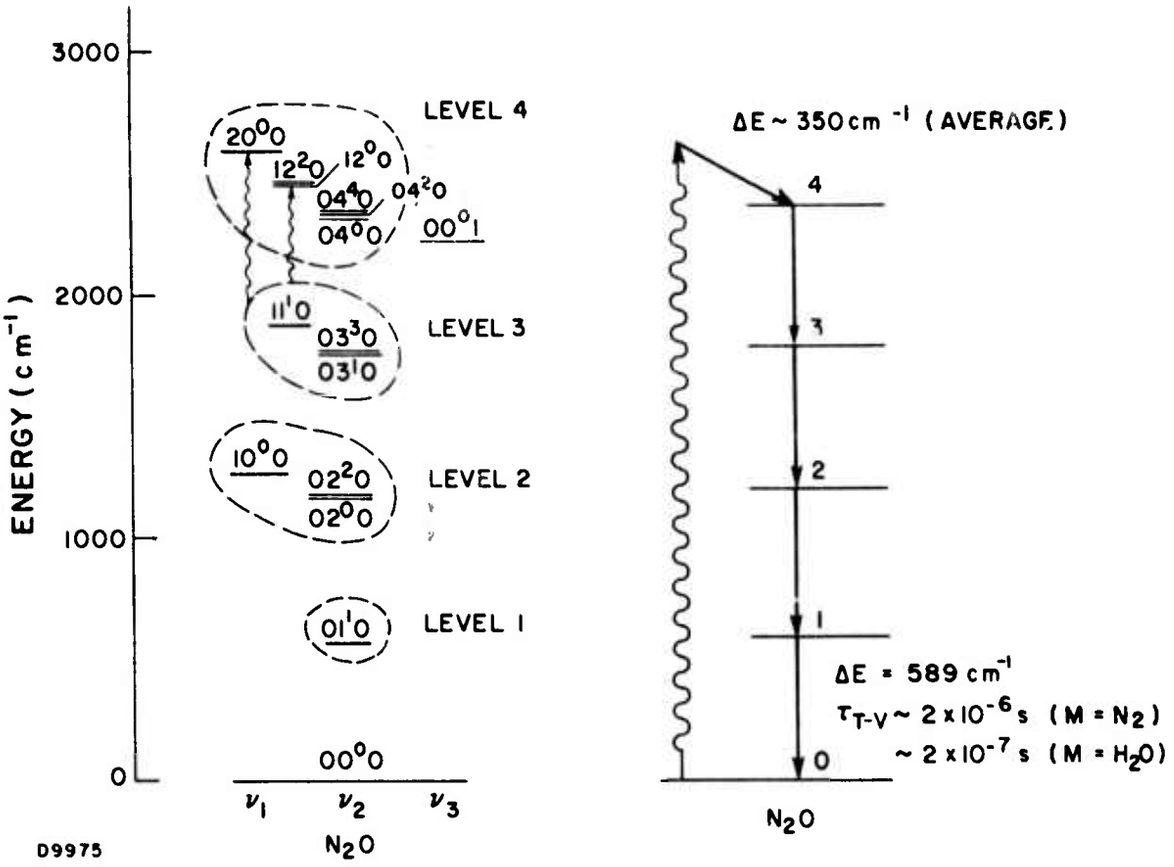

Fig. 5 Kinetics of Absorption of DF Laser Radiation by N_2O

5. Kinetics of Absorption of DF Laser Radiation by CH_4

DF laser radiation is absorbed by CH_4 on the ν_4 overtone band

$$CH_4(0000) + h\nu \rightarrow CH_4(0002) + \Delta E, \qquad (21)$$

and the combination band

$$CH_4(0000) + h\nu \rightarrow CH_4(0101) + \Delta E. \qquad (22)$$

In the experiments which have been done on CH_4 to date[24, 29-35] all the vibrational modes have been coupled very rapidly by CH_4-CH_4 collisions (on the order of 70 collisions to couple modes ν_3 and ν_4,[29] and less than 100 collisions to couple modes ν_2 and ν_4).[33] Since this coupling presumably takes place via intermolecular V-V transfer in high concentrations of CH_4, the modes are likely to be much more slowly coupled in dilute mixtures of CH_4. On the basis of his experimental data Yardley concludes[33] that the rate of coupling by rare gases is probably at least a factor of ten slower. Although atmospheric species such as N_2 and O_2 probably behave more like rare gases than like CH_4, we shall nevertheless, assume that all the modes are strongly coupled, since there is not enough data on vibrational relaxation in CH_4 to justify a more detailed description. Furthermore, the symmetric and asymmetric bending modes, ν_2 and ν_4, have comparable vibrational frequencies and are likely to behave similarly, whether coupled or not. The stretching modes, ν_1 and ν_3, have much larger vibrational frequencies and probably relax much more slowly than the bending modes. They will therefore have little effect on the relaxation of CH_4 except to increase the effective degeneracy of the bending levels to which they are coupled. On the basis of these considerations we adopt the model shown in Fig. 5.

The relaxation of CH_4 in the atmosphere is dominated by V-V transfer to O_2 and H_2O. The rate of transfer from CH_4 to O_2 is well documented,[32] although it is not known whether it takes place from the near-resonant (0100) level or the infrared active (0001) level. Under the assumption that these levels are in equilibrium with each other, we assign this process a room temperature rate equal to 6×10^{-13} cm^3/s in the exothermic direction (O_2 transfer to CH_4). The reverse rate is obtained by detailed balance, using the partition function of the combined $CH_4(0001)$ and $CH_4(0101)$ levels. To scale this rate to higher levels we use the harmonic oscillator rule, as before. To scale this rate to different temperatures we assume that the reaction is sufficiently near resonance for the probability per collision to vary as T^{-1} in the exothermic direction. The rate coefficient in this case varies as $T^{-1/2}$.

The rate of V-V transfer to H_2O (ν_2) is not so well documented, and there is some controversy regarding the extraction of rate coefficients from the limited data on CH_4/H_2O mixtures.[23, 31] If we accept Bauer's interpretation of the data, the rate of transfer from $H_2O(010)$ to CH_4 ($\nu_2 + \nu_4$)

is 6×10^{-11} cm^3/s at room temperature. To scale this rate to higher levels the harmonic oscillator rule is used, as before. To scale the rate to other temperatures we assume that the reaction is sufficiently near resonance that the rate varies as $T^{1/2}$, as was assumed for transfer to O_2. The subsequent relaxation of H_2O (ν_2) and O_2 is discussed in Section III. B. 3.

These processes are summarized in Fig. 6, where the relaxation times indicated correspond to the same atmospheric conditions as in Figs. 2 through 5. Only a very small amount of heating or cooling occurs at the absorption of a laser photon by CH_4. At sufficiently low H_2O concentrations ($\ll$ 0.2%) some cooling will occur on the fast time scale ($\sim 4 \times 10^{-6}$ s in Fig. 6) corresponding to transfer to O_2. Such small concentrations of H_2O can occur at high altitudes, since H_2O is not uniformly distributed throughout the atmosphere. Although V-V transfer from CH_4 (ν_2 and ν_4) to H_2O (ν_2) is endothermic, this process will not lead to cooling because the H_2O (ν_2) vibration is quenched on the same time scale with a large release of heat. Thus, under conditions of sufficiently high humidity ($\gg$ 0.2 percent H_2O), which ordinarily prevail at low altitudes, the laser energy absorbed by CH_4 will lead to heating on a fast time scale ($\sim 7 \times 10^{-7}$ s) corresponding to transfer to H_2O (ν_2) and quenching of the H_2O (ν_2) (principally by H_2O itself). The energy transferred to O_2 will appear as heat on a longer time scale ($\sim 10^{-4}$ s) corresponding to the relaxation of O_2 via H_2O (ν_2).

6. Kinetics of Absorption of DF Laser Radiation by HDO

HDO absorbs DF laser radiation on the ν_1 fundamental transition

$$HDO(000) + h\nu \rightarrow HDO(100) + \Delta E. \qquad (23)$$

No data exist regarding the relaxation of HDO (ν_1) (or ν_2 or ν_3, for that matter). However, preliminary data have been obtained at AERL regarding the relaxation of H_2O (ν_3) in collisions with H_2O.[36] These data indicate that modes ν_1, ν_2 and ν_3 are couples in less than 10 H_2O - H_2O collisions, despite the fact that the levels are separated by about 500 cm^{-1}. Because of the similarity of HDO and H_2O, we assume that HDO (ν_1) and (ν_2) are coupled to each other and to H_2O (ν_2) at every collision by the reactions

$$HDO(100) + H_2O \rightarrow HDO(020) + H_2O \qquad (24)$$

$$H_2O(010) + HDO(000) \rightarrow H_2O(000) + HDO(010). \qquad (25)$$

These reactions are assumed to have rate constants equal to 5×10^{-11} cm^3/s. To scale to higher levels, the harmonic oscillator rules are used. The T-V relaxation of HDO (ν_2) by H_2O, N_2 and O_2 is assumed to be the same as for H_2O (ν_2).

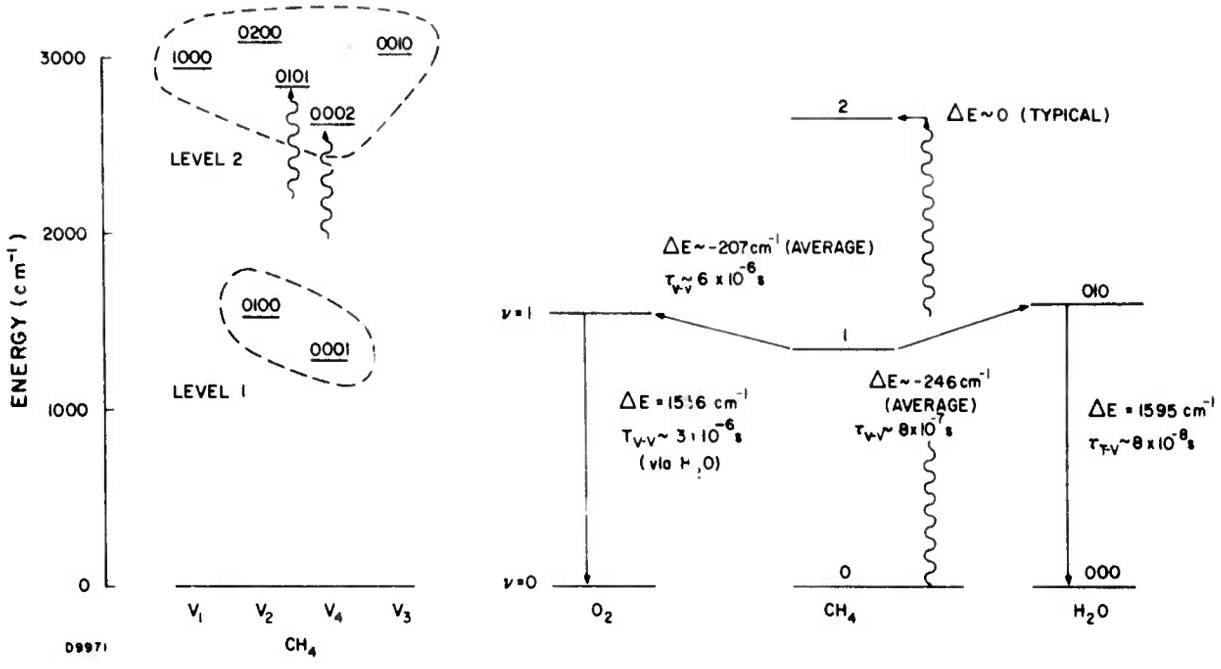

Fig. 6 Kinetics of Absorption of DF Laser Radiation by CH_4

In addition to these rapid H_2O - HDO processes, near resonant V-V transfer to N_2 and O_2 may be important, especially under conditions of low humidity:

$$O_2(v = 1) + HDO(000) \rightarrow O_2(v = 0) + HDO(010) + 153\ cm^{-1}, \qquad (26)$$

$$HDO(100) + N_2(v = 0) \rightarrow HDO(000) + N_2(v = 1) + 393\ cm^{-1}. \qquad (27)$$

The rate of reaction (26) is estimated to be about 1.0×10^{-12} cm^3/s. This is slightly slower (30 percent) than the corresponding rate of transfer between $H_2O(010)$ and O_2, which is more nearly resonant. It is more difficult to estimate the rate of reaction (27). Due to the larger nonresonance, compared with reaction (26), the rate of reaction (27) has somewhat arbitrarily been assumed to be 2×10^{-13} cm^3/s, which is a factor of five slower than reaction (26).

These processes are summarized in Fig. 7, where the times indicated correspond to the same atmospheric conditions as in Figs. 2 through 6. The dominant effect of absorption by HDO (ν_1) is seen to be rapid heating on a time scale of the order of 4×10^{-8} s, corresponding to the quenching of HDO (ν_2) and H_2O (ν_2) by H_2O.

C. RELAXATION EQUATIONS

With these approximations it is a simple matter to write down the kinetic equations describing the relaxation of the system. For this purpose we shall refer to a group of closely coupled vibrational and rotational states as "level i", and define the partition function Q_i and mean energy ϵ_i for level i by the expressions

$$Q_i = \sum_m g_m e^{-E_m/kT}, \qquad (28)$$

$$Q_i \epsilon_i = \sum_m g_m E_m e^{-E_m/kT}, \qquad (29)$$

where g_m is the degeneracy of state m, E_m is the energy of state m, k is Boltzmann's constant and T is the temperature. The partition functions for the levels of N_2O and CH_4 are described in Appendix A.

The density n_i of molecules in level i is assumed to satisfy the inviscid equation

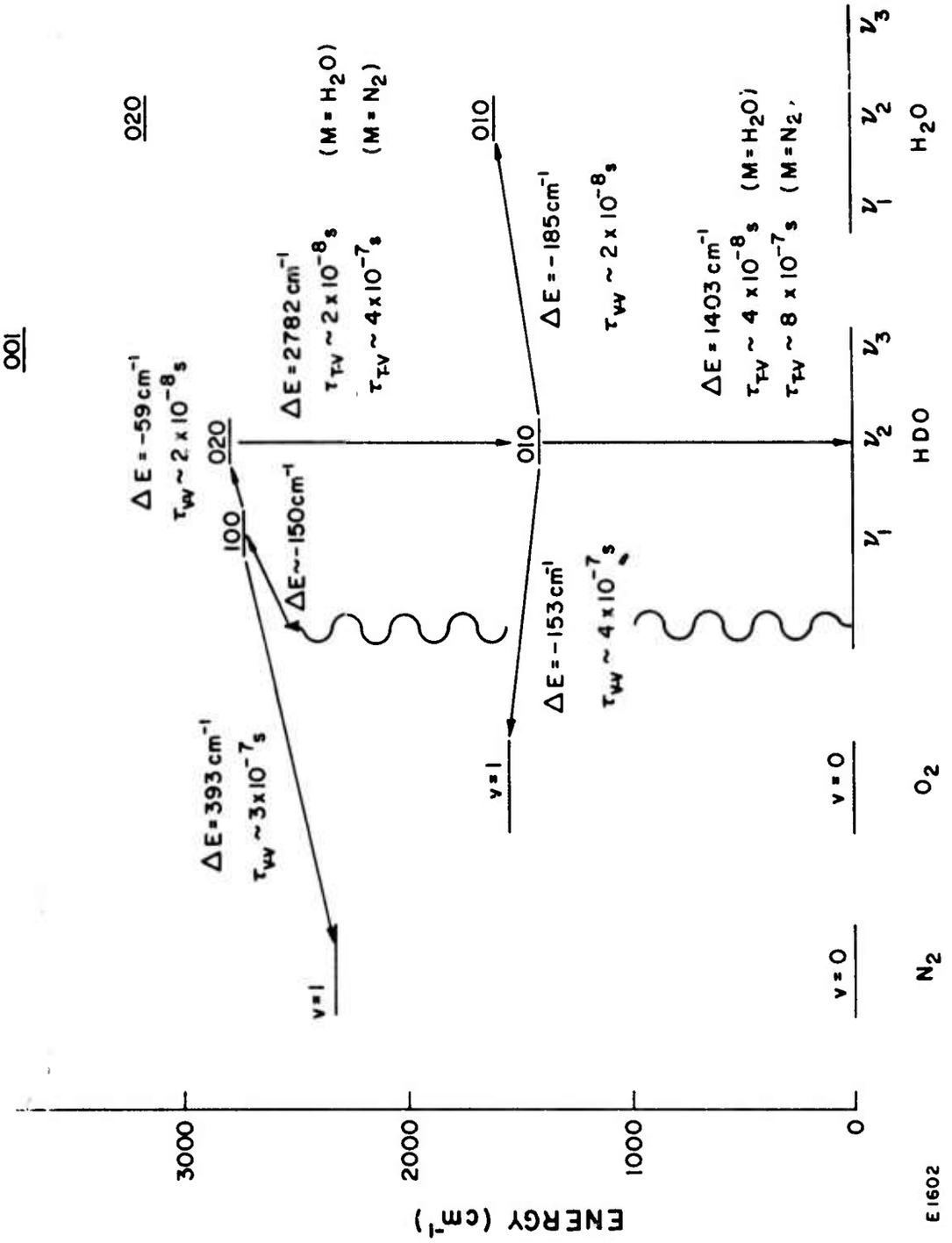

Fig. 7 Kinetics of Absorption of DF Laser Radiation by HDO

$$\frac{Dn_i}{Dt} + n_i \nabla \cdot \vec{v} = - \sum_{j,k,\ell} k_{i \to j}^{k \to \ell} \left(n_i n_j - \frac{Q_i Q_k}{Q_i Q_\ell} n_j n_\ell \right)$$

$$- \sum_{j,\nu} \bar{\sigma}_{i \to j}^{(\nu)} \Phi_\nu \left(n_i - \frac{Q_i}{Q_j} \exp - \frac{h\nu}{\bar{k}\bar{T}} n_j \right), \tag{30}$$

where D/Dt is the usual convective derivative and $\vec{v}$ is the local velocity. Thus, each level of each molecular species is treated as a chemical species capable of undergoing the reactions represented by the right-hand side of the equation. The first term on the right-hand side represents the effect of vibrational relaxation processes of the type

$$A_i + B_k \rightarrow A_j + B_\ell, \tag{31}$$

in which molecule A in level i reacts with molecule B in level k to form molecule A in level j and molecule B in level ℓ, with rate coefficient $k_{i \to j}^{k \to \ell}$. To express this term in the form shown, the usual detailed balance relation

$$k_{i \to j}^{k \to \ell} Q_j Q_\ell = k_{j \to i}^{\ell \to k} Q_i Q_k, \tag{32}$$

has been used. The rate coefficients used in the calculations are summarized in Appendix B. The second term on the right-hand side represents the effect of absorption processes of the type

$$A_i + h\nu \rightarrow A_j, \tag{33}$$

and stimulated emission processes of the type

$$A_j + h\nu \rightarrow A_i + 2h\nu. \tag{34}$$

In Eq. (30) $\bar{\sigma}_{i \to j}^{(\nu)}$ is the cross section at the frequency ν and Φ_ν is the flux of photons at this frequency. To express this term in the form shown, the detailed balance relation

$$\bar{\sigma}_{i \to j}^{(\nu)} Q_j = \bar{\sigma}_{j \to i}^{(\nu)} Q_i \exp - \frac{h\nu}{kT} \tag{35}$$

has been used. This relation is derived in Appendix C.

To solve completely the problem of laser beam propagation it is necessary to solve the vibrational relaxation equations together with the hydrodynamical momentum and energy equations describing the motion of the gas and Maxwell's equations (or an eiconal approximation) describing the propagation of the beam. However, to simplify the study of absorption kinetics, the effects of beam propagation are ignored, and the laser flux Φ_ν is specified as a function of time. To further streamline the problem, the hydrodynamic effects are approximated by assuming either constant pressure p or constant total density n, where

$$n = \sum_i n_i, \tag{36}$$

$$p = nkT. \tag{37}$$

The constant pressure approximation is appropriate when the laser pulse is so long that a pressure pulse generated by the heating of the gas can propagate beyond the width of the beam. Thus, if W is a characteristic width of the laser beam and Δt is the pulse duration (as seen by a "particle" of gas, in the case of a moving beam) then the constant pressure approximation is valid when

$$a\,\Delta t/W \gg 1, \tag{38}$$

where a is the speed of sound. For a sound speed $a = 3 \times 10^4$ cm/s, and a beam width W ~ 10 cm, we see that the constant pressure approximation is appropriate for pulse lengths $\Delta t > 1$ ms. The constant density approximation is appropriate when the laser pulse is so short that a pressure pulse has no time to propagate a significant distance, so that the gas cannot relax hydrodynamically. This limit is valid when

$$a\,\Delta t/W \ll 1. \tag{39}$$

Under the above assumptions, this corresponds to pulse lengths $\Delta t < 100\,\mu$s.

In the constant pressure limit the energy equation may be expressed

$$n \frac{D}{Dt} \left(\frac{5}{2} kT + \bar{\epsilon} \right) = \sum_{\nu, i} h\nu\, \Phi_\nu\, n_i\, \sigma_i(\nu). \tag{40}$$

where

$$n\bar{\epsilon} = \sum_i n_i\, \epsilon_i \tag{41}$$

is the total internal (rotational + vibrational) energy. This equation must be solved simultaneously with the relaxation equations. In the constant density limit the energy equation may be expressed

$$n \frac{D}{Dt} \left(\frac{3}{2} kT + \overline{\epsilon} \right) = \sum_{\nu, i} h\nu I_\nu n_i \sigma_i(\nu). \tag{42}$$

In the remainder of this report, only constant pressure solutions will be discussed. However, the temperature change ΔT is invariably small ($\Delta T/T \ll 1$), so that the relaxation equations are essentially decoupled from the energy equation. Under these conditions the constant density temperature change ΔT_n is simply related to the constant pressure temperature change ΔT_p by the formula

$$\Delta T_n = \frac{5}{3} \Delta T_p. \tag{43}$$

IV. VIBRATIONAL RELAXATION OF THE N_2O ν_1 MODE

A. VIBRATIONAL RELAXATION OF THE N_2O MODE BY N_2O

1. Introduction

In contrast to the ν_3 mode, the vibrational relaxation of the ν_1 mode (1285 cm^{-1}, 7.8 μm) of nitrous oxide has received little attention to date. The (001) level of the ν_3 mode and the (100) level of ν_1 mode are, respectively, the upper and lower lasing levels of the N_2O 10.5 μm laser,[37] and the relaxation times of both levels are important in determining laser performance. The relaxation of the (001) level can be conveniently studied by the laser fluorescence technique using an N_2O laser, and this technique has been applied by a number of investigators.[26, 27, 38-40] However, the lack of a convenient source of excitation for the (100) level has thus far deferred measurement of its relaxation process.

The near coincidence of the N_2O (200 ← 000) transition with a number of DF wavelengths lends itself conveniently to the excitation of the ν_1 mode. This section describes a fluorescence study at room temperature of the relaxation of the ν_1 mode following an overtone excitation via a DF laser operating on the $^3P_7$ transition.

Figure 8 is a schematic of the energy levels of N_2O. The great number of relaxation pathways can be grouped into three classes characterized by the amount of energy and the number of quanta exchanged during a collision. A few representative relaxation channels are given as follows:

(a) Intramode one quantum V-V exchange:

$$\left.\begin{array}{l} (2\overset{\ell}{0}0) + (0\overset{o}{0}0) \overset{\tau_{eq}}{\longleftrightarrow} (1\overset{o}{0}0) + (1\overset{o}{0}0) \\ (0\overset{\ell}{2}0) + (0\overset{o}{0}0) \longleftrightarrow (0\overset{1}{1}0) + (0\overset{1}{1}0) \end{array}\right\} \Delta E \sim 5 cm^{-1} \qquad (44)$$

(b) Intermode two quantum V-V exchange:

$$\left.\begin{array}{l} (1\overset{\ell}{2}0) + (0\overset{o}{0}0) \longleftrightarrow (0\overset{\ell}{4}0) + (0\overset{o}{0}0) \\ \qquad\qquad\quad \longleftrightarrow (0\overset{\ell}{2}0) + (0\overset{\ell}{2}0) \\ (1\overset{o}{0}0) + (0\overset{o}{0}0) \overset{\tau_{12}}{\longleftrightarrow} (0\overset{o}{0}0) + (0\overset{\ell}{2}0) \end{array}\right\} \Delta E \sim 125 cm^{-1} \qquad (45)$$

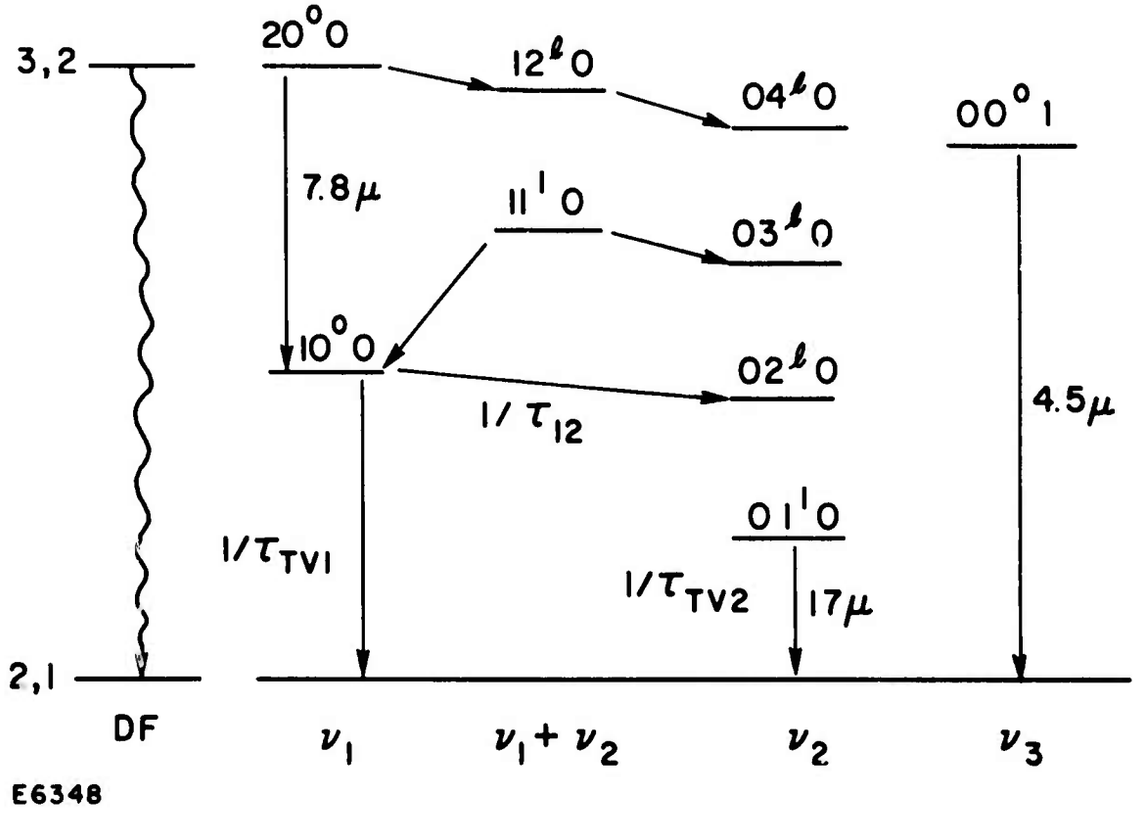

Fig. 8 Energy Level Diagram of N_2O

(c) V-T Relaxation:

$$(010)^{1} + M \quad \underset{}{\overset{\tau_{VT2}}{\longleftrightarrow}} \quad (000)^{o} + M \qquad \Delta E \sim 589 cm^{-1}$$

$$(100)^{o} + M \quad \underset{}{\overset{\tau_{VT1}}{\longleftrightarrow}} \quad (000)^{o} + M \qquad \Delta E \sim 1285 cm^{-1} \qquad (46)$$

Various relaxation time constants are associated with each of the three types of processes. The ability to resolve these time constants depends upon their relative magnitudes. The dipole-dipole V-V theory[41,42] suggests that $\tau_{eq} \ll \tau_{12}$. This is supported by the work of Stephenson, Wood and Moore[43] on the CO_2 molecule. The VT relaxation rate constants are in general much slower than the V-V rate constants[44] This work reports the results of the measurements on τ_{12} and τ_{VT2}. The sensitivity and resolution of the present experiment were not sufficient for the measurement of τ_{eq}.

2. Experimental

Figure 9 is a schematic of the experimental setup. The laser was operated with a 20-kV (12-nf storage capacitor) discharge at 10 pps between a copper bar anode and 100 resistive pin cathodes with an anode-cathode gap of 1 inch. The active medium was 50 cm. The 2-inch I. D. lucite tube was fitted with sapphire Brewster windows. The laser cavity length was 2 meters. The center of the fluorescence cell was placed intracavity and was coincident with the focal plane of a CaF_2 lens (6-inch focal length at 4 μm) and the radius of curvature (12. 5 inch) of an Ag-coated mirror. With this configuration, the beam waist (ω_o) at the center of the fluorescence cell is estimated to be ~1/2 mm using the Collins chart.[45] The grating (300 lines/mm, 4 μm blaze) selected the operating lasing wavelength. The lasing radiation scattered off one of the Brewster windows was monitored through a 1/2-meter Jarrell-Ash monochromator (dispersion ~8 cm^{-1}/mm) and an InSb detector. The Ge flat facilitated optical alignment and energy measurements. The output energy of the laser was measured with a TRG[46] energy meter in place of the 12. 5-inch mirror. The energy per pulse on a number of transitions ($3P_7$, $3P_8$ and $2P_{10}$) was ~1. 5 mJ, under the optimum pressure of around 100 Torr with SF_6 to D_2 ratio of ~4:1. Since the Ge flat was a 50-percent coupler, the intracavity energy with the 12. 5-inch mirror in place could be easily calculated to be a factor of three larger than the extracavity measurement, from the ratio of the scattered signals as measured by the InSb detector.

Two sapphire windows A. R. coated at 4 μm allowed the laser beam to pass through the fluorescence cell with little loss in intensity. The fluorescence signals at 7. 8 μm (ν_1 mode) and 4. 5 μm(ν_3 mode) were monitored through an Irtran 4 window and collected by a 1-inch diameter f-3/4 Irtran 4 lens, with a collection solid angle of ~1/20 steradian. The 7. 8 μm

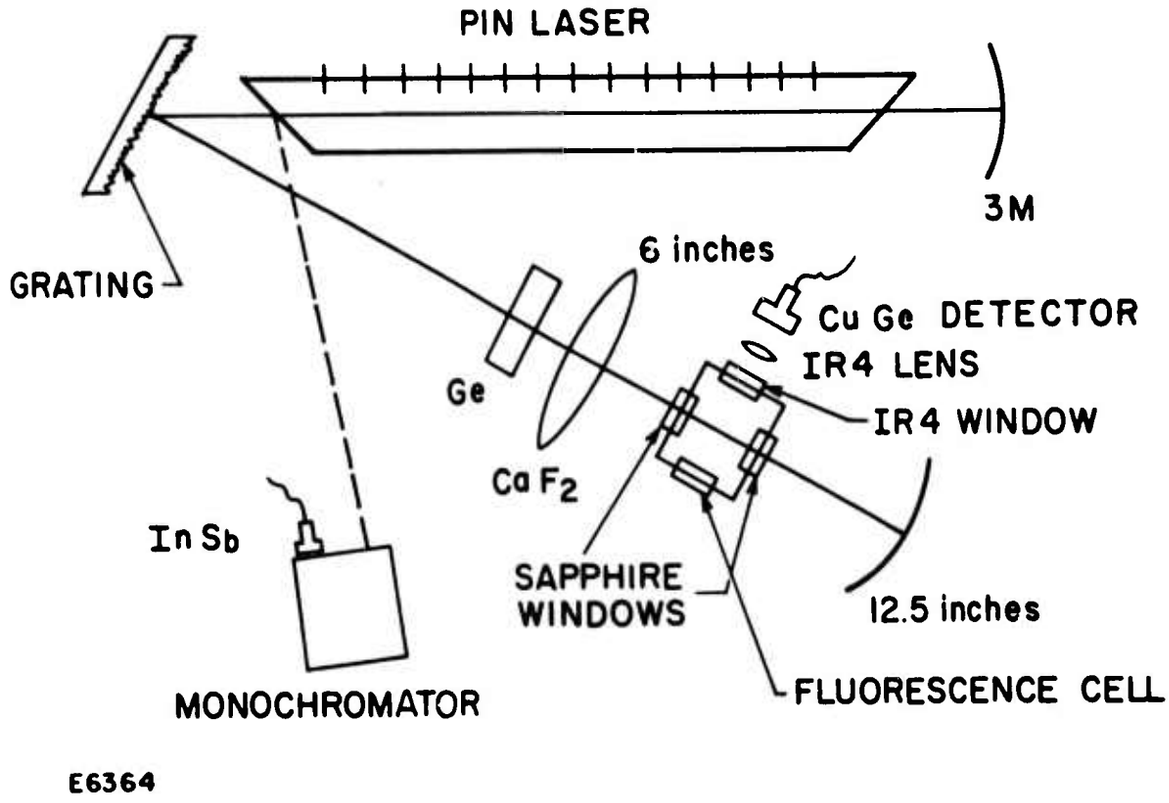

Fig. 9 Schematic of Laser Fluorescence Setup

fluorescence was focused onto a CuGe detector (Santa Barbara) equipped with liquid He-cooled filter ($\Delta\lambda$ ~5 to 8.25 μm), which blocked the ν_3 fluorescence and the possible presence of the ν_2 fluorescence at 17 μm. The output of the detector was fed into a 10-dB gain operational amplifier with a response time of <1 μs. The laser pulse width (FWHM) was between 0.75 and 1 μs under the aforementioned operating conditions. This resulted in a system response time of ~1μs. A PAR model 160 boxcar integrator and a Mosley recorder were used for signal retrieval. 3,000 to 12,000 pulses were averaged per scan (5 to 20 min). The boxcar integrator provided a 10-fold enhancement of the signal-to-noise (S/N). The time base on the recorder output was calibrated with Tektronix time mark generator.

The ν_3 fluorescence signal (4.5 μm) was monitored by an InSb detector. Due to its proximity to the excitation wavelength at 3.9 μm, a narrow band ($\Delta\lambda$ ~0.2-μm) filter centered about 4.5 μm was used.

The distance between the fluorescence region and the IR4 window was 1.3 cm. This provided a self-absorbing layer which trapped all of the radiation from $1 \rightarrow 0$ transitions for the ν_1 and ν_3 modes. An estimate of the optical thickness of the N_2O gas using band strength values of McClatchey[8] indicates that the transitions $100 \rightarrow 000$, $110 \rightarrow 010$, $001 \rightarrow 000$, and $011 \rightarrow 010$ were all black under the experimental conditions used in this experiment. Thus, the fluorescence signals from the ν_1 and ν_3 modes were predominantly radiation from the $200 \rightarrow 100$ and $002 \rightarrow 001$ transitions, respectively.

The vacuum system was pumped down to less than 1×10^{-4} Torr. The leak/outgasing rate was $<2 \times 10^{-4}$ Torr/min. The fluorescence signals were obtained under steady-flow conditions such that system-contributed impurities would have little effect on the relaxation rate. The cleanliness of the system was demonstrated by the consistent relaxation times obtained under flow and static conditions. A calibrated Wallace-Tiernan gauge measured the sample pressures.

The N_2O gas was purchased from Matheson and used without purification. The manufacturer claims a minimum purity of 98 percent. The major impurity species are N_2, CO, O_2, CO_2 and NO. Of these, NO is probably the most efficient relaxer of other molecules.[47] The extimated NO impurity is less than 0.5 percent.[48] This may contribute at most 10 percent to the relaxation rate constant.[49]

3. Results

Sample fluorescence scans at 7.8 μm on two different time scales for the same pressure are shown in Figs. 10 and 11. The initial positive spikes on the baseline scans were electrical pick-up from the laser discharge. The ratio of the electrical pick-up noise to the background detector noise was approximately a factor of 2 prior to averaging. This low level of pick-up noise was achieved after careful shielding of the laser tube and the power supply. Attempts at further pick-up suppression failed.

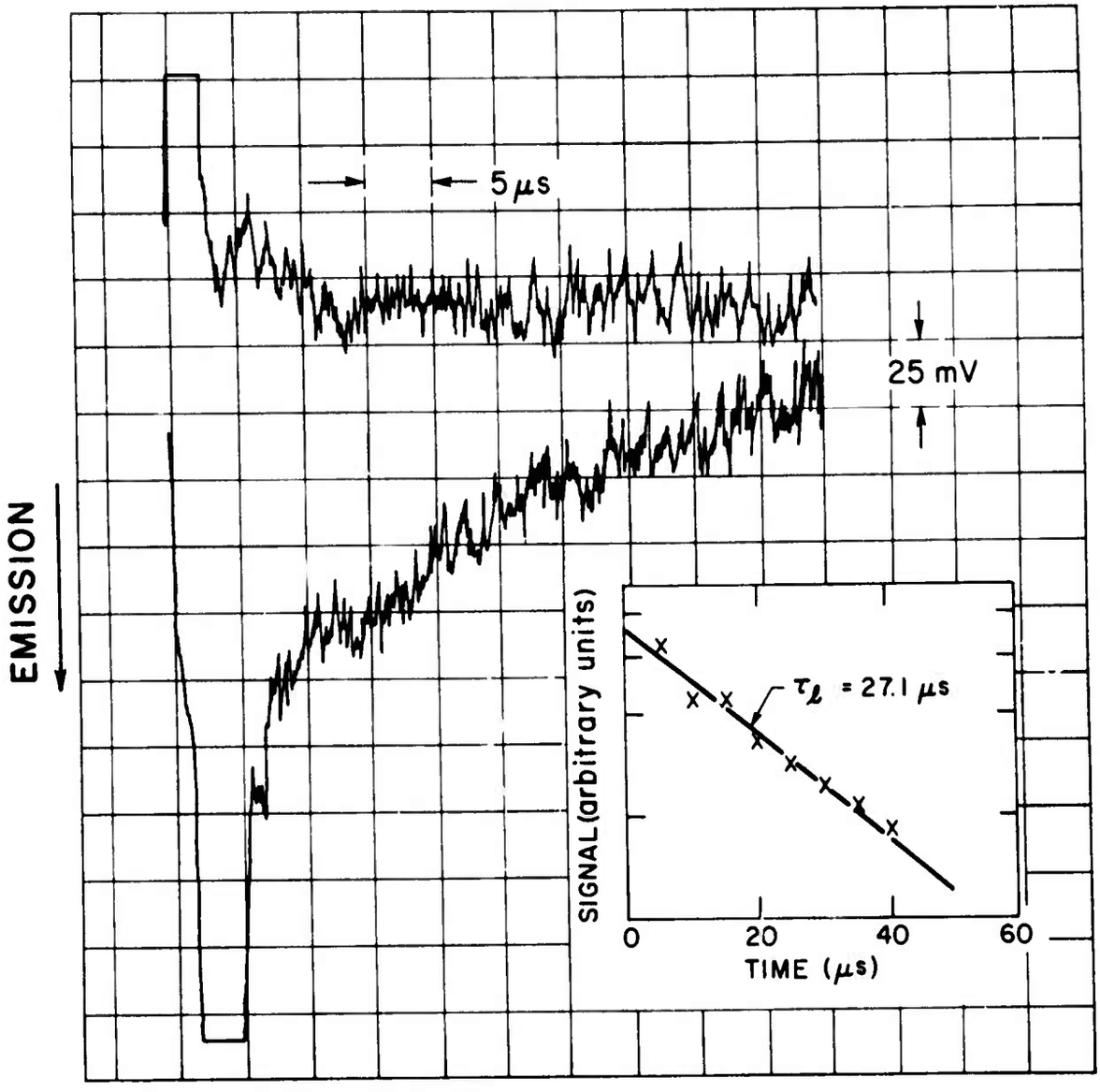

E6339

Fig. 10 Long Time Constant (V-T) Fluorescence Scan at 7.8 μm

p_{N_2O} = 21.5 Torr

Scan Time = 10 min

Aperture = 2.5 μs

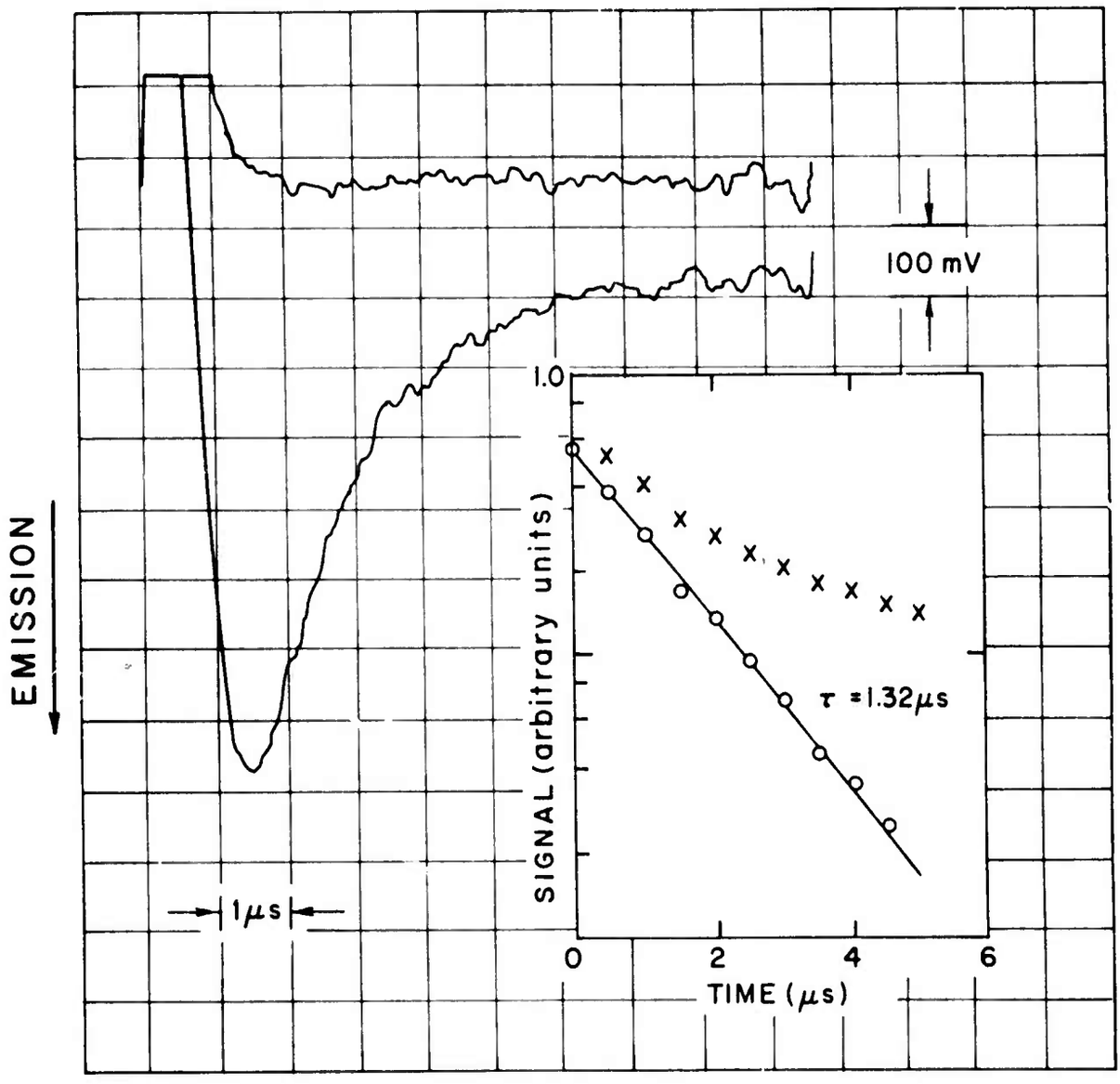

E6349

Fig. 11 Short Time Constant (V-V) Fluorescene Scan at 7.8 μm

P_{N_2O} = 21.5 Torr

Scan Time = 10 min

Aperture = 0.3 μs

The fluorescence signals are plotted vs time on a semi-log plot in the accompanying diagrams. The long time decay of Fig. 10 yields a single time constant. The crosses in Fig. 11 are corrected for the relaxation baseline shift, due to the presence of the longer time constant, to yield the straightline plot. The two time constants are easily resolved since they differ by one order of magnitude.

The reciprocals of the measured time constants are plotted vs pressure for a number of runs in Fig. 12. The slopes yield long (τ_ℓ) and short (τ_s) time constants of 0.72 μs-atm and 0.031 $\pm$ 0.006 μs-atm, respectively. The pressure range (6 to 21 Torr) covered for the short time constant measurements was limited by S/N at low pressures and by time resolution at high pressures. The long time constant measurements were limited by S/N on the low pressure side (~20 Torr) and translational heating as the pressure was increased beyond 60 Torr. The latter effect resulted from pressure-broadened absorption, in which the amount of absorbed energy per molecule is approximately proportional to the pressure. Absorption measurements on the $3P_7$ and $2P_{10}$ DF lasing lines were made with the same system by replacing the 12.5-inch radius of curvature mirror with an InSb PEM detector. The transmittance per unit length $(\ell n\, I_o/I)/\ell$ is plotted vs p_{N_2O} on a log-log plot in Fig. 13. The absorption length, ℓ, was 10 cm in the present measurement. Also plotted in the same figure are the results of Spencer, et al.[50] In the region of pressure overlap, the results are in good agreement. The slopes yield a pressure dependence of $p^{1.8}$ and $p^{1.74}$, respectively, for the $3P_7$ and $2P_{10}$ lines. The results of Spencer, et al, tend to deviate from our extrapolation to higher pressure. This is consistent with the fact that under pressure-broadened conditions the transmittance should vary as the second power of the pressure at low density and transforms into a dependence of 1 to 0 at high pressures depending upon the density of states of the absorber near the absorption line.

The two time constants are interpreted, respectively, as processes (45) and (46) for the short and long time constants. Further justification of this interpretation will be given in a subsequent discussion.

τ_ℓ is interpreted as the VT relaxation of the ν_2 mode. A direct verification of this was to follow the 17 μm (ν_2 mode) fluorescence. The radiative lifetime of the ν_2 mode (6.5 s)[51] is approximately 100 times longer than that of the ν_1 mode (80.7 ms).[51] A pressure of 200 Torr was necessary to detect any signal. At this pressure, the amount of energy absorbed per molecule was estimated to be nearly 20 percent (Eq. (52)) of the translational and rotational energy of N_2O at room temperature. The resultant fluorescence signal was indicative of thermal difusion and conductivity of a heated gas[39] on a time scale of the order of milliseconds. The V-T relaxation time constant at this pressure would correspond to ~2 μs and was completely masked by the heating of the gas sample.

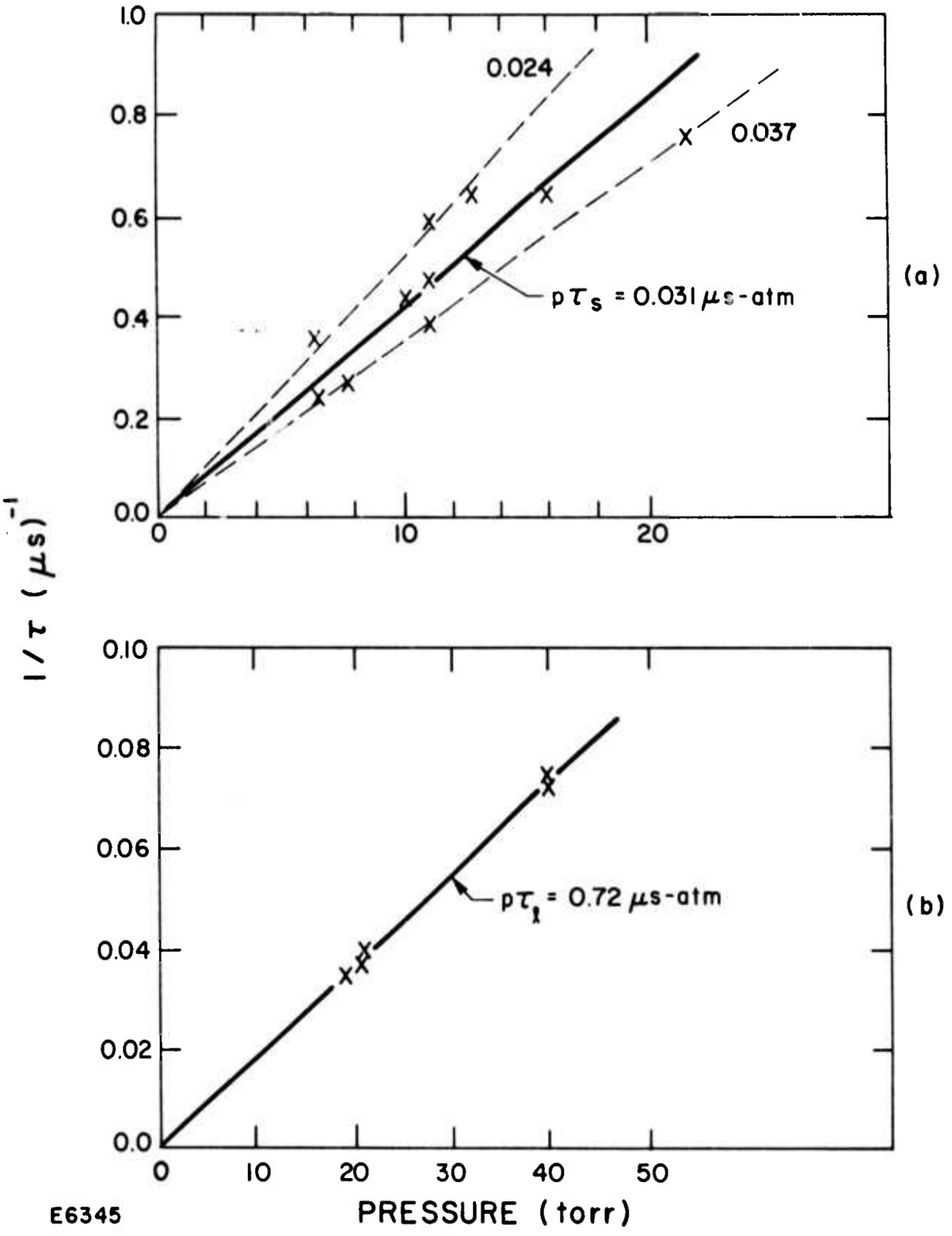

Fig. 12 $1/\tau$ vs Pressure Plot for the (a) Short and (b) Long Time Constants at 7.8 μm

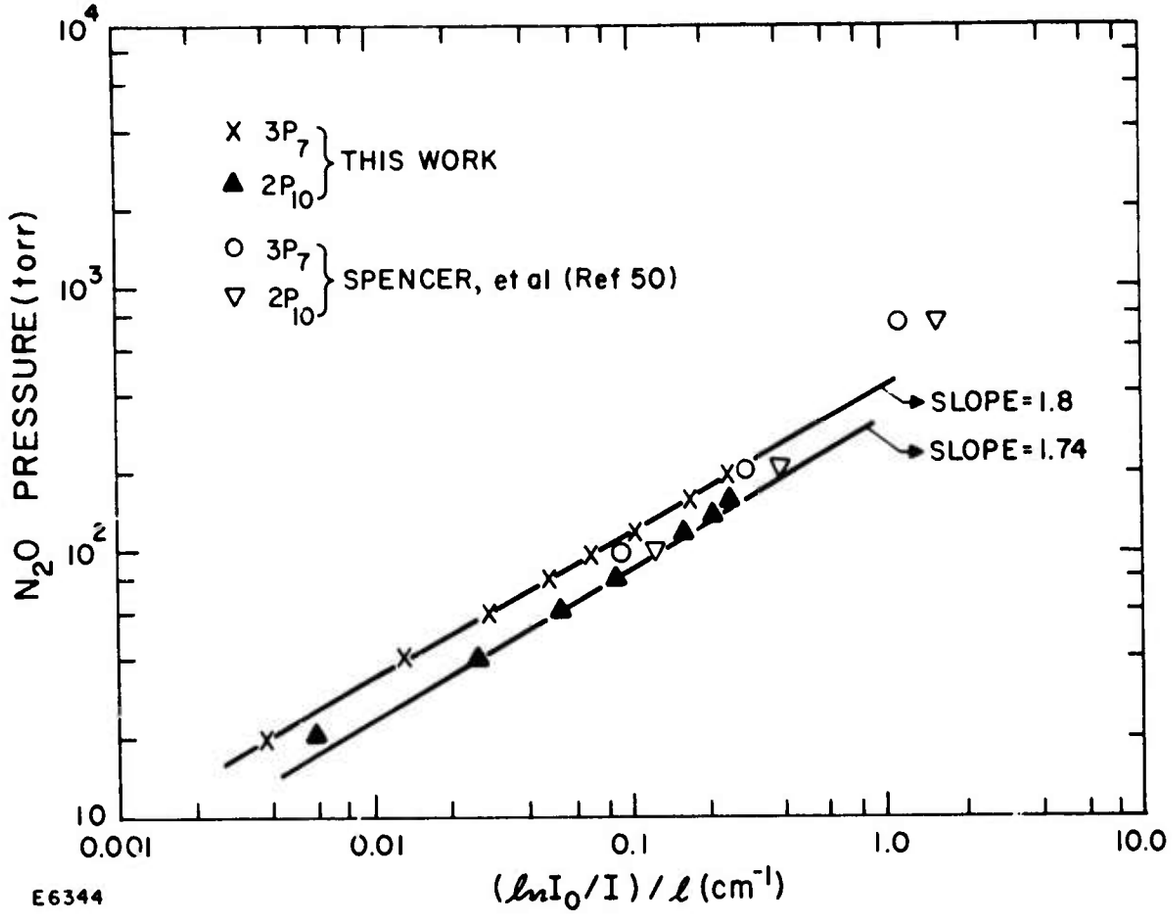

Fig. 13 Absorption Measurements of N_2O at the DF $3P_7$ and $2P_{10}$ Lasing Lines. Plot of p_{N_2O} vs transmittance /unit length.

Fluorescence at 4.5 μm was observed as shown in Fig. 14. System resolution prevented any risetime measurement. The decay yielded a single time constant. Fig. 15(a) is a plot of $1/\tau$ vs pressure. The slope yeilds a time constant of 1.05 $\pm$ 0.15 μs-atm. The peak fluorescence signals, I_p, vs pressures are plotted in Fig. 15(b). The resultant functional relationship is $I_p \propto p^{3.8}$. This relationship will be shown to be significant in identifying the level from which the fluorescence originated.

4. Interpretation and Discussion

There are three assumptions implicit in the interpretation of the results which will be justified in the following discussion.

(a) Intramode relaxation times are too fast to be resolved under the experimental conditions.
(b) The ν_1-ν_2 V-V relaxation is much faster than the ν_1-ν_3 V-V relaxation.
(c) The ν_1 V-T relaxation is much slower than that of the ν_2 mode.

The two relaxation times obtained from the ν_1 fluorescence are interpreted as processes (45) and (46). An estimate of the collisional probability of process was made using the dipole-dipole V-V theory.[42] The transition moments for the processes (200 $\leftarrow$ 100) and (100 $\leftarrow$ 000) were calculated from the band strength values of McClatchey, et al.[8] The N_2O-N_2O collision diameter used was that compiled in Hirschfelder, Curtis and Bird.[52] The calculated probability is ~1/6, which is equivalent to a time constant of ~0.001 μs-atm. This is more than an order of magnitude smaller than the measured τ_s, suggesting that assumption (a) is justified.

The assumption that $\tau_{12} < \tau_{13}$ can be justified by the transition moments and exothermicities of some main reaction paths listed in Table VI. Although the transition moments of the $\nu_1 \rightarrow \nu_2$, and ν_1, $\nu_2 \rightarrow \nu_3$ reaction paths are comparable, the energy exchanged with translation is smaller for the $\nu_1 \rightarrow \nu_2$ equilibration, implying that $\tau_{12} < \tau_{13}$. Yardley[27] suggests that the main depopulating pathway of the (001) level in collisions with inert gases is the reverse of reaction (k). In populating the (001) level, it is more likely that the exothermic reactions (h), (i), and (j) are the main pathways rather than reaction (k). In fact, reaction (k) probably governs the decay of the ν_3 mode as observed in this experiment.

The V-T channel of the ν_1 mode has been ruled out from two considerations. First, the ν_1 spacing is twice that of the ν_2 mode, implying[44] a much slower V-T relaxation rate. Secondly, in order for the ν_1 V-T relaxation to be competitive with the corresponding ν_2 relaxation, the rate constant of the former channel has to be at least a factor of 10 faster than the latter due to the much higher population in the ν_2 mode after the initial equilibration between the ν_1, ν_2 modes. Furthermore the magnitude of the

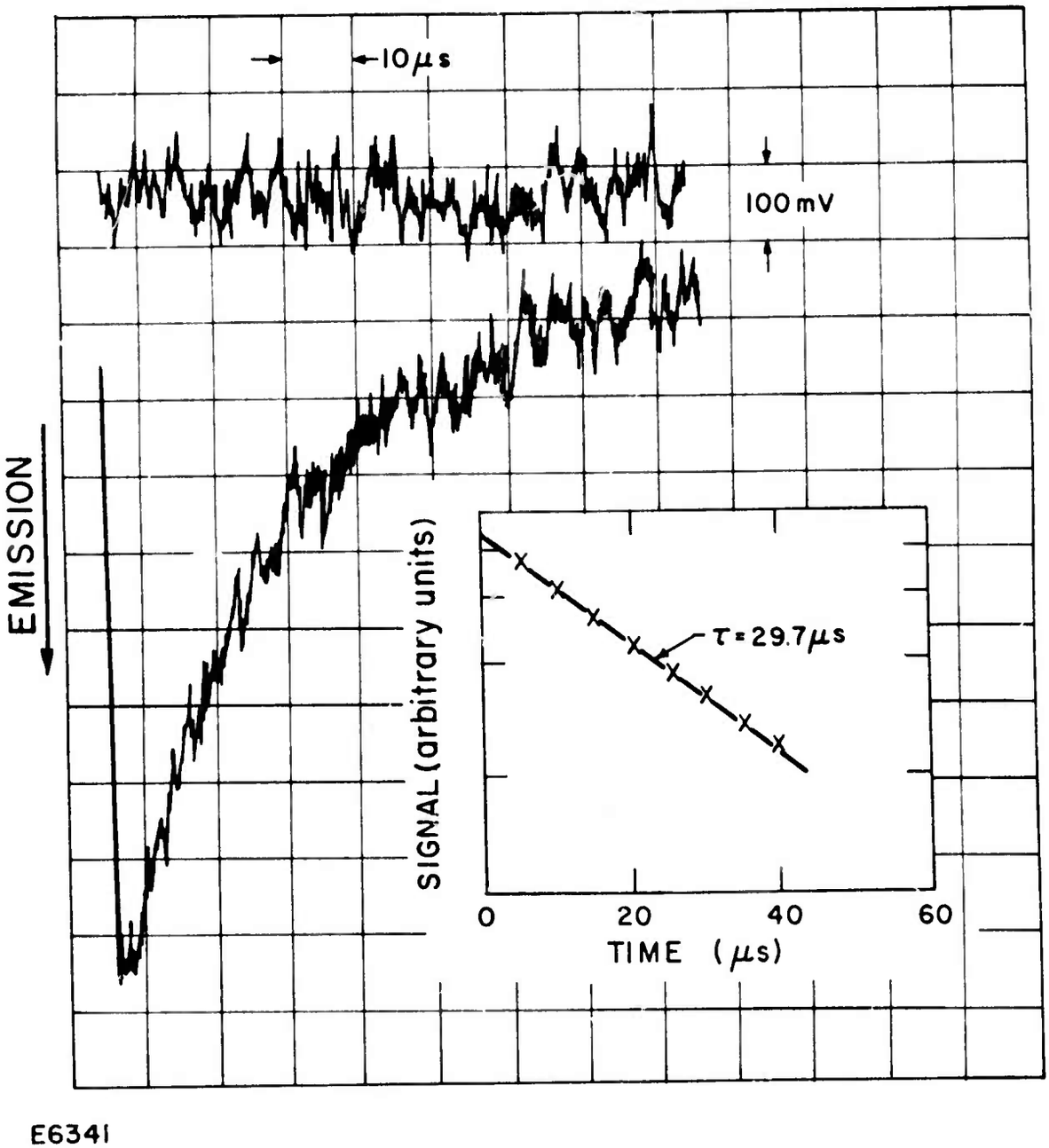

Fig. 14 Fluorescence Scan at 4.5 μm

P_{N_2O} = 32.3 Torr

Scan Time = 20 min

Aperture = 3.8 μs

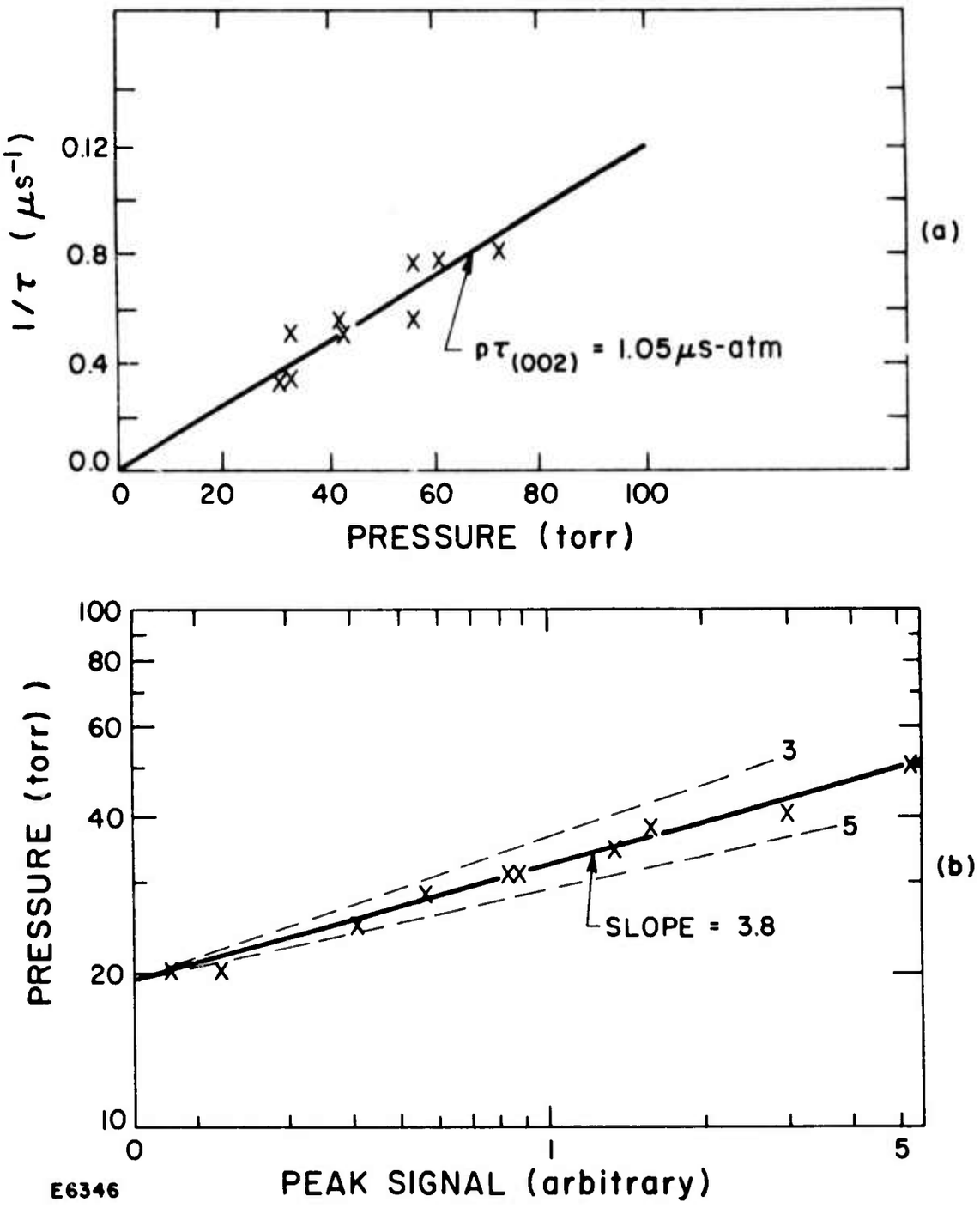

Fig. 15 (a) Observed Peak 4.5 μm Fluorescence Signal (Arbitrary Units) vs N_2O Pressure

(b) $1/\tau$ vs Pressure Plot at 4.5 μm

TABLE VI

TRANSITION MOMENTS

Reference	Pathway	$\langle \mu_1 \mu_2 \rangle$ (stat $c^2 \cdot cm^2$)	ΔE (cm^{-1})
a	100 + 000 → 000 + 020	3.8×10^{-39}	116.8
b	110 + 000 → 010 + 020	5.0×10^{-39}	123.4
c	120 + 000 → 020 + 020	4.4×10^{-39}	125.7
d	200 + 000 → 000 + 120	6.4×10^{-40}	101.3
e	200 + 010 → 100 + 030	8.5×10^{-39}	118.1
f	120 + 000 → 000 + 040	9.6×10^{-41}	139.4
g	200 + 000 → 000 + 040	1.9×10^{-40}	241.0
h	200 + 000 → 000 + 001	8.8×10^{-39}	339.6
i	120 + 000 → 000 + 001	4.5×10^{-39}	238.0
j	040 + 000 → 000 + 001	1.3×10^{-39}	98.6
k	110 + 000 → 000 + 001	8.0×10^{-40}	-344

long time constant strongly suggests that it is the V-T relaxation time of the ν_2 mode, in view of the impact tube results of Huetz, et al.[53] The latter experiment measured directly the ν_2 relaxation with a reported time constant of 1.12 μs-atm. A direct comparison of the two results cannot be made without a detailed examination of the kinetics involved, which will be discussed presently.

Immediately following the laser excitation, the population in the (200) level redistributes itself through process (44), establishing a vibrational temperature in the ν_1 mode. Subsequent relaxation is mainly through the $(100) \xrightarrow{k_1} (020)$ channel, during which time, equilibrium is established between the (200) and (100) levels through the relationship

$$(200) = \frac{(100)^2}{(000)} \exp(\Delta E/kT), \tag{47}$$

where ΔE is the anharmonicity in the ν_1 mode. The overall decay rate of the (100) level can be expressed as

$$\frac{d(100)}{dt} = -k_1 (100)(000), \tag{48}$$

where k_1 is the decay rate constant. Differentiating Eq. (47) and using Eq. (48), one obtains

$$\frac{d(200)}{dt} = -2k_1 (200)(000). \tag{49}$$

It is evident from Eqs. (48) and (49), that the (200) level decays twice as fast as the (100) level as long as Eq. (47) holds. Since the detector sees only the $(200 \rightarrow 100)$ radiation, the measured time constant can be related to the relaxation times of the lowest levels through the relationships

$$\tau_{12} = 2\tau_s \tag{50}$$

$$\tau_{VT2} = 2\tau_\ell \frac{C_2}{C_1 + C_2} \tag{51}$$

where the heat capacity ratio correction is necessary for the V-V, V-T series relaxation process.[54] In order to calculate the heat capacity ratio, the vibrational temperatures of the two modes during the final V-T relaxation process must be known. Since most of the energy resides in the ν_2 mode, due to its smaller spacing and higher degeneracy, the following equation can be used to estimate T_{V2}:

$$\frac{2}{\exp(\theta_2/T_{V2})-1} = \frac{\delta E_\ell}{Ah\nu_\ell} + \frac{2}{\exp(\theta_2/T_t)-1}\ , \tag{52}$$

where θ_2 = 589 cm^{-1}

δ = 8.4×10^{-21} cm^2 (at 30 Torr pressure deduced from Fig. 13.

E_ℓ = 4.5 mJ

A = $1 \times 10^{-2} cm^2$ ($\approx (2\omega_o)^2$, laser waist area)

ν_ℓ = laser frequency

T_t = translational temperature (300^oK)

T_{V2} = vibrational temperature of the ν_2 mode.

The estimated T_{V2} is 350^oK. The heat capacity ratio, $C_2/(C_1 + C_2)$, for this temperature is 0.9. The variation of this ratio with temperature is small, as evidenced by the respective values of 0.93 and 0.81 at 300^o and 500^oK. $C_2/(C_1 + C_2) = 0.9$ is used in Eq. (51) to calculate τ_{VT2}. A $\pm$ 10 percent uncertainty in τ_{VT2} is assigned. The deduced value of 1.3 ± 0.13 μs-atm for τ_{VT2} is 15 percent larger than the impact tube measurements.(53)

The decay of the (200) level can thus be represented by the equation

$$(200) = (200)_o \left[(1-q)\, e^{-t/\tau_s} + q\, e^{-t/\tau_\ell}\right], \tag{53}$$

where $(200)_o$ is the level population after intra-mode equilibration. It is related to the initial population $(200)_i$ excited by the laser through the relationship,

$$(1/2)(100)_o + (200)_o = (200)_i. \tag{54}$$

q is the ratio of the population of the (200) level after intermode, $\nu_1 \longleftrightarrow \nu_2$ equilibration to $(200)_o$. The overall time variation of the (001) level can be given as

$$\frac{d(001)}{dt} = \frac{(200)}{\tau_{13}} - \frac{(001)}{\tau_{32}}\ , \tag{55}$$

where $1/\tau_{13}$ is the feeding rate from the ν_1 mode and $1/\tau_{32}$ is the decay rate from the ν_3 mode.

Integrating Eq. (55) with Eq. (53) yields

$$\frac{(001)}{(200)_o} = A\, e^{-t/\tau_s} + B\, e^{-t/\tau_\ell} - [A + B]\, e^{-t/\tau_{32}} \qquad (56)$$

where

$$A = \frac{(1-q)1/\tau_{13}}{\frac{1}{\tau_{32}} - \frac{1}{\tau_s}} \quad \text{and} \quad B = \frac{(q)1/\tau_{13}}{\frac{1}{\tau_{32}} - \frac{1}{\tau_\ell}}.$$

The ν_3 fluorescence risetime was not resolved ($< 1\ \mu s$) for pressures > 30 Torr, at which pressure $\tau_s \sim 0.8\ \mu s$ and $\tau_\ell \sim 18\ \mu s$. This suggests that the coefficient $A > B$, or $q \ll 1$. For $\tau_{32} \gg \tau_s$, the late time history of the (002) level can be shown to be

$$(002) \sim \frac{(200)_o^2}{(000)} A^2\, e^{-2t/\tau_{32}} \qquad (57)$$

using the fast intramode equilibration assumption.

Since the 001→000 transition is optically black, the observed fluorescence (002→001) can be represented by Eq. (57). Bates, et al[26] and Yardley[27] have measured the relaxation time constant τ_{32} yielding, respectively, 1.96 and 1.74 μs-atm. The measured value of $\tau_{32}/2$ in this work is 1.05 μs-atm, thus agreeing very well with available data.

Further supporting evidence that the 002→001 transition was the dominant ν_3 fluorescence is given by the results of Fig. 15(b). The predicted exponent dependence of the pressure vs peak signal can be easily derived as follows. For $(200)_o/(100)_o \ll 1$, and using Eq. (54),

$$(100)_o \propto (200)_i \propto p^{1.8}, \qquad (58)$$

as given by the results of Fig. 13. Using Eqs. (47), (56) and (57), it is evident that $(001)_p \propto p^{2.6}$ and $(002)_p \propto p^{4.2}$, where the subscript p denotes peak value. The results of Fig. 15(b) yielded $I_p \propto p^{3.8}$. This is in good agreement with the predicted result. The lower measured exponent probably resulted from the lack of system time resolution which prevented the fluorescence signal from attaining peak value before the decay set in.

It is also evident from Eq. (57) that τ_{13} could be obtained if the detectors were calibrated to yield absolute quantities for $(002)_p$ and $(200)_o$. Calibrations were not attempted because (a) the initial electrical noise in the ν_1 signal prevented accurate measurement of the magnitude of $(200)_o$, and (b) the pressure regime at which the ν_3 signal could be detected, did not overlap with that of the ν_1 signal under conditions in which τ_s can be resolved.

Table VII lists the results of the present work and the available data from the literature. The results of the ν_2 V-T and $\nu_3 \rightarrow \nu_2/\nu_1$ relaxation times agree very well with measurements by other investigators. The $\nu_1 \rightarrow \nu_2$ relaxation is the first attempted measurement of this process.

In view of the similarity between N_2O and CO_2 (except for the lack of infrared activity in the ν_1 mode of CO_2), it should prove interesting to compare the $\nu_1 \rightarrow \nu_2$ relaxation process of the two molecules. The 100 and 020 levels of both molecules are coupled through Fermi resonance. The Fermi matrix element of CO_2[55] is slightly larger than that of N_2O[56] The resonance mixing between the levels should render the relaxation process $100 \rightarrow 020$ very rapid.

A number of investigators have attempted to measure this rate constant in CO_2. Only recently [57] have there been suggestions on the consistent interpretation of various results[57-60] In these laser probing experiments, the 9.4- and 10.6-μm radiation were used to probe the levels of interest. A number of relaxation time constants were observed[57, 58] Bulthius and Ponsen[57] identified a fast rate constant ($\sim 3.3 \times 10^{-3}$ μs-atm) as the $100 \rightarrow 020$ relaxation and a slow rate constant (~ 0.13 μs-atm) as the $100 \rightarrow 010$ relaxation. The measured $\nu_1 \rightarrow \nu_2$ relaxation time (~ 0.062 μs-atm) in this work has been interpreted as the $100 \rightarrow 020$ transition. In view of the CO_2 results, it is quite possible that this measured relaxation time pertains to the process $100 \rightarrow 010$. If the $100 \rightarrow 020$ process of N_2O were as fast as that of CO_2, the time resolution in this experiment for the given sensitivity would not allow the measurement of this rate constant. An absorption experiment using an N_2O laser operating on the $020 \rightarrow 001$ transition would specifically monitor the 020 level. Experiments of this type would serve to resolve the various possible channels.

B. VIBRATIONAL RELAXATION OF THE N_2O ν_1 MODE BY Ar, N_2, H_2O AND NO

1. Introduction

The self-relaxation of the ν_1 mode of N_2O was investigated first, because of its important effects in any experiment with N_2O. This section describes an investigation of the effect of some foreign gases, namely, Ar, N_2, H_2O and NO on the relaxation of the ν_1 mode of N_2O. The ν_2 relaxation by Ar, N_2 and H_2O was also measured.

TABLE VII

EXPERIMENTAL RESULTS

Process	$\tau(\mu s\text{-atm})$	P*	$(\tau)_{lit.}$	Reference
$\nu_1 \rightarrow \nu_2$	0.062±20%	1/280	-	
$\nu_2 \rightarrow$ Translation	1.3 ± 10%	1/5900	1.12	53
$\nu_3 \rightarrow \nu_2/\nu_1$	2.1 ± 10%	1/9500	1.96 1.74 1.84	26 27 40

*P is the collision probability calculated from measured τ' s and the collision diameter of 3.85Å.[52]

The N_2O-N_2, N_2O-H_2O rates are important in the propagation of DF chemical laser (3.9 μm) radiation through the atmosphere. A major absorber of this radiation is N_2O, which is present at a concentration of ~ 0.5 ppm.[61] The N_2O-N_2O self-relaxation would thus be negligible. The absorbed laser energy appears as translational energy mainly due to N_2O-N_2 and N_2O-H_2O collisions. The former collision pair is important since N_2 is the major constituent in the atmosphere, while the importance of the latter is due mainly to the unique property of water vapor as an efficient relaxer of other molecules.

The N_2O-NO relaxation rate was investigated due to the possible presence of NO in the N_2O gas, as discussed in Section IV A. The NO V-T self-relaxation rate constant is ~ 6 orders of magnitude faster than the corresponding CO self-relaxation rate, while the intramolecular V-V relaxation is comparable to CO.[62] In this work, the unusual property of NO as an efficient V-T relaxer will be examined from the point of view of its effect on the measured N_2O rate constants.

The relaxations under study are the V-V exchange process

$$N_2O(\nu_1) + M \xrightarrow{\tau_{12}} N_2O(\nu_2) + M \qquad (59)$$

and the V-T process.

$$N_2O(\nu_2) + M \xrightarrow{\tau_{TV2}} N_2O + M \qquad (60)$$

2. Experimental

The experimental setup used is as described in Section IV A with the addition of a water vapor feed-in system similar to that of Kung and Center.[63] A schematic of this system is shown in Fig. 16. The incoming carrier gas was divided into two parallel streams, one of which flowed through the water bubbler and was mixed with the bypassed carrier gas flow. Needle valves were used to obtain the desired total pressure and partial pressure of water vapor in the mixture. Needle valve 3 was heated to prevent possible H_2O condensation during the expansion through the valve. A Wallace-Tiernan gauge and a Panametric hygrometer probe[64] monitored the total pressure and the water vapor partial pressure in the fluorescence chamber. The fluorescence measurements commenced only after the pressure and hygrometer readings were constant over a 1/2-hour duration. The flow velocities were small and did not affect the pressure measurements. The hygrometer probe was calibrated against a Validyne diaphragm gauge[65] (Model DP-0.1 PSID) which in turn was calibrated against a cold trapped McLeod gauge. The overall uncertainty in the water vapor partial pressure measurement was ~ ±10 percent, as reflected in the scatter of the calibration curve over a range of 0.1 to 3 Torr. Partial pressures of H_2O over the range of 0.3 to 1.6 Torr were used in this experiment.

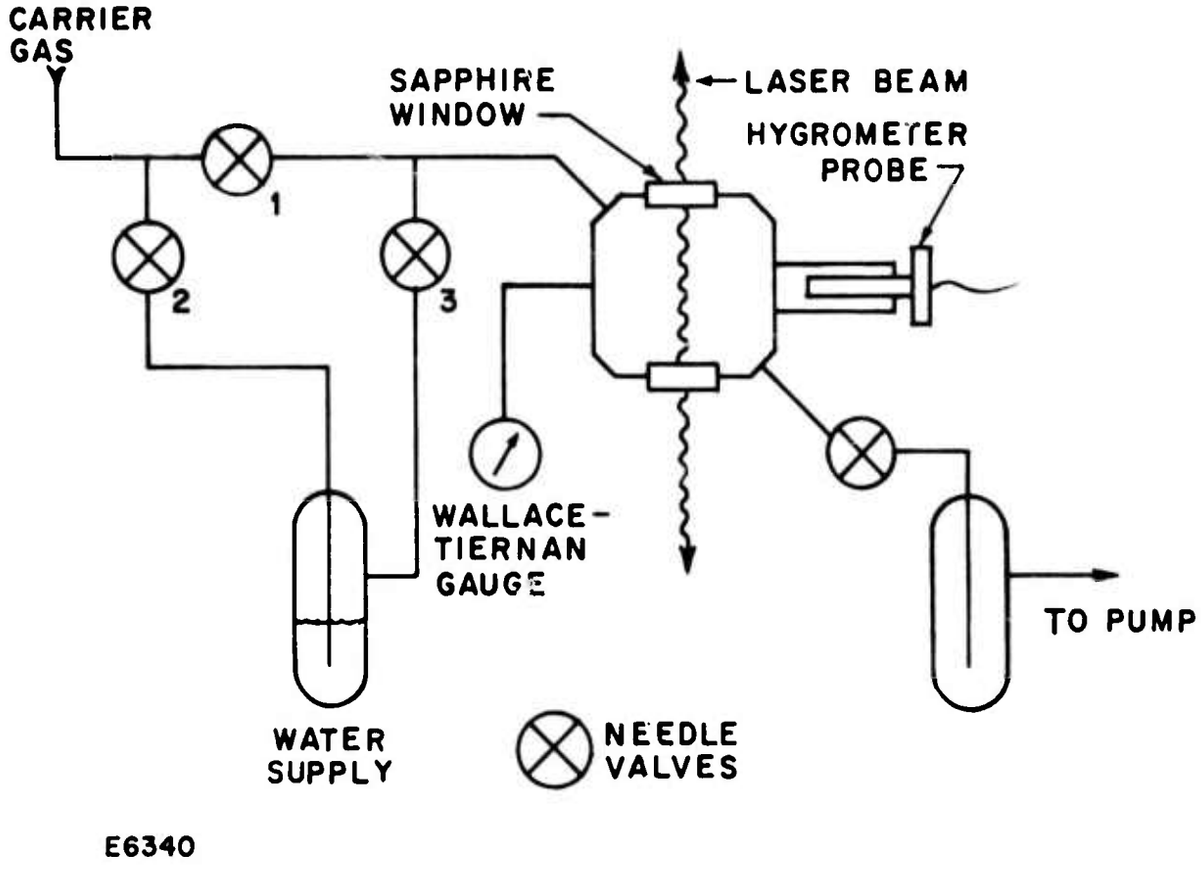

Fig. 16 Schematic of Water Vapor Feed-in System

The N_2O ν_1(7.8 μm) fluorescence was monitored by a CuGe detector (Santa Barbara) equipped with liquid He-cooled filter ($\Delta\lambda \sim 5$ to 8.5 μm). Within this bandwidth there is a possibility of interference from the ν_2-bending mode of water vapor (6.3 μm) due to the comparable band strengths of N_2O ν_1-mode (268 ama^{-1} cm^{-2})[8] and H_2O ν_2-mode (250 ama^{-1} cm^{-2}).[66] Since the mole fraction of H_2O vapor used in this experiment was less than 0.07, the possible presence of vibrationally excited H_2O molecules due to the V-V exchange between N_2O and H_2O would contribute little to the fluorescence signals.

The N_2O gas was obtained from Matheson with a minimum purity of 98 percent. Some premixed N_2O-N_2 and N_2O-Ar mixtures were purchased from Mass Oxygen[67] with compositions of 10.2 percent N_2O in N_2 and 9.73 percent N_2O in Ar. The nominal purities were 99.5 percent for these mixtures. Mixtures of other compositions used were prepared in a 2-liter stainless steel chamber with either N_2 or Ar of 99.995 percent nominal purity. The NO gas used was obtained from Matheson and was purified in an acetone slush bath, thus separating out tne NO_2 impurity.

3. Results

The fluorescence (7.8 μm, ν_1 mode) decay time constants of various mixtures were measured. The decay time constants τ_M, of N_2O-M collisions were reduced from the Eq. (61)[68]

$$\frac{1}{\tau} = \frac{\psi_{N_2O}}{\tau_{N_2O}} + \frac{\psi_M}{\tau_M} \qquad (61)$$

where τ and τ_{N_2O} are, respectively, the measured time constant and the relaxation time constant of pure N_2O. ψ_{N_2O} and ψ_M are the respective mole fractions of N_2O and M gases.

Two distinct time constants were observed in all cases except for NO. The short τ_s and long τ_ℓ time constants are attributed to the V-V and V-T relaxation processes, respectively.

a. N_2O-Ar and N_2O-N_2 Mixtures

The V-V relaxation time constants were obtained from the slopes of the $1/\tau$ vs pressure plot for the 9.73 percent N_2O in Ar and 10.2 percent N_2O in N_2 mixtures as shown in Fig. 17(a) and (b). The slopes yielded time constants of 0.13 and 0.10 μs-atm for Ar and N_2 mixtures, respectively. Using Eq. (61), the short time constants for N_2O-Ar and N_2O-N_2 collisions were found to be 0.19 and 0.13 μs-atm, respectively.

The V-T relaxation results for a number of runs are listed in Table VIII for the N_2O-N_2 and N_2O-Ar mixtures. The average values of the long time constants are, respectively, 6.72 and 0.97 μs-atm for the N_2O-Ar and N_2O-N_2 collisions.

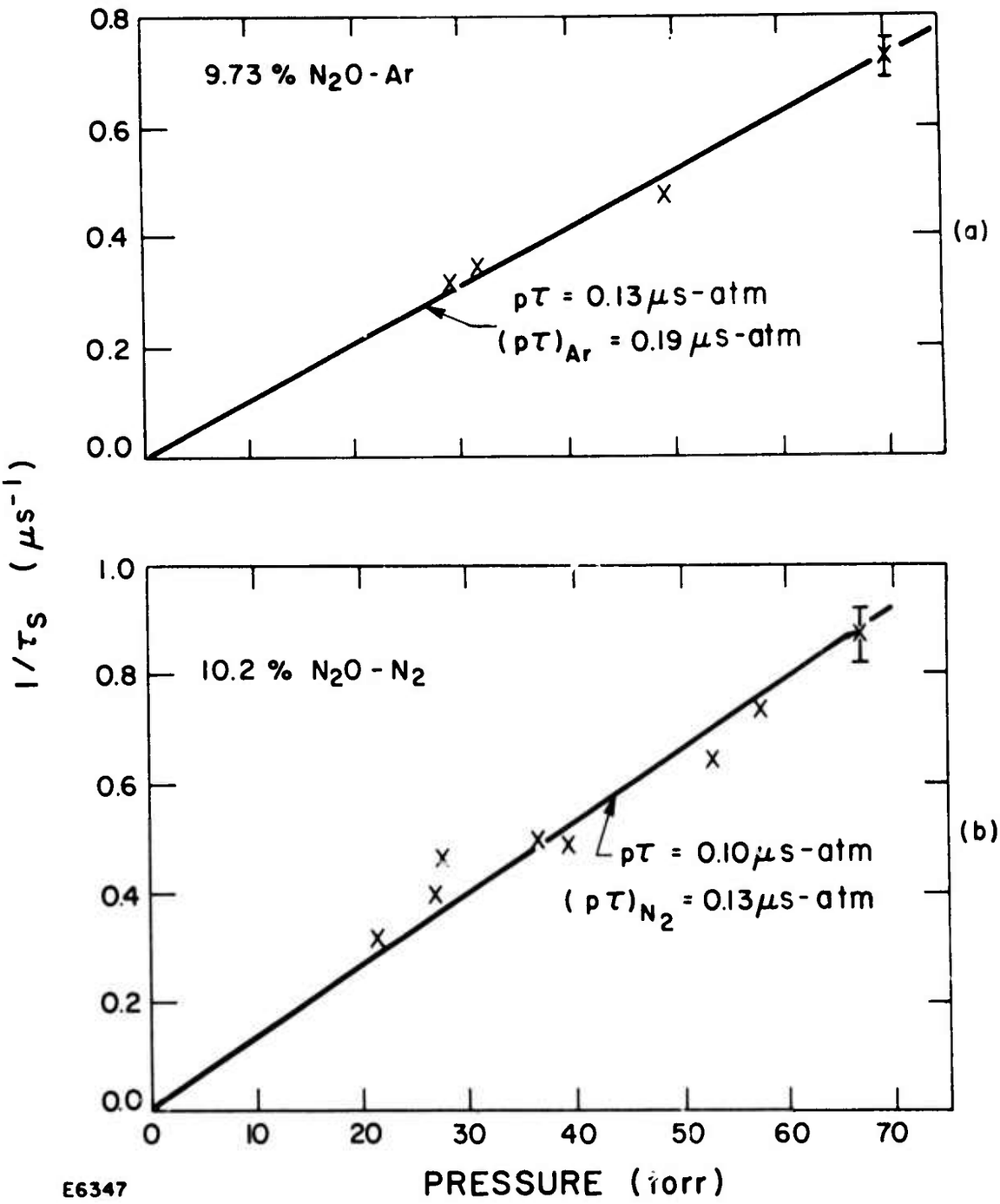

Fig. 17 (a) Short Time Constant (V-V) Measurements of 9.73 Percent N_2O in Ar Mixture. Plot of $1/\tau_s$ vs Pressure

(b) Short Time Constant (V-V) Measurements of 10.2 Percent N_2O in N_2 Mixture. Plot of $1/\tau_s$ vs Pressure

TABLE VIII

Ar AND N_2 V-T RELAXATION RESULTS

p (Torr)	ψ_{N_2O}	$p\tau$ (μs-atm)	τ_{Ar} (μs-atm)	p (Torr)	ψ_{N_2O}	$p\tau$ (μs-atm)	τ_{N_2}
100	0.097	3.68	6.90	98.0	0.102	0.91	0.94
60	0.082	3.96	6.62	68.5	0.102	0.97	1.01
100	0.050	4.72	6.63	45.7	0.20	0.91	0.97
				89.9	0.20	0.91	0.97
	Average		6.72 ± 3%				0.97 ± 3%

b. N_2O-H_2O Mixtures

The V-V time constant τ_s of N_2O-H_2O collisions was measured at ~10 Torr N_2O pressure and various mole fractions of H_2O. The results are plotted as $1/\tau$ vs ψ_{H_2O} in Fig. 18(a). A straight line was drawn through the data and made to pass through the previously measured value for pure N_2O at $\psi_{H_2O} = 0$. A similar plot for the long time constant is displayed in Fig. 18(b). The slopes yield $(1/\tau_{H_2O} - 1/\tau_{N_2O})$'s, from which τ_{H_2O}'s of 1.5×10^{-3} and 5.2×10^{-3} μs-atm are obtained, respectively, for the short and long-time constants. The large scatter, especially in the short time constant results, was due mainly to S/N and time resolution limitations. This is evident in the fluorescence scan shown in Fig. 19.

c. N_2O-NO Mixtures

The results of the effect of NO on the N_2O long time constant fluorescence are shown in Fig. 20. The measured time constant is 0.031 μs-atm.

It was shown in Section IV.A that the measured relaxation times can be related to those of the lowest levels through the relationships

$$\tau_{12} = 2\tau_s \tag{50}$$

$$\tau_{VT2} = 2\tau_\ell \frac{C_2}{C_1 + C_2} \tag{51}$$

where C_i is the specific heat capacity of mode i. The ratio $C_2/(C_1+C_2)$ was shown to be $\sim 0.9^{+0.03}_{-0.09}$. Equations (50) and (51) hold under the condition that the $100 \rightarrow 00^0 1$ transition is optically thick through a cold gas layer. The estimated optical depth is $\gtrsim 10$ as calculated from the band strength values of McClatchey et al.[8]

The results of the present investigation along with other related works are listed in Table IX. The errors quoted in Table IX result from (a) uncertainty of pure N_2O measurements propagated through Eq. (61) (V-V, $< \pm 10\%$; V-T, ~0); (b) errors from individual measurements (H_2O V-V, $< \pm 40\%$; N_2 and Ar V-V, $< \pm 20\%$; H_2O V-T $< \pm 15\%$; N_2 and Ar V-T $< \pm 5\%$); (c) uncertainty in the estimate of the specific heat ratio (V-T ~ $\pm 10\%$).

4. Discussion

No other measurement of the N_2O $\nu_1 \rightarrow \nu_2$ relaxation by foreign gases is available for comparison. The V-T relaxation of the ν_2 mode

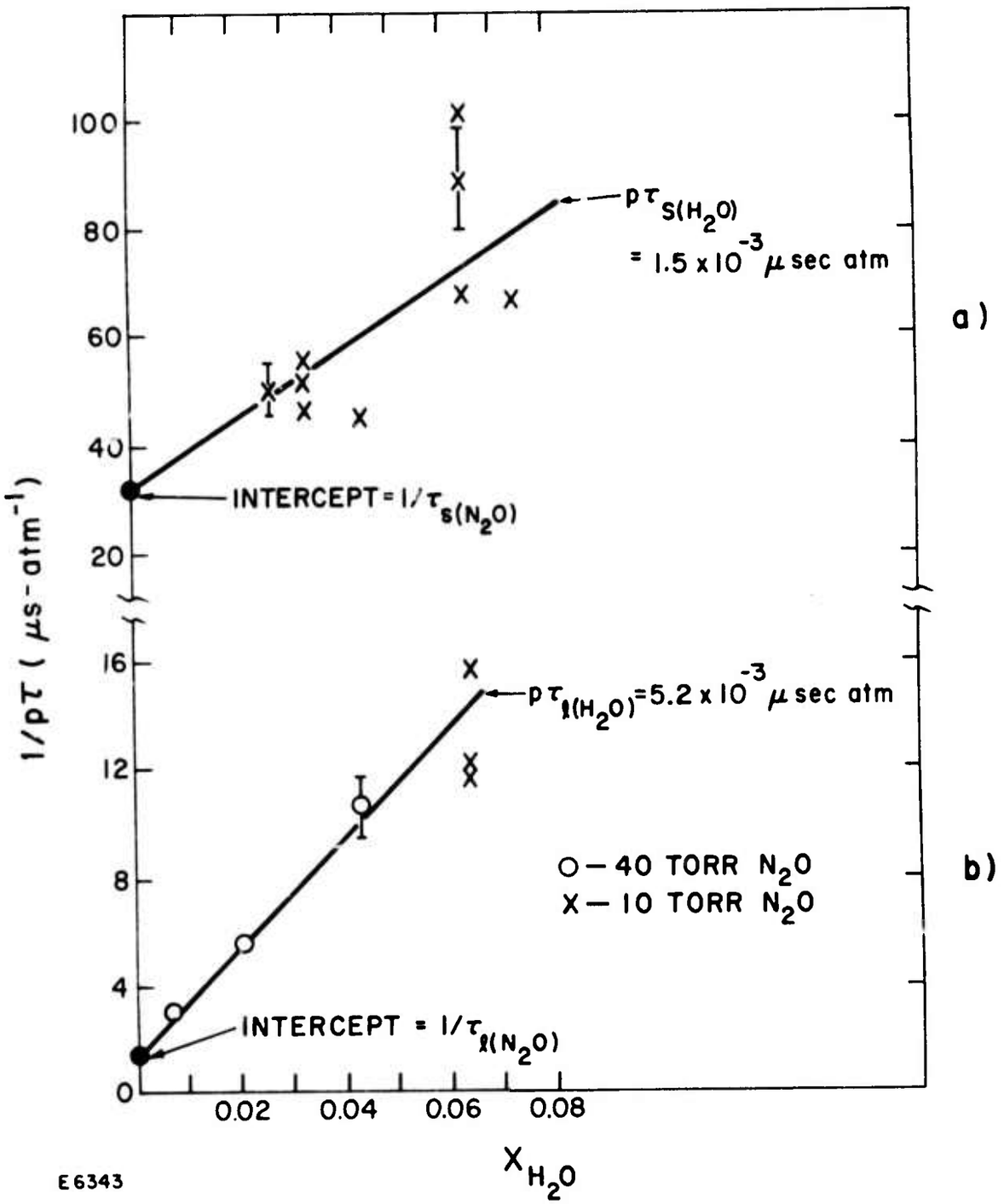

Fig. 18 (a) Short Time Constant (V-V) Measurements of N_2O - H_2O Mixtures. Plot of $1/p\tau_s$ vs Mole Fractions of H_2O (X_{H_2O})

(b) Long Time Constant (V-T) Measurements of N_2O - H_2O Mixtures. Plot of $1/p\tau_\ell$ vs (X_{H_2O})

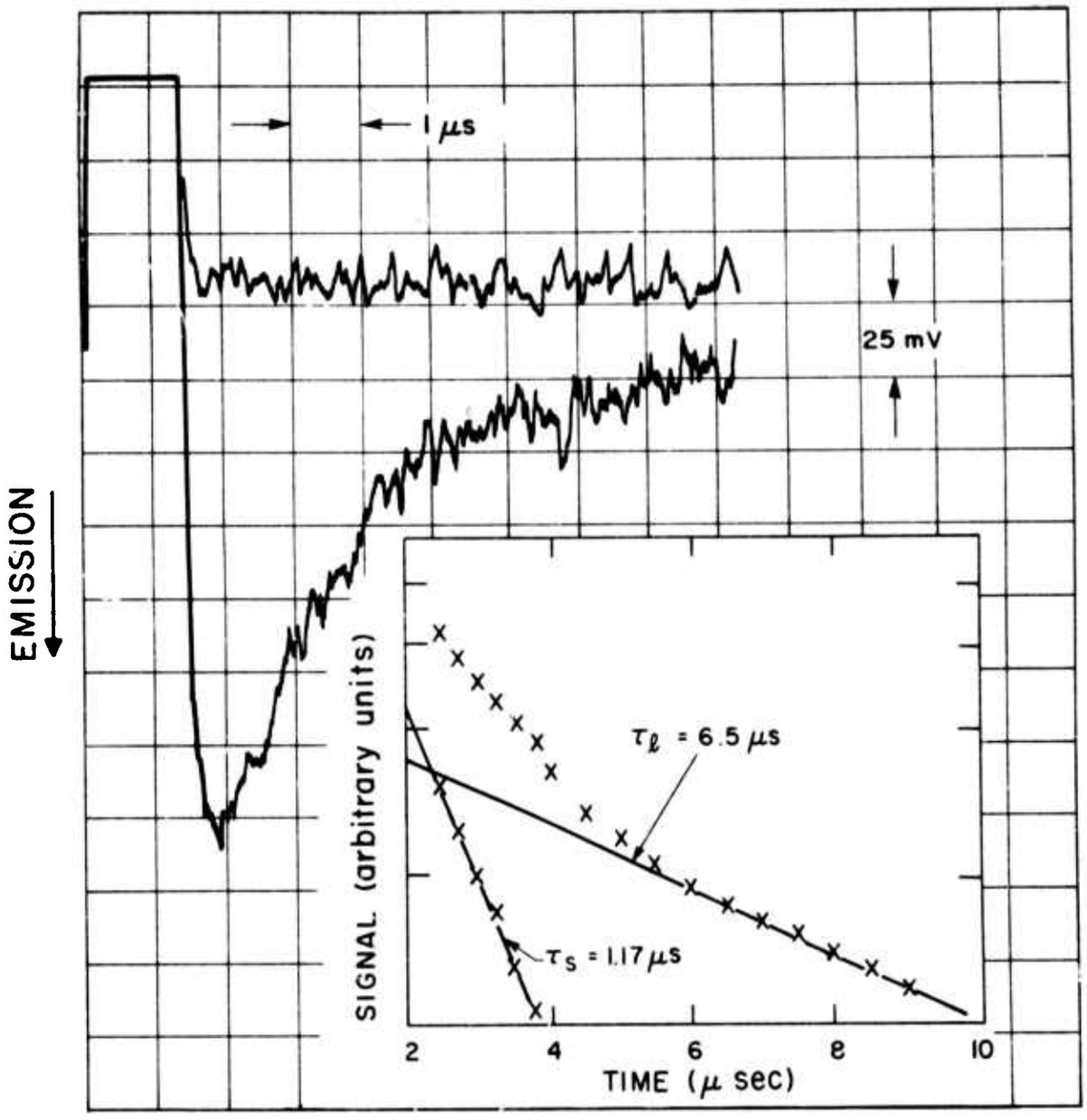

E6350

Fig. 19 Fluorescence Scan at 7.8 μm for a N_2O - H_2O Mixture.

$N_2O + H_2O = 9.6$ Torr

$H_2O = 0.61$ Torr

Scan = 20 min

Aperture = 0.36 μs

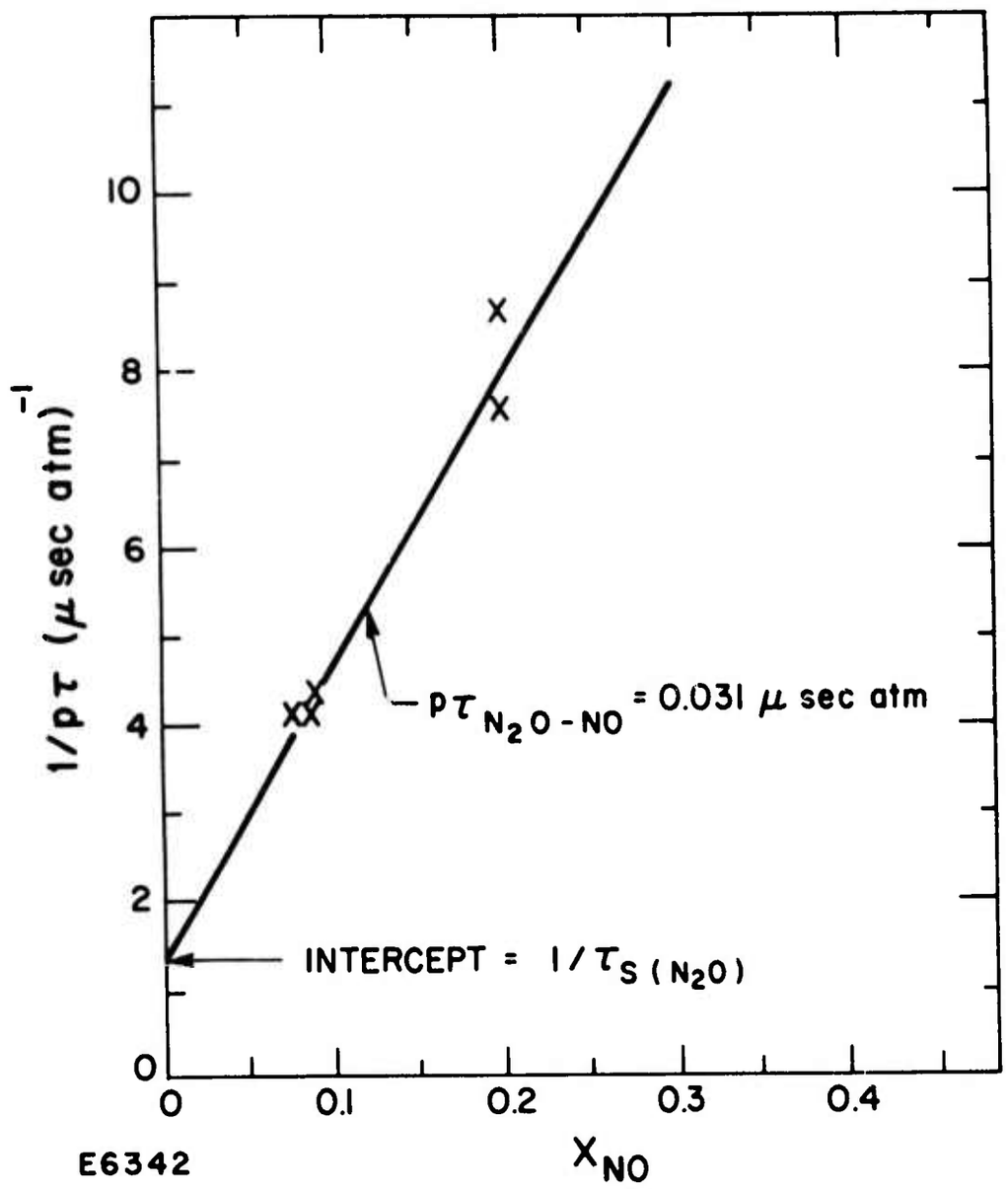

Fig. 20 Plot of $1/p\tau$ vs Mole Fraction of No in Mixtures of N_2O-NO

TABLE IX

EXPERIMENTAL RESULTS

Process	Collision Partner	τ (μ s-atm)	P[a]	τ_{lit}
$\nu_1 \rightarrow \nu_2$	N_2O	0.062 ± 20%	1/280	---
	Ar	0.38 ± 30%	1/1800	---
	N_2	0.26 ± 30%	1/1200	---
	H_2O	3.0×10^{-3} ± 50%	1/15	---
$\nu_2 \rightarrow T$	N_2O	1.3 ± 10%	1/5900	1.2(b)
	Ar	12.1 ± 15%	$1/5.4 \times 10^4$	6.0 (b)
	N_2	1.75 ± 15%	1/7900	1.5(b)
$\nu_2 \rightarrow T$	H_2O	9.4×10^{-3} ± 25%	1/47	---
	NO	0.062		

(a) P is the collision probability calculated from measured τ's and the collision diameters of Hirschfelder, Curtis and Bird.[52]
(b) Ref. (53).

has been measured by Heutz, et al.,[55] using the impact tube method. Their results on N_2O and N_2 agree very well with the results of this work. Their Ar rate constant is a factor of two larger than that measured here. There is no obvious reason for this discrepancy.

The comparable efficiency of Ar and N_2 in quenching the N_2O ν_1-mode is in direct contrast to the quenching of the ν_3-mode. Yardley[27] found N_2 to be a factor of 60 more efficient than Ar in relaxing the N_2O (00^01) level. This was attributed to the near resonant V-V exchange ($\Delta E \sim 100\ cm^{-1}$) between $N_2O(00^01)$ and N_2 vibration. Long-range dipole-quadruple forces were suggested as the dominant interaction in the latter system. The results on N_2O ν_1 relaxation suggests that the quenching rate is not strongly dependent on the inert collision partner in the presence of strong Fermi resonance interaction between the $\nu_1 \sim \nu_2$ modes. The apparent resonance between N_2O (12^00) and $N_2(1)$ ($\Delta E \sim 131\ cm^{-1}$) and $N_2O(04^00)$ and $N_2(1)$($\Delta E \sim 10\ cm^{-1}$) do not seem to enhance the N_2 quenching rate on N_2O. Although the populations of the $(12^{\ell}0)$ and $(04^{\ell}0)$ levels in the present experiment are probably too small to realize the effects of these V-V coupling channels, the multi-quantum change involved in these processes undoubtedly would yield very small transition probabilities.

The factor of ~5 faster V-V exchange between N_2O-N_2O as compared to N_2O-N_2(Ar) collisions can be attributed to the available vibrational energy exchanges between colliding pairs not available to the N_2O-N_2(Ar) pairs.

H_2O is an extremely efficient relaxer of both the V-V and V-T processes as indicated by the measured rate constants. Since CO_2 and N_2O are very similar, a comparison of their relaxation rate is illuminating. The quenching of CO_2 (ν_2) by H_2O requires about 20 collisions.[69] Widom and Bauer[70] suggest that this rapid relaxation may be due to the chemcial interaction between H_2O and CO_2 through the carbonic acid molecule H_2CO_3. Sharma[71] suggests that multipolar interaction is responsible for the rapid quenching rate of $CO_2(\nu_2)$ by H_2O. Both theories yield reasonable agreement with experimental results.[71] However, the latter explanation suggests that the $N_2O(\nu_2)$-H_2O quenching rate should be comparable to that of $CO_2(\nu_2)$-H_2O, while the former suggestion would predict a large difference in the relaxation rate, since no known chemical complex of H_2O-N_2O exists. The results of the present work tend to support Sharma's theory.

The N_2O-NO relaxation rate constant was measured in order to shed some light on the effect of NO present as an impurity in the N_2O gas. A close examination of the fluorescence scans of a mixture of N_2O-NO indicated that in the pure N_2O long time constant relaxation region, two time constants appeared by the addition of NO; a short time constant (as plotted in Fig. 20) and a long time constant characteristic of the pure N_2O V-T relaxation time. This implies that the observed N_2O-NO relaxation time is not a V-T process. A perusal of the energy levels of N_2O and NO immediately suggests that the observed quenching rate may be a result of the V-V coupling process.

$$N_2O(11^10) + NO \xrightarrow{\tau_c} N_2O(000) + NO(1)\ \Delta E = 4\ cm^{-1}. \qquad (62)$$

Since $N_2O(11^10)$ is present only after the equilibration of the $\nu_1 - \nu_2$ mode, process (62), initially competes with process (60), followed by the V-T relaxation of the whole vibrational manifold through the latter process. The rate constant of process (62) cannot be simply related to the measured value of Fig. 20 because the $N_2O(11^10)$ level was not directly monitored. Since the fluorescence is from the $20^00 \rightarrow 10^00$ transition, the drain on the (11^10) level through process (62) is reflected through the reshuffling of energy in the ν_1-ν_2 mode. For $1/\tau_c > 1/\tau_{12}$ (where τ_{12} is the V-V quenching time constant of pure N_2O), the measured quenching rate constant due to the drain of process (62) is just $1/\tau_{12}$. If the agreement between the measured relaxation time constant in N_2O-NO mixtures and τ_{12} is not fortuitous, the above interpretation suggests that $\tau_c < 6 \times 10^{-2}$ μs-atm. This time constant cannot be directly measured in the present system.

The presence of a small impurity level of NO in the N_2O gas would cause a small perturbation of the V-T relaxation time of N_2O. For a possible maximum NO impurity level of 0.5 percent at most a 10 percent change results in the measured V-T relaxation times. The effect of NO on the V-V quenching of N_2O was not measured and is not expected to influence the measured V-V rates.

According to Section IV. A, the V-V relaxation process can be interpreted as either

$$10^00 + M \rightarrow 02^\ell0 + M$$

$$\text{or} \quad 10^00 + M \rightarrow 01^10 + M\ .$$

In the atmosphere, the DF laser excited N_2O (200) molecules would not be equilibrated within the ν_1 mode due to the extremely low N_2O concentration. Under this condition, the dominant quenching out of the (200) level would be the processes

$$(20^0) + M \rightarrow (12^\ell0) + M$$

$$\rightarrow (11^10) + M$$

It was not possible to measure these rates directly in this experiment, since the increased signal due to foreign gas broadening is offset by the reasonably large V-V quenching rates of the respective foreign gases. The rate constant for these processes can be evaluated through the Landau-Teller probability relationships[44]

$$P_{\ell \to \ell + 2}^{\lambda \to \lambda - 1} = (\ell + 2)(\ell + 1)\, \lambda\, P_{0 \to 2}^{1 \to 0} ;$$

(44)

$$P_{\ell \to \ell + 1}^{\lambda \to \lambda - 1} = (\ell + 1)\, \lambda\, P_{1 \to 0}^{0 \to 1}$$

and the values measured in this work.

V. RESULTS

In order to properly assess the thermal response of the atmosphere to high-power CO and DF laser pulses, it is necessary to survey wide variations in atmospheric properties, especially humidity, and laser parameters. The situation is particularly complicated in the case of DF, since the various laser lines are absorbed by different species and produce a different response in the atmosphere. Consequently, a complete survey would generate an enormous amount of data which would be difficult, at best, for the reader to absorb. For this reason, as well as limitations in time and money, the calculations have been limited to a few representative atmospheric models. In addition, the most important features of the atmospheric response have been parameterized in a well-defined fashion so that these parameters can be simply summarized rather compactly in tables. These ideas are discussed in the following paragraphs, and the results are presented at the end of this section.

The properties of the atmosphere have been widely studied. On the basis of the available data, five model atmospheres have been proposed corresponding to tropical, mid-latitude summer, mid-latitude winter, sub-arctic summer and sub-arctic winter conditions. The properties of these model atmospheres are summarized as a function of altitude by McClatchy, et al.[8] Most of the species of importance for infrared laser propagation are uniformly distributed throughout the atmosphere in the concentrations listed in Table X. The concentration of water vapor, however, varies widely. To represent the variations expected at sea level, calcuations have been performed for the two model atmospheres summarized in Table XI. The high humidity case corresponds to tropical conditions (approximately 80 % relative humidity). The low humidity case corresponds to "desert conditions" (about 8 % relative humidity). The contributions of the various species to the equilibrium absorption coefficients at a number of CO and DF laser wavelengths are summarized in Table XII for these two atmospheric conditions.

The thermal response of the atmosphere to a typical laser pulse is shown in Fig. 21 where the temperature rise ΔT is plotted as a function of the time t. The laser pulse in this case is switched on at $t = 0$ and remains constant thereafter. At early times, the heating rate goes through an unsteady period while the vibrational degrees of freedom of the molecules relax to a steady state with the laser radiation. During the unsteady period, the temperature rise is a fairly complicated function of the time and may even be negative as in the case of CO_2. At the end of the unsteady period, the rate of temperature rise asymptotically approaches a steady value $(dT/dt)_s$. The duration of the unsteady period will be referred to as the relaxation time, τ_R, defined as shown in Fig. 21. Both τ_R and $(dT/dt)_s$ depend

TABLE X

COMPOSITION OF THE ATMOSPHERE

Species	Concentration (Mole Fraction)
N_2	7.9×10^{-1}
O_2	2.1×10^{-1}
CO_2	3.3×10^{-4}
N_2O	2.8×10^{-7}
CO	7.5×10^{-8}
CH_4	1.6×10^{-6}
H_2O	Variable

TABLE XI

MODEL ATMOSPHERES

	Temperature (^oK)	Pressure (b)	Water Vapor (Mole Fraction)
High Humidity	300	1.013	2.6×10^{-2}
Low Humidity	300	1.013	2.6×10^{-3}

TABLE XII (A)

COEFFICIENTS FOR THE ABSORPTION OF DF LASER RADIATION BY ATMOSPHERIC SPECIES AT SEA LEVEL - HIGH HUMIDITY CASE (20 TORR WATER VAPOR)

Laser Transition	a (N_2) (%/km)	a (N_2O) (%/km)	a (CH_4) (%/km)	a (CO_2) (%/km)	a (H_2O) (%/km)	a (HDO) (%/km)	a (Total) (%/km)
2P(8)	0.12	-	0.08	-	0.44	0.98*	1.6
2P(9)	0.18	0.03	0.006	-	0.007	2.9*	3.1
2P(10)	0.28	2.0*	-	-	0.009	0.35	2.6
2P(11)	0.51	0.70*	-	-	0.0005	0.072	1.3
3P(8)	0.60	2.0*	0.10	-	0.005	0.11	2.8
3P(9)	1.0*	0.03	-	0.26	0.005	0.023	1.3
3P(10)	2.0*	0.02	-	0.54	0.60	0.006	3.2
3P(11)	3.0*	0.29	-	1.2	0.72	0.13	5.4

*Strongest Absorber

TABLE XII (B)

COEFFICIENTS FOR THE ABSORPTION OF DF LASER RADIATION BY ATMOSPHERIC SPECIES AT SEA LEVEL - LOW HUMIDITY CASE (2 TORR WATER VAPOR)							
Laser Transition	a (N_2) (%/km)	(a N_2O) (%/km)	a (CH_4) (%/km)	a (CO_2) (%/km)	a (H_2O) (%/km)	a (HDO) (%/km)	a (Total) (%/km)
2P(8)	0.02*	-	0.08	-	0.04	0.098	0.34
2P(9)	0.18	0.03	0.006	-	0.0007	0.29*	0.51
2P(10)	0.28	2.0*	-	-	0.00009	0.04	2.3
2P(11)	0.51	0.70*	-	-	0.00005	0.007	1.2
3P(8)	0.60	2.0*	0.10	-	0.0005	0.01	2.7
3P(9)	1.0*	0.03	-	0.26	0.0005	0.002	1.3
3P(10)	2.0*	0.02	-	0.54	0.06	0.0006	2.6
3P(11)	3.0*	0.29	-	1.2	0.07	0.01	4.6

*Strongest Absorber

TABLE XII (C)

COEFFICIENTS FOR THE ABSORPTION OF CO LASER RADIATION BY ATMOSPHERIC WATER VAPOR AT SEA LEVEL FOR HIGH HUMIDITY (20 TORR WATER VAPOR) AND LOW HUMIDITY (2 TORR WATER VAPOR) CASES

Laser Transition	High Humidity α (km^{-1})	Low Humidity α (km^{-1})
2P(8)	0.31	0.031
2P(9)	0.28	0.028
2P(15)	0.34	0.034
3P(10)	0.60	0.060
3P(15)	0.47	0.047
3P(16)	1.60	0.160
4P(8)	0.47	0.047
4P(9)	0.48	0.048
4P(15)	0.73	0.073
5P(9)	0.87	0.087
6P(9)	1.00	0.100
6P(10)	1.13	0.113

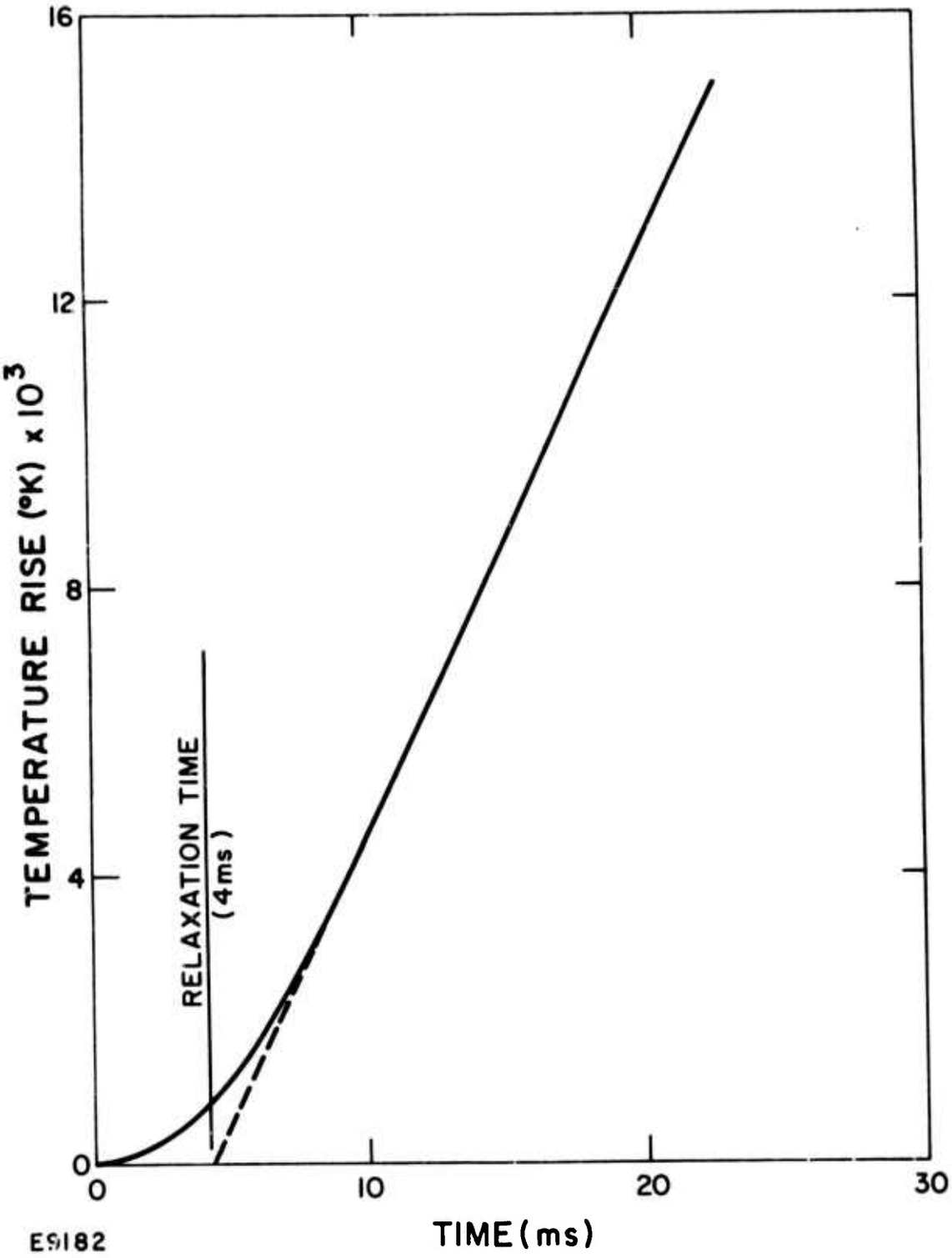

Fig. 21 Thermal Response of the Atmosphere to DF Laser Radiation ($10^5 W/cm^2$ on the 3 P(9) Transition) under Sea Level, Low Humidity Conditions

upon the laser flux I. Some typical results for the dependence of the heating rate on the laser intensity are shown in Fig. 22. At low values of the laser intensity, vibrational degrees of freedom are not perturbed too far from equilibrium. The heating rate is therefore given by the expression

$$\left(\frac{dT}{dt}\right)_s = \frac{I\bar{a}}{\rho c_p}, \tag{63}$$

where $\bar{a}$ is the equilibrium absorption coefficient, ρ is the density and c_p is the specific heat of the gas. At sufficiently high laser intensities, however, the absorber becomes bleached. Under these conditions, the rate of absorption is controlled not by the laser intensity, but by the rate at which the absorbing species can relax. Thus the heating of the laser intensity. The bleaching intensity I_B at which these effects become important is defined as shown in Fig. 22.

To indicate the importance of thermal heating on laser propagation through the atmosphere, it is useful to introduce two further parameters. For laser intensities below the bleaching flux I_B, the important parameter is E_p, the total laser pulse energy per unit area at which thermal distortion effects become important. For high laser intensities in excess of I_B, the important parameter is Δt_p, the pulse length at which thermal distortion effects become important. In general, thermal distortion becomes important when the phase shift in the laser wavefront is of the order of unity, that is when the change in the optical path length is of the order of $\lambda/2\pi$. Mathematically, this is expressed by the formula

$$2\pi \int_0^L (n - 1) \frac{\Delta T}{T} dx = O(\lambda), \tag{64}$$

where x is the distance along the ray, n is the local index of refraction of the atmosphere and L is the distance to the target. If we assume uniform conditions between the source and the target, the threshold temperature rise at which optical distortion becomes important is given by the expression

$$\Delta T = \frac{\lambda}{2\pi L} \frac{T}{n - 1} = \frac{E\,(\text{absorbed})}{\rho c_p}, \tag{65}$$

where E (absorbed) is the laser energy absorbed per unit volume, ρ is the atmospheric density and c_p is the specific heat. At low laser intensities below the threshold for bleaching, the absorbed laser energy is given by the expression

$$E\,(\text{absorbed}) = \bar{a}\, I\, \Delta t = \bar{a}\, E\,(\text{laser}), \tag{66}$$

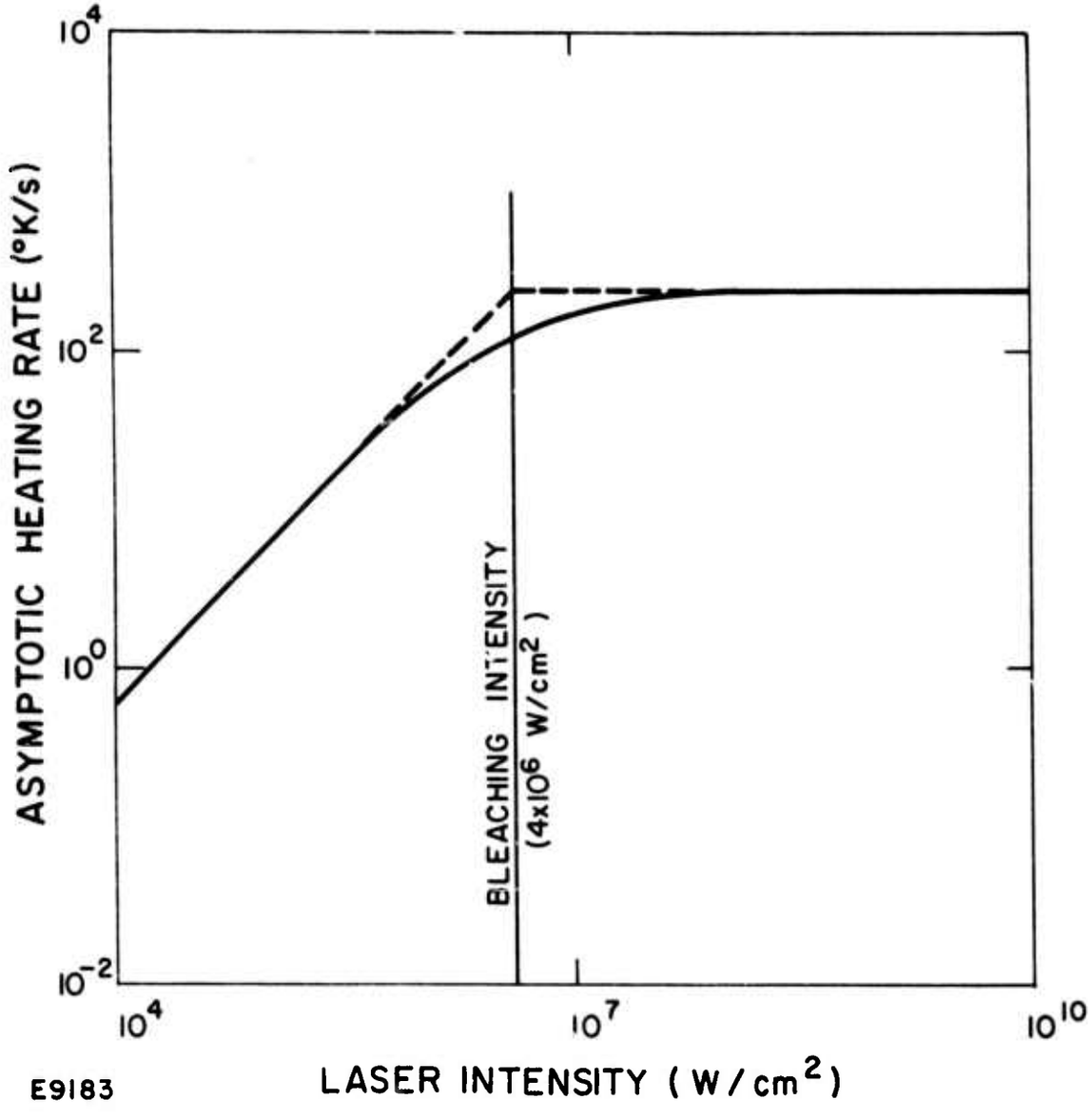

Fig. 22 Asymptotic Heating Rate due to the Absorption of DF 2P(11) Laser Radiation by Air at Sea Level, Low Humidity

where $\bar{a}$ is the equilibrium absorption coefficient and E (laser) is the laser pulse energy per unit area. The laser pulse energy per unit area at which distortion effects become important is therefore given by the expression

$$E_P = \frac{\rho c_p}{n-1} \frac{\lambda T}{2\pi \bar{a} L}. \tag{67}$$

In commonly used units, this expression becomes

$$E_P \ (J/cm^2) = 9 \times 10^{-5} \frac{\lambda \ (\mu m) \ T \ (^oK)}{\bar{a} L}. \tag{69}$$

For high laser intensities above the bleaching intensity I_B, the absorbed energy is given by the expression

$$E \ (absorbed) = \bar{a} I_B \Delta t. \tag{68}$$

The laser pulse duration at which distortion effects become important is therefore given by the expression

$$\Delta t_P = \frac{\rho c_p}{n-1} \frac{\lambda T}{2\pi I_B \bar{a} L} \tag{69}$$

In commonly used units this corresponds to the expression

$$\Delta t_P \ (\mu s) = 9 \times 10^{-5} \frac{\lambda \ (\mu m) \ T \ (^oK)}{I_b \ (MW/cm^2) \ \bar{a} L} \tag{69}$$

Calculated values of the relaxation time τ_R, bleaching flux I_B, threshold pulse energy E_P and threshold pulse length Δt_P for DF and CO lasers are presented in Table XIII. The relaxation time τ_R has been computed only for the low-intensity case. At high intensities, however, the relaxation time should be comparable, since it is principally a function of the molecular relaxation times. In some cases, where the relaxation time was very short, it was difficult to extract the relaxation time from the computed temperature time histories due to truncation and round-off errors in the computer results. A better way to establish these relaxation times would be to linearize the vibrational relaxation equations and solve them analytically in terms of the eigenvalues and eigenfunctions of the set of relaxation equations. For the present, it was not necessary to do this, since such short relaxation times are not of practical interest.

TABLE XIII (A)

PARAMETERS DESCRIBING THE KINETICS OF ABSORPTION OF DF LASER RADIATION BY THE ATMOSPHERE AT SEA LEVEL-HIGH HUMIDITY CASE

Laser Transition	Threshold Energy E_p (J/cm^2)	Relaxation Time* τ_R (μs)	Bleaching Intensity I_B (MW/cm^2)	Threshold Pulse Length Δt_p (μs)
2P(8)	7	< 1	> 10^3	-
2P(9)	3	< 1	> 10^3	-
2P(10)	4	< 1	> 10^3	-
2P(11)	8	< 1	30	< 1
3P(8)	4	< 1	100	< 1
3P(9)	8	400	> 10^3	-
3P(10)	3	400	> 10^3	-
3P(11)	2	400	> 10^3	-

*Strongest Absorber

TABLE XIII (B)

PARAMETERS DESCRIBING THE KINETICS OF ABSORPTION OF DF LASER RADIATION BY THE ATMOSPHERE AT SEA LEVEL-LOW HUMIDITY CASE

Laser Transition	Threshold Energy E_p (J/cm^2)	Relaxation Time* τ_R (μs)	Bleaching Intensity I_B (MW/cm^2)	Threshold Pulse Length Δt_p (μs)
1P(8)	30	4000	$> 10^3$	-
2P(9)	20	50	300	< 1
2P(10)	5	1	20	< 1
2P(11)	9	1	4	2
3P(8)	4	1	4	1
3P(9)	8	4000	$> 10^3$	-
3P(10)	4	4000	$> 10^3$	-
3P(11)	2	4000	$> 10^3$	-

*Strongest Absorber

TABLE XIII (C)

PARAMETERS DESCRIBING THE KINETICS OF ABSORPTION OF CO LASER RADIATION BY THE ATMOSPHERE AT SEA LEVEL-HIGH HUMIDITY CASE

Laser Transition	Threshold Energy E_p (J/cm^2)	Relaxation Time τ_R (μs)	Bleaching Intensity I_B (MW/cm^2)	Threshold Pulse Length Δt_p (μs)
2P(8)	0.4	< 1	> 10^3	-
2P(9)	0.5	< 1	> 10^3	-
2P(15)	0.4	< 1	> 10^3	-
3P(10)	0.2	< 1	> 10^3	-
3P(15)	0.3	< 1	> 10^3	-
3P(16)	0.1	< 1	> 10^3	-
4P(8)	0.3	< 1	> 10^3	-
4P(9)	0.3	< 1	> 10^3	-
4P(15)	0.2	< 1	> 10^3	-
5P(9)	0.2	< 1	> 10^3	-
6P(9)	0.1	< 1	> 10^3	-
6P(10)	0.1	< 1	> 10^3	-

TABLE XIII (D)

PARAMETERS DESCRIBING THE KINETICS OF ABSORPTION OF CO LASER RADIATION BY THE ATMOSPHERE AT SEA LEVEL-LOW HUMIDITY CASE

Laser Transition	Threshold Energy E_p (J/cm^2)	Relaxation Time τ_R (μs)	Bleaching Intensity I_B (MW/cm^2)	Threshold Pulse Length Δt_p (μs)
2P(8)	4	4	$> 10^3$	-
2P(9)	5	4	$> 10^3$	-
2P(15)	4	4	$> 10^3$	-
3P(10)	2	4	$> 10^3$	-
3P(15)	3	4	$> 10^3$	-
3P(16)	1	4	$> 10^3$	-
4P(8)	3	4	$> 10^3$	-
4P(9)	3	4	$> 10^3$	-
4P(15)	2	4	$> 10^3$	-
5P(9)	2	4	$> 10^3$	-
6P(9)	1	4	$> 10^3$	-
6P(10)	1	4	$> 10^3$	-

VI. SUMMARY

The DF chemical laser at 3.9 μm operates in a good atmospheric window, i.e., there are no major atmospheric absorbers at this wavelength. The absorption of DF radiation by the atmosphere is dominated by a number of small weak absorbers. The situation is complicated by the fact that different laser lines are absorbed by different absorbers. For purposes of the present calculations, the eight strongest lines of a pulsed DF laser were chosen. The strongest lines of a CW laser may be different, but the absorption will be due to the same group of molecules. The kinetics of CO laser absorption are simpler since there is only one important absorber, namely water vapor. Twelve laser lines from the vibrational levels 2 to 6 were chosen. These are characteristic of larger, high-gain lasers and propagate better than the longer wavelength transitions originating from higher vibrational levels in smaller, lower-gain CO lasers and are therefore of more interest for high-power applications. The principal absorbers for DF radiation include N_2 (collision-induced fundamental), N_2O (combination and overtone bands), CO_2 (ν_3 fundamental band), CH_4 (overtone and combination bands), H_2O and HDO. The magnitude of the absorption by the latter two species as well as the precise vibrational assignments of the absorbing transitions, is a matter of some controversy in the literature. Since these species provide the largest amount of absorption for some DF lines, this uncertainty probably represents the greatest uncertainty in the results.

Both the vibrational and rotational kinetics of these absorbers have been studied. The effects of kinetics manifest themselves in the form of transients in the heating rate at the beginning of the laser pulse and in the form of bleaching at high laser fluxes. Rotational relaxation is, of course, much too fast to give rise to transients of interest for high-power lasers. Bleaching was studied in more detail. The results show that although rotational bleaching may be important for some lasers, it is not important for CO or DF lasers at intensities below about 10^9 W/cm^2. The vibrational relaxation of the absorbing species has been studied in considerable detail using a computer model. Most of the important vibrational relaxation rates were known from experiments described in the open literature. The most important unknown rates were those for the relaxation of N_2O by water. These were measured under the current program using a DF laser fluorescence technique. Two important assumptions were made in constructing the model. In the first place, certain near-resonant vibrational levels in N_2O, CO_2, H_2O and CH_4 are assumed to be in equilibrium. Evidence accumulated at AERL indicates that this assumption is good in N_2O and H_2O. There is no evidence that it is not equally valid for the other species. The second important assumption in the model involves the neglect of absorption by vibrationally excited molecules. When the absorbing species is bleached, the number of molecules in the

vibrationally excited level is equal to the number of molecules in the ground state. Consequently, if the vibrationally excited molecules have absorbing transitions to higher levels, this must be added to the total absorption of the gas. Unfortunately, nothing is known about absorption transitions originating from the excited vibrational levels, and it was necessary to make this assumption even though it is probably in error. The effect of absorption from higher levels will be to raise the intensity at which the gas bleaches. Since most of the transitions bleach at intensities beyond those of interest, the error is of no consequence. For those transitions which bleach at intensities of interest, the bleaching intensities quoted must be regarded as lower bounds.

Numerical calculations have been carried out for two model atmospheres corresponding to sea level, high humidity and sea level, low humidity. The results for CO indicate that the relaxation time during which transient non-steady heating occurs is generally less than 1 μs and therefore of no practical interest. The laser flux at which bleaching occurs is generally found to be greater than 10^9 W/cm^2 and therefore, again, of no practical interest. For DF, however, the kinetics of absorption may be significant. Certain of the lines, specifically those for which the N_2 collision-induced continuum is the strongest absorber, show relaxation times of the order of milliseconds under conditions of low humidity. During this time, the heating rate is less than the equilibrium heating rate since the absorbed energy is being stored in nitrogen vibrations. No kinetic cooling is predicted. For other lines, notably those for which N_2O is the principal absorber, bleaching fluxes as low as 4 MW/cm^2 are predicted. However, as noted above, this prediction really represents a lower bound on the bleaching intensity. It will be necessary to do further experiments to determine the true bleaching intensity.

REFERENCES

1. Wood, A. D., Camac, M., and Gerry, E. T., Appl. Opt. 10, 1877 (1971).

2. Hayes, J. N., Ulrich, P. B., and Aitkin, A. H., Appl. Opt. 11, 257 (1972).

3. Gebhardt, F. G. and Smith, D. C., Appl. Phys. Letters 128, 20 (1972).

4. Deutsch, T. F., Appl. Phys. Letters 10, 8, 234 (15 April 1967).

5. Basov, N. G., et al., Appl. Optics 10, 8, 1814 (August 1971).

6. Spencer, D. J., et al., "Atmospheric Gas Absorption at DF Laser Wavelengths," Paper presented at "Absorption of Infrared Laser Radiation in the Atmosphere" Meeting, MITRE Corporation (April 1973).

7. McClatchey, R. A., et al., "Atmospheric of HF and DF Laser Radiation," Air Force Cambridge Research Laboratories Report AFCRL-72-0312 (23 May 1972).

8. McClatchey, R. A., et al., AFCRL Atmospheric Absorption Lane Parameters Compilation, Air Force Cambridge Research Laboratories, AFCRL-TR-73-0096, (26 January 1973).

9. Winters, B. H., et al., "Line Shape in the Wing Beyond the Band Head of the 4.3μ Band of CO_2," JQSRT 4, 527 (1964).

10. Burch, D. E., Gryvnak, D. A., and Pembrook, J. D., "Investigation of the Absorption of Infrared Radiation by Atmospheric Gases: Water, Nitrogen and Nitrous Oxide," Philco-Ford Corporation, Aeronutronic Division Report U-4897 (January, 1971).

11. Bates, David M., et al., "Line Parameters and Computer Spectra for Water Vapor Bands at 2.7 Microns," National Bureau of Standards Monograph 71, (3 August 1964).

12. Shapiro, M. M. and Gush, H. P., Can. J. Physics 44, 949 (1966).

13. Mantz, A. W., Nichols, E. R., Alpert, B. D. and Rao, K. N., "CO Laser Spectra Studied with a 10-Meter Vacuum Infrared Grating Spectrograph," J. Mol. Spectry 35, 325 (1970).

14. Mantz, A. W., Watson, J. K. G., Rao, K. N. Albritton, D. L., Schmeltekopf, A. L. and Zare, R. N., "Rydberg-Klein-Rees Potential for the $X^1\Sigma^+$ State of the CO Molecule," J. Mol. Spectry 39, 180 (1971).

15. Long, R. K., Mills, F. S. and Trusty, G. L., "Experimental Absorption Coefficients for Eleven CO Laser Lines," Ohio State University Research Foundation Report 3271-3 (March 1973).

16. McClatchey, R. A., AFCRL, private communication.

17. McClatchey, R. A., "Atmospheric Attenuation of CO Laser Radiation," Air Force Cambridge Research Laboratories Report, AFCRL-71-0370 (1 July 1971).

18. Burch, D. E., France, W. L. and Williams, D., "Total Absorptance of Water Vapor in the Near Infrared," Appl. Opt. 2, 585 (1963).

19. Harris, E. L. and Glowacki, W. J., "Absorption of CO Laser Radiation by Water Vapor Near 5 μm," Naval Ordnance Laboratory Technical Report 73-206 (26 November 1973).

20. Carroll, T. O. and Marcus, S., Phys. Letters 27A, 590 (1968).

21. Evans, L. B., "Rotational Relaxation in Polar Gases," Ph. D. Thesis, Oklahoma State University (August 1969).

22. Kley, D. and Welge, K. H., J. Chem. Phys. 49, 2870 (1968).

23. For surveys of vibrational relaxation rates and references to the original papers see: Taylor, R. L. and Bitterman, S., Rev. Mod. Phys. 41, 26, (1969), Moore, C. B., Adv. Chem. Phys. 23, 41 (1973), Lewis, P., et al., "Survey of Vibrational Relaxation Data," Avco Everett Research Laboratory Technical Memorandum (unpublished).

24. Cottrell, T. L., Macfarlane, I. M., Read, A. W. and Young, A. H., Trans. Faraday Soc. 62, 2655 (1966).

25. Cottrell, T. L., Macfarlane, I. M. and Read, A. W., Trans. Faraday Soc. 63, 2093 (1967).

26. Bates, R. D., Flynn, G. W. and Ronn, A. M., J. Chem. Phys. 49, 1432 (1968).

27. Yardley, J. T., J. Chem. Phys. 49, 2816 (1968).

28. The authors are indebted to Moore, C. B., for pointing out this interpretation of Yardley's data.

29. Yardley, J. T. and Moore, C. B., J. Chem. Phys. 45, 1066 (1966).

30. Monkewicz, A. A., J. Acoust. Soc. Am. 42, 258 (1966).

31. Bauer, H. J., J. Acoust. Soc. Am. 44, 285 (1968).

32. Yardley, J. T. and Moore, C. B., J. Chem. Phys. 48, 14 (1968).

33. Yardley, J. T. and Moore, C. B., J. Chem. Phys. 49, 1111 (1968).

34. Evans, L. B. and Winter, T. G., J. Acoust. Soc. Am. 45, 515 (1969).

35. Yardley, J. T., Fertig, M. N. and Moore, C. B., J. Chem. Phys. 52, 1450 (1970).

36. Kung, R. T. V., private communication.

37. Chang, T. Y. and Wood, O. R., Appl. Phys. Lett. 24, 182 (1974).

38. Margottin-Maclou, M., Doyennette, L. and Henry, L., Appl. Optics, 10, 1768 (1971).

39. Doyennette, L., Margottin-Maclou, M., Gueguen, H., Carion, A. and Henry, L., J. Chem. Phys. 60, 697 (1974).

40. Starr, D. F. and Hancock, J. K., J. Chem. Phys. 62, 3747 (1975).

41. Mahan, B. H., J. Chem. Phys., 46, 98 (1967).

42. Levron, M., Palke, W. E. and Millikan, R. C., Int. J. of Chem. Kinetics, 5, 753 (1973).

43. Stephenson, J. C., Wood, R. E. and Moore, C. B., J. Chem. Phys., 48, 4790 (1968).

44. Schwartz, R. N., Slawsky, Z. I. and Herzfeld, K. F., J. Chem. Phys., 20, 1591 (1952).

45. Collins, S. A., Jr., Appl. Optics, 3, 1263 (1964).

46. Model 102 and Model 100, Korad Division of Hadron Corp., Santa Monica, Cal.

47. Taylor, R. L., Can. J. of Chem., 52, 1436 (1974).

48. This is a manufacturer's quoted maximum impurity. No analysis was made on the specific sample used in this experiment. Yardley (Ref. 27) in his experiment analyzed an NO impurity of < 0.2% for the N_2O gas obtained from the same manufacturer.

49. See Section IV. B.

50. Spencer, D. J., Denault, G. C., Takimoto, H. H., Appl. Opt. 13, 2855 (1974).

51. Calculated from bandstrength values given in Ref. 8.

52. Hirschfelder, J. O., Curtis, C. F. and Bird, R. B., Molecular Theory of Gases and Liquids, Wiley, New York, 1964, p. 1111.

53 Huetz, M., Chevalier, P. and Sanson, B., Astronautica Acta, 17, 645 (1972).

54. Cottrell, T. L. and McCourbrey, J. C., Molecular Energy Transfer in Gases, Butterworths, London, 1961, pp. 27-29.

55. Suzuki, I., J. Mol. Spectrosc. 32, 54 (1969).

56. Suzuki, I., J. Mol. Spectrosc. 25, 479 (1968).

57. Bulthius, K. and Ponsen, G. J., Chem. Phys. Lett., 21, 415 (1973).

58. Rhodes, C. K., Kelley, M. J. and Javan, A., J. Chem. Phys. 48, 5730 (1968).

59. Rosser, W. A., Jr., Hoag, E. and Gerry, E. T., J. Chem. Phys., 57, 4153 (1972).

60. Stark, E. E., Jr., Appl. Phys. Letters 23, 335 (1973).

61. Handbook of Geophysics and Space Environments, Air Force Cambridge Research Laboratories, 1965.

62. Weitz, E. and Flynn, G., Annual Review of Phys. Chem. Ed., H. Eyring, C. J. Christensen, and H. S. Jonston, Palo Alto, California, Annual Reviews, Inc., 1974, Vol. 25, pp. 275-315.

63. Kung, R. T. V. and Center, R. E., J. Chem. Phys. 62, 2187 (1975).

64. Parametrics, Inc., Waltham, Mass., 02154.

65. Validyne Engineering Corp., Northridge, Calif. 91324.

66. Ferriso, C. C., Ludwig, C. B. and Thomson, A. L., J. Quan. Spect. Rad. Transfer, 6, 241 (1966).

67. Mass. Oxygen and Equipment Co., Westboro, Mass., 01581.

68. Ref. 54, p. 31.

69. Original references can be found in the review work of R. L. Taylor and S. Bitterman, Modern Phys. 41, 1670 (1953).

70. Widom, B. and Bauer, S.H., J. Chem. Phys. 21, 1670 (1953).

71. Sharma, R.D., J. Chem. Phys. 54, 810 (1971).

APPENDIX A

PARTITION FUNCTIONS

1. N_2C "States"

Referred to the elemental chemical species, the partition function (Q) for a molecule in vibrational level $(v_1 v_2 \ell v_3)$ is given by the expression

$$Q_{v_1 v_2 \ell v_3} = \exp(-\Delta H_F^{\circ}/kT) Q^{(T)} Q^{(VR)}_{v_1 v_2 \ell v_3}, \qquad \text{(A-1)}$$

where ΔH_F° is the heat of formation of $0^{\circ}K$, k is Boltzmann's constant and T is the temperature. The transitional partition function $[Q^{(T)}]$ is given by the expression

$$Q^{(T)} = (2\pi mkT/h^2)^{3/2}, \qquad \text{(A-2)}$$

where m is the molecular mass and h is Planck's constant. According to the classical rigid rotor approximation, the vibration-rotation partition function $[Q^{(VR)}]$ may be expressed

$$Q^{(VR)}_{v_1 v_2 \ell v_3} = g_\ell \, kT/B_{v_1 v_2 \ell v_3}$$

$$X \exp\left[\left(B_{v_1 v_2 \ell v_3} \ell^2 - G_{v_1 v_2 \ell v_3}\right)/kT\right], \qquad \text{(A-3)}$$

where $B_{v_1 v_2 \ell v_3}$ is the rotational constant and $G_{v_1 v_2 \ell v_3}$ is the vibrational energy. The vibrational degeneracy is given by the formula

$$g_\ell = 1 \text{ for } \ell = 0,$$

$$= 2 \text{ otherwise.} \qquad \text{(A-4)}$$

When the vibrational levels are grouped into closely coupled "states", we obtain the following partition functions:

$$Q_0 = Q_{00^0 0} \tag{A-5a}$$

$$Q_1 = Q_{01^1 0} \tag{A-5b}$$

$$Q_2 = Q_{02^0 0} + Q_{02^2 0} + Q_{100} \tag{A-5c}$$

$$Q_3 = Q_{03^1 0} + Q_{03^3 0} + Q_{11^1 0} \tag{A-5d}$$

$$Q_4 = Q_{04^0 0} + Q_{04^2 0} + Q_{04^4 0} + Q_{12^0 0} + Q_{12^2 0} + Q_{20^0 0} \tag{A-5e}$$

2. CH_4 "States"

Referred to the elemental chemical species, the partition function for a molecule in vibrational level $(v_1 v_2 v_3 v_4)$ is given by the expression

$$Q_{v_1 v_2 v_3 v_4} = \exp(-\Delta H_F^{\circ}/kT)\, Q^{(T)} Q^{(VR)}_{v_1 v_2 v_3 v_4} \tag{A-6}$$

where ΔH_F° is the heat of formation of $0^{\circ}K$, k is Boltzmann's constant and T is the temperature. The translational partition function is given by the expression

$$Q^{(T)} = (2\pi\, mkT/h^2)^{3/2} \tag{A-7}$$

where m is the molecular mass and h is Planck's constant. To calculate the vibration-rotation partition function we ignore the fine multiplet splitting of the intercombination levels, and neglect vibration-rotation interaction. The vibration-rotation partition function may then be expressed

$$Q^{(VR)}_{v_1 v_2 v_3 v_4} = \frac{g_v}{12} \left(\frac{kT}{B}\right)^{3/2} \exp\left(-\frac{G_{v_1 v_2 v_3 v_4}}{kT}\right), \tag{A-8}$$

where $B = 5.24059\ cm^{-1}$ is the rotational constant and $G_{v_1 v_2 v_3 v_4}$ is the vibrational energy. The vibrational degeneracy is given by the formula

$$g_v = \frac{1}{4} (v_2+1) (v_4+1) (v_4+2) (v_3+1) (v_3+2), \qquad \text{(A-9)}$$

and the factor 12 accounts for the rotational symmetry.

When the vibrational levels are grouped into closely coupled "states", we obtain the following partition functions:

$$Q_0 = Q_{0000} \qquad \text{(A-10a)}$$

$$Q_1 = Q_{0001} + Q_{0100} \qquad \text{(A-10b)}$$

$$Q_2 = Q_{0002} + Q_{0101} + Q_{0200} \qquad \text{(A-10c)}$$

$$+ Q_{1000} + Q_{0010} \qquad \text{(A-10d)}$$

APPENDIX B

SUMMARY OF VIBRATIONAL RELAXATION PROCESSES AND RATES

	Process	Rate k (cm^3/sec)
(1)	$N_2(v=1) + H_2O \rightarrow N_2(v=0) + H_2O$	3.6×10^{-15}
(2)	$N_2(v=1) + N_2 \rightarrow N_2(v=0) + N_2$	2.5×10^{-24}
(3)	$N_2(v=1) + O_2 \rightarrow N_2(v=0) + O_2$	2.5×10^{-24}
(4)	$N_2(v=1) + O_2(v=0) \rightarrow N_2(v=0) + O_2(v=1)$	1.6×10^{-18}
(5)	$CO_2(001) + N_2(v=0) \rightarrow CO_2(000) + N_2(v=1)$	5.4×10^{-13}
(6)	$CO_2(001) + H_2O \rightarrow CO_2(030) + H_2O$	4.3×10^{-13}
(7)	$CO_2(001) + N_2 \rightarrow CO_2(030) + N_2$	1.9×10^{-15}
(8)	$CO_2(001) + O_2 \rightarrow CO_2(030) + O_2$	1.9×10^{-15}
(9)	$CO_2(001) + CO_2 \rightarrow CO_2(030) + CO_2$	4.2×10^{-15}
(10)	$CO_2(001) + H_2O \rightarrow CO_2(000) + H_2O$	4.2×10^{-15}
(11)	$CO_2(030) + CO_2(000) \rightarrow CO_2(020) + CO_2(010)$	1.0×10^{-11}
(12)	$CO_2(020) + CO_2(000) \rightarrow CO_2(010) + CO_2(010)$	6.9×10^{-12}
(13)	$CO_2(100) + M \rightarrow CO_2(020) + M$	1.0×10^{-10}
(14)	$CO_2(010) + H_2O \rightarrow CO_2(000) + H_2O$	1.8×10^{-11}
(15)	$CO_2(020) + H_2O \rightarrow CO_2(010) + H_2O$	3.6×10^{-11}
(16)	$CO_2(030) + H_2O \rightarrow CO_2(020) + H_2O$	5.4×10^{-11}
(17)	$CO_2(010) + N_2 \rightarrow CO_2(000) + N_2$	3.8×10^{-15}
(18)	$CO_2(020) + N_2 \rightarrow CO_2(010) + N_2$	7.6×10^{-15}
(19)	$CO_2(030) + N_2 \rightarrow CO_2(020) + N_2$	1.1×10^{-14}
(20)	$CO_2(010) + O_2 \rightarrow CO_2(000) + O_2$	3.8×10^{-15}

	Process	Rate k (cm^3/sec)
(21)	$CO_2(020) + O_2 \rightarrow CO_2(010) + O_2$	7.6×10^{-15}
(22)	$CO_2(030) + O_2 \rightarrow CO_2(030) + O_2$	1.1×10^{-14}
(23)	$CO_2(010) + CO_2 \rightarrow CO_2(000) + CO_2$	7.2×10^{-15}
(24)	$CO_2(020) + CO_2 \rightarrow CO_2(010) + CO_2$	1.4×10^{-14}
(25)	$CO_2(030) + CO_2 \rightarrow CO_2(020) + CO_2$	2.2×10^{-14}
(26)	$H_2O(010) + H_2O \rightarrow H_2O(000) + H_2O$	4.2×10^{-11}
(27)	$H_2O(020) + H_2O \rightarrow H_2O(010) + H_2O$	8.3×10^{-11}
(28)	$H_2O(010) + N_2 \rightarrow H_2O(000) + N_2$	6.0x10-14
(29)	$H_2O(020) + N_2 \rightarrow H_2O(010) + N_2$	1.2×10^{-13}
(30)	$H_2O(010) + O_2 \rightarrow H_2O(000) + O_2$	2.7×10^{-15}
(31)	$H_2O(020) + O_2 \rightarrow H_2O(910) + O_2$	5.4×10^{-15}
(32)	$H_2O(010) + O_2(v=0) \rightarrow H_2O(000) + O_2(v=1)$	1.5×10^{-12}
(33)	$H_2O(020) + O_2(v=0) \rightarrow H_2O(010) + O_2(v=1)$	3.0×10^{-12}
(34)	$O_2(v=1) + H_2O \rightarrow O_2(v=0) + H_2O$	4.3×10^{-14}
(35)	$O_2(v=1) + N_2 \rightarrow O_2(v=0) + N_2$	3.6×10^{-19}
(36)	$O_2(v=1) + O_2 \rightarrow O_2(v=0) + O_2$	3.6×10^{-19}
(37)	$O_2(v=1) + CO_2(000) \rightarrow O_2(v=0) + CO_2(010)$	6.6×10^{-15}
(38)	$N_2O(010) + H_2O \rightarrow N_2O(000) + H_2O$	4.3×10^{-12}
(39)	$N_2O(020) + H_2O \rightarrow N_2O(010) + H_2O$	8.6×10^{-12}
(40)	$N_2O(030) + H_2O \rightarrow N_2O(020) + H_2O$	1.3×10^{-11}
(41)	$N_2O(040) + H_2O \rightarrow N_2O(030) + H_2O$	1.7×10^{-11}
(42)	$N_2O(010) + N_2 \rightarrow N_2O(000) + N_2$	2.0×10^{-14}
(43)	$N_2O(020) + N_2 \rightarrow N_2O(010) + N_2$	4.0×10^{-14}
(44)	$N_2O(030) + N_2 \rightarrow N_2O(020) + N_2$	6.0×10^{-14}

	Process	Rate k (cm^3/sec)
(45)	$N_2O(040) + N_2 \rightarrow N_2O(030) + N_2$	8.0×10^{-14}
(46)	$N_2O(010) + O_2 \rightarrow N_2O(000) + O_2$	2.0×10^{-14}
(47)	$N_2O(020) + O_2 \rightarrow N_2O(010) + O_2$	4.0×10^{-14}
(48)	$N_2O(030) + O_2 \rightarrow N_2O(020) + O_2$	6.0×10^{-14}
(49)	$N_2O(040) + O_2 \rightarrow N_2O(030) + O_2$	8.0×10^{-14}
(50)	$H_2O(010) + N_2O(000) \rightarrow H_2O(000) + N_2O(020)$	1.0×10^{-12}
(51)	$H_2O(010) + N_2O(010) \rightarrow H_2O(000) + N_2O(030)$	1.0×10^{-12}
(52)	$H_2O(010) + N_2O(020) \rightarrow H_2O(000) + N_2O(040)$	2.0×10^{-12}
(53)	$O_2(v=1) + CH_4(0000) \rightarrow O_2(v=0) + CH_4(0001)$	6.0×10^{-13}
(54)	$O_2(v=1) + CH_4(0001) \rightarrow O_2(v=0) + CH_4(0002)$	1.2×10^{-12}
(55)	$H_2O(010) + CH_4(0000) \rightarrow H_2O(000) + CH_4(0001)$	6.4×10^{-11}
(56)	$H_2O(010) + CH_4(0001) \rightarrow H_2O(000) + CH_4(0002)$	1.3×10^{-10}
(57)	$HDO(100) + H_2O \rightarrow HDO(020) + H_2O$	2.0×10^{-10}
(58)	$HDO(010) + H_2O(010) \rightarrow HDO(010) + H_2O(000)$	2.0×10^{-10}
(59)	$HDO(010) + H_2O(010) \rightarrow HDO(020) + H_2O(000)$	4.0×10^{-10}
(60)	$HDO(000) + H_2O(020) \rightarrow HDO(010) + H_2O(010)$	4.0×10^{10}
(61)	$HDO(010) + H_2O \rightarrow HDO(000) + H_2O$	4.2×10^{-11}
(62)	$HDO(020) + H_2O \rightarrow HDO(010) + H_2O$	8.3×10^{-11}
(63)	$HDO(010) + N_2 \rightarrow HDO(000) + N_2$	6.0×10^{-14}
(64)	$HDO(020) + N_2 \rightarrow HDO(010) + N_2$	1.2×10^{-13}
(65)	$HDO(010) + O_2 \rightarrow HDO(000) + O_2$	2.7×10^{-15}
(66)	$HDO(020) + O_2 \rightarrow HDO(010) + O_2$	5.4×10^{-15}
(67)	$HDO(100) + N_2(v=0) \rightarrow HDO(000) + N_2(v=1)$	2.0×10^{-13}
(68)	$O_2(v=1) + HDO(000) \rightarrow O_2(v=0) + HDO(010)$	1.0×10^{-12}
(69)	$O_2(v=1) + HDO(010) \rightarrow O_2(v=0) + HDO(020)$	2.0×10^{-12}

APPENDIX C

DETAILED BALANCE FOR OPTICAL TRANSITIONS

We consider a molecule N whose manifold of internal levels may be grouped into two sets of levels, with one set loosely referred to as the ground state, N^o, and the other loosely referred to as the excited state N^*. The total populations of these states are

$$N^o = \sum_i N_i, \tag{C-1a}$$

$$N^* = \sum_j N_j, \tag{C-1b}$$

where N_i and N_j are the populations of the individual levels i and j, respectively. We shall assume that rapid collisional processes keep the relative populations of the levels within each state in equilibrium with each other at the temperature T. That is,

$$N_i = \frac{g_i \exp(-E_i/kT)}{Q^o} N^o, \tag{C-2a}$$

$$N_j = \frac{g_j \exp(-E_j/kT)}{Q^*} N^*, \tag{C-2b}$$

where g_i and g_j are the degeneracies of levels i and j, respectively and E_i and E_j are the energies (referred to the same zero) of level i and j, respectively, and k is Boltzmann's constant. The partition functions are defined by the expressions

$$Q^o(T) = \sum_i g_i \exp(-E_i/kT), \tag{C-3a}$$

$$Q^*(T) = \sum_j g_j \exp(-E_j/kT). \tag{C-3b}$$

We now suppose that the molecules are subjected to radiation of intensity I_ν and frequency ν, where

$$h\nu = E_j - E_i, \tag{C-4}$$

and h is Planck's constant. The rate of induced transitions is then

$$N^* = -N^o = N_i B_{ij} I - N_j B_{ji} I, \tag{C-5}$$

where B_{ij} and B_{ji} are Einstein's coefficients for the transitions i→j and j→i, respectively. These coefficients satisfy the relation

$$g_i B_{ij} = g_j B_{ji}. \tag{C-6}$$

Substituting Eqs. (C-2), (C-4) and (C-6) into Eq. (C-5) we obtain the result

$$N^* = -N^o = \sigma_{\nu i} \Phi_\nu \left[N^o - \frac{Q^o}{Q^*} e^{-h\nu/kT} N^* \right], \tag{C-7}$$

where the flux of photons is

$$\Phi_\nu = I_\nu / h\nu, \tag{C-8}$$

and the absorption cross section for a ground state molecule is defined by the expression

$$\sigma_{\nu i}(T) \sigma \frac{g_i \exp(-E_i/kT)}{Q^o} h\nu B_{ij}. \tag{C-9}$$

It should be noted that if several transitions are absorbing at the frequency ν, Eq. (C-7) may be used simply by replacing $\sigma_{\nu i}$ by σ_ν, where

$$\sigma_\nu = \sum_i \sigma_{\nu i}. \tag{C-10}$$

If several frequencies ν are being absorbed, separate equations must be written for each frequency.

DISTRIBUTION LIST

Director
Defense Advanced Research Projects Agency
1400 Wilson Boulevard
Arlington, Virginia — 2 copies

Defense Documentation Center
Cameron Station
Alexandria, Virginia 22314 — 12 copies

STOIAC
Battelle Memorial Institute
505 King Avenue
Columbus, Ohio 43201 — 1 copy

Office of Naval Research
800 North Quincy Street
Arlington, Virginia 22217
Attention: Code 421 — 3 copies

Office of Naval Research
Branch Office
495 Summer Street
Boston, Massachusetts 02210
Attention: Dr. A. D Wood — 1 copy

DCASD
666 Summer Street
Boston, Massachusetts 02210
Attention: DBCS-C7 — 1 copy

Director
Naval Research Laboratory
Washington, D. C. 20390
Attention: Code 2627 — 6 copies